Příloha 1a

OXFORD

ORIGINAL ARTICLE

Acadian variant of Fanconi syndrome is caused by mitochondrial respiratory chain complex I deficiency due to a non-coding mutation in complex I assembly factor NDUFAF6

Hana Hartmannová[1,†], Lenka Piherová[1,†], Kateřina Tauchmannová[2,†], Kendrah Kidd[3], Philip D. Acott[4,5], John F. S. Crocker[4,5], Youcef Oussedik[6], Marcel Mallet[7], Kateřina Hodaňová[1], Viktor Stránecký[1], Anna Přistoupilová[1], Veronika Barešová[1], Ivana Jedličková[1], Martina Živná[1], Jana Sovová[1], Helena Hůlková[1], Vicki Robins[3], Marek Vrbacký[2], Petr Pecina[2], Vilma Kaplanová[2], Josef Houštěk[2], Tomáš Mráček[2], Yves Thibeault[8], Anthony J. Bleyer[3] and Stanislav Kmoch[1,3,*]

[1]Institute for Inherited Metabolic Disorders, First Faculty of Medicine, Charles University in Prague, 120 00 Prague 2, Czech Republic, [2]Institute of Physiology of the Czech Academy of Sciences, Vídeňská 1083, Prague, Czech Republic, [3]Section on Nephrology, Wake Forest School of Medicine, Medical Center Blvd, Winston-Salem, NC, USA, [4]Section of Pediatric Nephrology, Department of Pediatrics, Dalhousie University, Halifax, Nova Scotia, Canada, [5]IWK Health Center, Halifax, Nova Scotia, Canada, [6]Department of Pathology, [7]Section of Pulmonology and [8]Section of Nephrology, Dr. Georges L. Dumont University Hospital Centre, Moncton, New Brunswick, Canada

*To whom correspondence should be addressed at: First Faculty of Medicine, Institute for Inherited Metabolic Disorders, Prague, Charles University in Prague, 120 00 Prague, Czech Republic. Tel: +420 224967691; Fax: +420 224967119; Email: skmoch@lf1.cuni.cz

Abstract

The Acadian variant of Fanconi Syndrome refers to a specific condition characterized by generalized proximal tubular dysfunction from birth, slowly progressive chronic kidney disease and pulmonary interstitial fibrosis. This condition occurs only in Acadians, a founder population in Nova Scotia, Canada. The genetic and molecular basis of this disease is unknown. We carried out whole exome and genome sequencing and found that nine affected individuals were homozygous for the ultra-rare non-coding variant chr8:96046914 T > C; rs575462405, whereas 13 healthy siblings were either heterozygotes or lacked the mutant allele. This variant is located in intron 2 of *NDUFAF6* (NM_152416.3; c.298-768 T > C), 37 base pairs upstream from an alternative splicing variant in *NDUFAF6* chr8:96046951 A > G; rs74395342 (c.298-731 A > G). *NDUFAF6* encodes NADH:ubiquinone oxidoreductase complex assembly factor 6, also known as C8ORF38. We found that rs575462405—either alone or in combination with rs74395342—affects splicing and synthesis of NDUFAF6 isoforms. Affected kidney and lung

1

51

showed specific loss of the mitochondria-located NDUFAF6 isoform and ultrastructural characteristics of mitochondrial dysfunction. Accordingly, affected tissues had defects in mitochondrial respiration and complex I biogenesis that were corrected with NDUFAF6 cDNA transfection. Our results demonstrate that the Acadian variant of Fanconi Syndrome results from mitochondrial respiratory chain complex I deficiency. This information may be used in the diagnosis and prevention of this disease in individuals and families of Acadian descent and broadens the spectrum of the clinical presentation of mitochondrial diseases, respiratory chain defects and defects of complex I specifically.

Introduction

Renal Fanconi Syndrome (RFS) is a rare condition associated with decreased proximal tubular uptake of electrolytes and organic compounds, resulting in metabolic acidosis, aminoaciduria, phosphaturia and uricosuria (1,2). RFS may be caused by medications (3), toxins (4) or genetic mutations affecting the function of the proximal tubule (1,5). RFS is often caused also by mitochondrial defects because bulk transport in the proximal tubule is highly energy dependent (6–10). For many familial RFS cases, the genetic and molecular basis remains unknown. The Acadian variant of Fanconi Syndrome (AVFS) refers to a form of RFS found only in Acadians, a founder population in Nova Scotia, Canada. This specific form of RFS is associated with abnormalities in proximal tubular reabsorption, chronic kidney disease leading to the need for renal replacement therapy and pulmonary fibrosis (11,12). In this investigation, we identified a causative non-coding mutation in NADH:ubiquinone oxidoreductase complex assembly factor 6 (NDUFAF6) that leads to aberrant splicing of NDUFAF6 mRNA and loss of the mitochondria-located NDUFAF6 isoform, resulting in NADH:ubiquinone oxidoreductase complex (mitochondrial respiratory chain complex I) deficiency. These findings are in contrast to a previously reported mutation in NDUFAF6 that resulted in loss of both the mitochondrial and cytoplasmic isoforms and causes Leigh syndrome and early death (13).

Results

AVFS is characterized by proximal tubular dysfunction, slowly progressive chronic kidney disease, pulmonary interstitial fibrosis and autosomal recessive inheritance

Acadian variant of Fanconi Syndrome has been characterized by generalized proximal tubular dysfunction from birth, slowly progressive chronic kidney disease and pulmonary interstitial fibrosis occurring later in life (11,12). In this study, all affected individuals presented with genu valgum (a sign of phosphate deficiency due to phosphaturia associated with RFS) before age 10 years (Table 1). Due to the historical characterization of affected individuals, all laboratory analyses were not available in each participant. However, when available, all results consistently pointed to a proximal tubular defect with the following characteristics: (a) proximal renal tubular acidosis, (b) the absence of potassium wasting, (c) generalized aminoaciduria, (d) phosphaturia with hypophosphatemia requiring phosphate replacement, (e) hyperuricosuria with hypouricemia, (f) absence of nephrocalcinosis and (g) elevated urinary lactate (Supplementary Material, Table S1). Over time, each affected individual developed slowly progressive kidney failure. Renal ultrasound examination was unremarkable. Pathologic findings from kidney biopsies in two individuals yielded similar results. The majority of glomeruli were normocellular. The interstitium showed patchy fibrosis associated with tubular atrophy and focal collections of chronic mononuclear inflammatory cells.

An occasional cystic dilated tubule was present. There was no tubulitis. Affected individuals progressed to end-stage kidney disease between ages 25 and 40 years (Fig. 1A). One individual died of uremia prior to the onset of renal replacement therapy. Six individuals received a kidney transplant, and three individuals were placed on maintenance dialysis.

Individuals affected with AVFS developed symptoms of dyspnea in their third to fifth decades of life. Initial pulmonary function studies revealed a low carbon monoxide diffusing capacity (DLCO) in the presence of a well-preserved forced vital capacity (FVC) and forced expiratory volume at 1 s (FEV1). The DLCO declined gradually over time, leading to respiratory failure (Fig. 1B). None of the affected individuals received lung transplantation, with all older individuals involved in the study eventually dying from respiratory failure. Lung biopsies and pathologic specimens from autopsies showed pulmonary interstitial fibrosis as the predominant finding. Computerized axial tomographic scans revealed diffuse interstitial fibrosis, emphysema, and in one individual pulmonary microlithiasis. One individual suffered from the premature onset of lung cancer. Table 1 provides a summary of the individual characteristics.

In total, 12 affected individuals from eight families were studied retrospectively (see Fig. 2). There were five individuals from one family with six affected individuals (F1), one family with two affected individuals (F4), two cases were from families with two (F2) and one (F3) unaffected siblings, respectively, and three cases were singletons (F5–7). The pedigree structures and expected founder effect in Acadian population suggested that the disease is inherited in an autosomal recessive manner (Fig. 2).

Homozygosity mapping and genome sequencing identified a candidate intronic variant in a gene encoding NADH:ubiquinone oxidoreductase complex assembly factor, NDUFAF6

Given the known genetic heterogeneity of RFS, we initially sequenced all coding and miRNA exons (NimbleGen SeqCap V2) in four individuals (F1_IV.1, F1_IV.7, F1_IV.19 and F1_V.2) from family 1 using SOLiD™ 4 System (Applied Biosystems, Carlsbad, CA) at the Institute for Inherited Metabolic Disorders (Prague, Czech Republic). Data analysis was performed according to the expected autosomal recessive model with an assumption of a founder effect. We therefore searched for homozygous CNVs, homozygous genomic regions > 2 Mb or homozygous single nucleotide variants (SNVs) or indels shared by all three affected individuals (F1_IV.7, F1_IV.19 and F1_V.2) but not present in the healthy individual (F1_IV.1). We identified only one such region on chromosome 8 (chr8:90958422-96960058). This region did not contain any candidate causal variant except for two low-frequency variants in OTUD6B (chr8:92097062 G/A; rs3210518) and RBM12B (chr8: 94746049 T/G; rs16916188).

We next confirmed the rs3210518 genotypes in all four individuals from Family 1 and genotyped the other nine healthy

Příloha 1a

Table 1. Clinical characteristics of affected individuals

Participant	Age of last follow-up	Status	Genu valgum	Kidney biopsy	Current eGFR or ESRD	Age ESRD	Age of kidney transplantation	Tobacco usage	Age of dx of pulmonary disease	Pulmonary diagnosis
F1_IV.2	47	Deceased	Yes	Not done	ESRD	37	42	Yes	39	Autopsy: pulmonary fibrosis in accelerated phase
F1_IV.7	52	Deceased	Yes	Tubulointerstitial fibrosis	ESRD	40	41	Yes	39	Lung biopsy at age 50 years: chronic interstitial fibrosis. No emphysema
F1_IV.13	22	Deceased	Yes	Not done	ESRD	22	Not transplanted	No	22	Pulmonary microlithiasis on chest x-ray
F1_IV.19	56	Deceased	Yes	Tubulointerstitial fibrosis	ESRD	36	37	No	50	Non-specific micronodular interstitial fibrosis
F1_V.2	25	Alive	Yes	Tubulointerstitial fibrosis	30	N/A	Not transplanted	Yes	20	Decreased DLCO of unknown cause
F2_II.1	32	Alive	Yes	Not done	ESRD	N/A	18	Yes	25	Decreased DLCO of unknown cause
F3_II.1	27	Alive	Yes	Not done	ESRD	19	Not transplanted	Yes	19	Decreased DLCO of unknown cause, CT scan of chest normal
F4_II.1	38	Deceased	Yes	Not done	ESRD	28	30	Yes	37	Adenocarcinoma of lung at 37 and bullous emphysema
F4_II.2	48	Alive	Yes	Tubulointerstitial fibrosis	ESRD	37	37	Yes	37	Bullous emphysema and lung biopsy with emphysematous changes
F5_II.1	35	Alive	Yes	Not done	ESRD	20	Not transplanted	No	30	Centrilobular emphysema, granulomas present
F6_II.1	42	Alive	Yes	Not done	ESRD	35	35	No	30	Decreased DLCO of unknown cause
F7_II.1	44	Alive	Yes	Not done	ESRD	26	38	No	31	Decreased DLCO of unknown cause

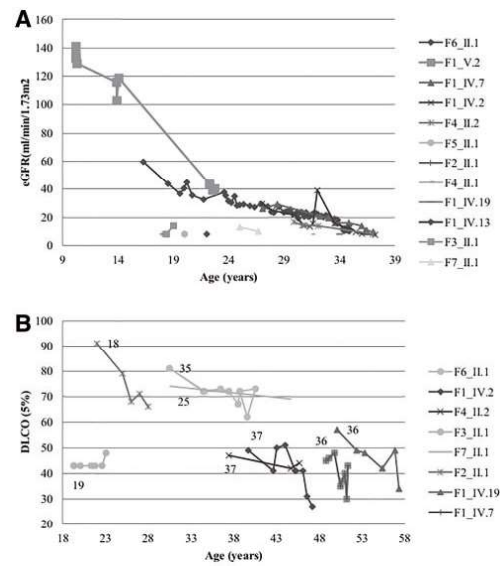ESRD, end-stage renal disease; N/A, not applicable; DLCO, carbon monoxide diffusing capacity.

Figure 1. Clinical characteristics of individuals affected with the Acadian variant of Fanconi syndrome. (**A**) Change in estimated glomerular filtration rate (eGFR) over time for affected individuals. Laboratory values were obtained by chart review. eGFR at the start of renal replacement therapy was estimated at 10 ml/min/1.73 m². eGFR was calculated with the modified Modification of Diet in Renal Disease (MDRD) equation (14). (**B**) Change in the diffusion coefficient of carbon monoxide (DLCO) over time in affected individuals. The number at the beginning of each individual's data series is the age of onset of end-stage kidney disease (ESRD) for that individual. This value is included in the figure to enable the reader to see the relationship between progression of kidney disease and pulmonary disease.

family members using Sanger sequencing. This analysis confirmed the relevance of the homozygous region in this family, as all affected individuals were homozygous for the minor rs3210518 variant, whereas all healthy individuals were either heterozygotes or lacked the minor allele (homozygous for the major allele). We also genotyped rs3210518 in three other unrelated individuals affected with AVRFS (F4_II.2, F5_II.1 and F6_II.1). We found that one individual (F4_II.2) was homozygous but two individuals (F5_II.1 and F6_II.1) were heterozygous for the minor rs3210518 allele, excluding this variant as causative.

To identify mutations that we may have missed in the first round of exome sequencing (NimbleGen SeqCap EZ Exome v2) and to identify homozygous regions in both affected individuals that were heterozygous for the minor rs3210518 allele, we sequenced all coding exons and 5′- and 3′-untranslated regions of their corresponding mRNAs (UTRs) in a pool of genomic DNA obtained from three affected individuals from Family 1 (F1_IV.7, F1_IV.19 and F1_V.2) and DNA samples from two affected individuals (F5_II.1 and F6_II.1) who have been found to be heterozygous for rs3210518; (SeqCap EZ Human Exome +UTR library, Illumina HiSeq 1500). Using this approach, we again did not identify any plausible candidate variants. Nevertheless, using homozygosity mapping, we detected in F5_II.1 and a pooled DNA sample recombination events at the centromeric and telomeric ends of their corresponding homozygous regions, which delimited the candidate homozygous to chr8:94242350-97172487 (Fig. 3A and B).

To identify non-coding variants within the candidate region, we sequenced the whole genomes of F5_II.1 and F1_IV.7 at 30X coverage using the Illumina HiSeq X Ten System. Homozygosity
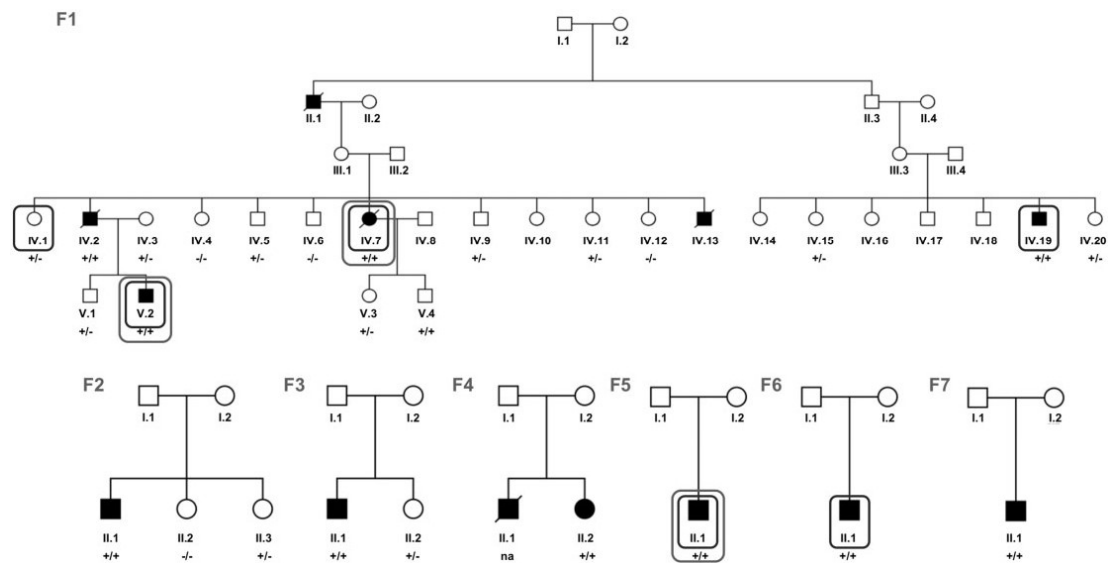
Figure 2. Pedigrees of Acadian families (F1–F7) affected by Fanconi syndrome. Black symbols denote affected individuals, open symbols denote unaffected parents and siblings. Black and gray boxes indicate individuals who underwent whole exome (black boxes) and/or whole genome (gray boxes) sequencing, respectively. (+/−) denotes presence (+) or absence (−) of the chr8:96046914 T > C mutation. na indicates DNA was unavailable for investigation.
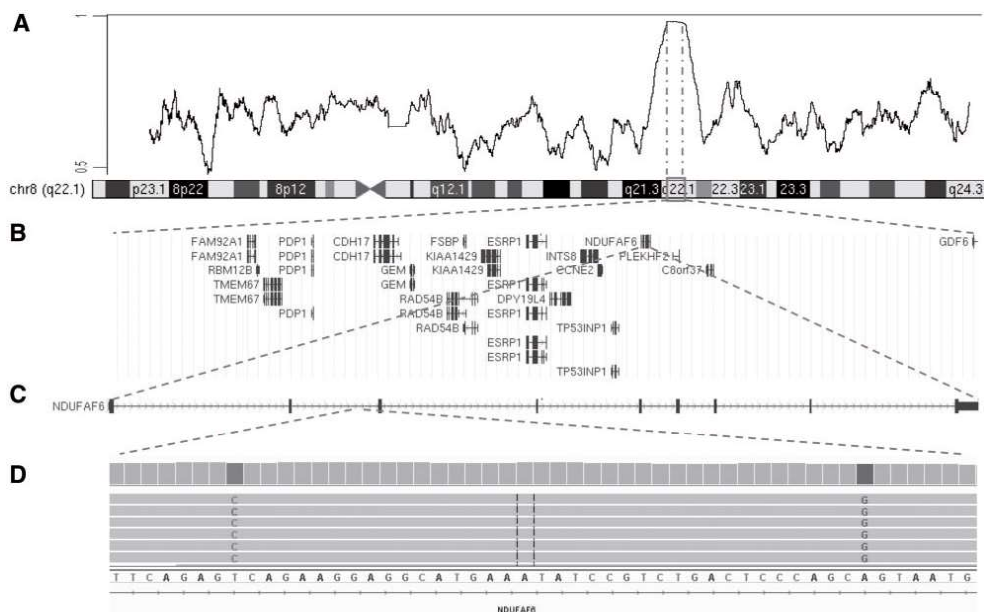

Figure 3. Identification of non-coding mutation in *NDUFAF6*. (**A**) Candidate region on chromosome 8 identified by homozygosity mapping. Allele frequency was calculated and visualized using TTR R-package. The Y-axis shows the proportion of individuals homozygous for a given genomic region, and the *x*-axis shows the position of the homozygous region on chromosome 8. (**B**) Annotated transcripts within the homozygous interval. (**C**) Schematic illustration of the *NDUFAF6* transcript. (**D**) Visualization in the Integrative Genomics Viewer of the homozygous non-coding variants rs575462405 (chr8:96046914 T > C) and rs74395342 (chr8:96046951 A > G) located in intron 2 of *NDUFAF6* identified in all affected individuals.

mapping further narrowed candidate homozygous region to chr8: 94423201-96206283. From the 322 variants identified within the candidate homozygous region, we searched for those that were either novel or present at frequencies <0.005 in the 1000 Genomes database, dbSNP database and our internal genome database (10 genomes). We found 16 non-coding variants; 11 variants were intronic, 1 downstream, 3 intergenic and one was located in the 5′-UTR (Supplementary Material, Table S2). We prioritized the variants according to conservancy (GERP conservation score) (15,16) and predicted deleteriousness of

SNV's (raw and scaled CADD scores) (17). Using this approach we defined one candidate variant, chr8:96046914 T > C, in the gene *NDUFAF6* (Fig. 3C and D). This variant, rs575462405, is located in intron 2 of *NDUFAF6* (NM_152416.3; c.298-768 T > C), 37 base pairs upstream from another variant in *NDUFAF6* (chr8:96046951 A > G (c.298-731 A > G), rs74395342, minor allele frequency 0.1), which creates an alternative splice donor site. To predict the possible effects of the c.298-768 T > C mutation on *NDUFAF6* splicing, we used SpliceSiteFinder, MaxEntScan, NNSPLICE, GeneSplicer and Human Splicing Finder algorithms that are incorporated in the Alamut Mutation Interpretation Software. These programs predicted that the c.298-768 T > C nucleotide change would create a novel splice acceptor site. The Alamut splicing window also includes exonic splice enhancer prediction software, ESEFinder, which predicted that the mutation creates a putative binding site for the pre-mRNA-splicing factor SRp40 (Supplementary Material, Fig. S1).

Using Sanger sequencing, we confirmed homozygosity for the chr8:96046914 T > C variant in all 3 affected individuals from Family 1 as well as in the other 6 individuals affected with AVFS; 13 healthy siblings were either heterozygotes or lacked the mutant allele (Fig. 2). This variant was absent in 13 200 genomes reported in the Kaviar database (18). Interestingly, it was found once among 104 individuals from a Puerto Rican sample set that was analyzed within the 1000 genome project; (1000 Genomes Browser).

Identified mutation affects splicing and synthesis of NDUFAF6 isoforms

NDUFAF6 encodes assembly factor 6 of the NADH dehydrogenase (ubiquinone) complex I (NDUFAF6), also known as C8ORF38. Knockdown of NDUFAF6 reduces the abundance and activity of mitochondrial complex I (19) and a previously reported mutation of NDUFAF6 led to clinical symptoms of respiratory chain deficiency (OMIM 612392) (13,20). RFS is caused by generalized proximal tubular dysfunction, often of mitochondrial origin (7,9,21). We therefore considered that mitochondrial dysfunction resulting from complex I deficiency due to alternative splicing of *NDUFAF6* mRNA might be responsible for this phenotype.

Three transcript variants of human *NDUFAF6* resulting from alternative mRNA splicing have been proposed to exist (20). Isoform 1 (NM_152416), (*v_1*), encodes a 38-kDa protein of 333 amino acids (Q330K2-1), V_1. The protein contains a mitochondrial targeting sequence leading to association of this isoform with the matrix face of the inner mitochondrial membrane (20). Compared to isoform *v_1*, isoform 2 (AY444560.1), (*v_2*), has different exons 1 and 2 and encodes for a protein of 281 amino acids that lack the N-terminal mitochondrial targeting sequence (Q330K2-2), V_2. Isoform 3 (BC028166), (*v_3*), encodes for a protein of 121 amino acids (Q330K2-3), V_3, which is predicted to have the same N-terminal mitochondrial targeting sequence as V_1 and is truncated due to a stop codon, resulting from alternative splicing of the exon 4/intron 4 boundaries and inclusion of a unique exon 5. This NDUFAF6 isoform is predicted to be targeted to mitochondria (20), though this has not been proven experimentally.

To explore why AVFS predominantly affects the kidney and lung, we looked at *NDUFAF6* expression in the Genotype-Tissue Expression, (GTEX) portal (http://www.gtexportal.org/home/) (22). *NDUFAF6* is ubiquitously expressed in all tissues with lower expression in kidney and lung compared to heart, brain or

skeletal muscle. The splicing pattern is more complex than previously reported.

To assess the effect of the c.298-768 T > C mutation on *NDUFAF6* mRNA expression, splicing and stability, we isolated total RNA from a participant's skin fibroblasts and autoptic lung tissue and performed reverse transcription polymerase chain reaction (RT-PCR) analyses of the three *NDUFAF6* mRNA isoforms. In fibroblasts and lung tissue from affected individuals, we found an altered profile of RT-PCR products (Fig. 4A). The amounts of RT-PCR products were similar but larger in size than those of control specimens that were obtained from individuals who were either wild-type, heterozygous or homozygous for the c.298-731 A > G splicing SNP. The analysis thus showed that the G nucleotide in this position itself is preferentially used for splicing in the presence of the causative c.298-768 T > C mutation. In both, control and affected samples there were also additional PCR products suggestive of a more complex mRNA splicing pattern. To identify the differences in the splicing pattern of *NDUFAF6* in control and affected individuals we isolated and Sanger sequenced major RT-PCR fragments. In parallel we also pair-end sequenced the obtained RT-PCR products using the Illumina HiSeq 1500 system. In addition to the known isoforms *v_1*, *v_2* and *v_3* this analysis revealed the existence of several other isoforms. In control samples we identified novel isoforms that we name *v_4*, *v_5*, *v_6*, *v_7*, *v_8*, *v_9* and *v_10* (Supplementary Material, Table S3). These isoforms may encode several novel NDUFAF6 isoforms (Supplementary Material, Table S4). In affected samples we did not identify isoforms *v_1*, *v_7* and *v_8*. All other identified cDNA isoforms that we name (*v_Nm*) had the insertion of 102 nucleotides corresponding to chr8:96046850-96046951 (Fig. 4B, e_mut). This sequence represents the exonized intronic fragment that contains the c.298-768 T > C mutation and uses the alternative splice donor site created by the chr8:96046951 A > G variant (minor variant of rs74395342). Excluding *v_3m* and *v_5m*, the exonized intronic fragment introduces a premature stop codon to identified cDNA variants. This encodes for several classes of truncated NDUFAF6 proteins that either contain the N-terminal mitochondrial targeting sequence or correspond to the truncated N-terminal part of the cytoplasmic isoform V_2. Interestingly all these cDNA isoforms contain the alternative initiation codon beyond the premature stop codon in exon 6. This encodes in all cases for cytoplasmic NDUFAF6 proteins that lack 67 amino acid residues on their N-terminal end compared to the V_2 variant (Fig. 4B and Supplementary Material, Table S5).

To test whether these alternative initiation codons are used for translation, we translated the *v_1* and *v_2* NDUFAF6 cDNA isoforms *in vitro*. This analysis revealed the presence of polypeptides of molecular weights corresponding to nascent V_1 and V_2 isoforms (at ~38 and 33 kDa) together with polypeptides of isoforms ~29 and 26 kDa, theoretically corresponding to cytoplasmic isoforms translated from the alternative initiation codons (Fig. 5A). This indicates that affected individuals may lose the mitochondrial NDUFAF6 but may have preserved cytoplasmic function by the expression of this truncated cytosolic NDUFAF6 forms.

To assess the effect of the identified splicing mutation on NDUFAF6 expression and intracellular localization we performed Western-blot analysis of affected and control skin fibroblasts along with HeLa and HEK cells transiently expressing recombinant human mitochondrial NDUFAF6 isoform V_1. For Western-blot detection we used three types of commercially available polyclonal antibodies that were raised against different epitopes of NDUFAF6. In agreement with the cDNA analysis
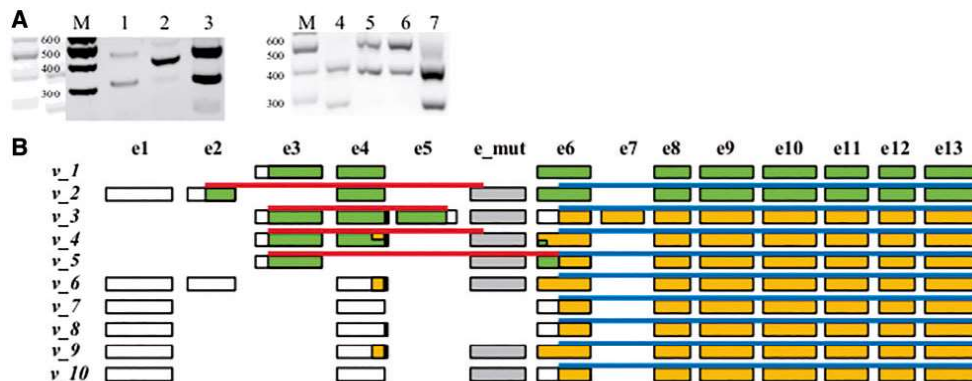
Příloha 1a

Figure 4. *NDUFAF6* cDNA analysis. (**A**) Agarose gel electrophoresis profiles of RT-PCR products amplified from total RNA isolated from fibroblasts of control and proband F2_II.1. Lane 1—RT-PCR analysis of isoforms *v_1* and *v_3* in control sample that is homozygous (A;A) for the major allele of rs74395342. Two RT-PCR products with sizes 325 and 444 base pairs expected for *NDUFAF6* isoforms *v_1* and *v_3*, respectively are detected. Lane 2—RT-PCR analysis of isoforms *v_1* and *v_3* in the proband sample demonstrate multiple RT-PCR products that are longer than the control bands. Lane 3—RT-PCR analysis of isoforms *v_1* and *v_3* in control sample that is homozygous (G;G) for the minor allele of rs74395342 show similar profile to (A;A) in Lane 1. Lane 4—RT-PCR analysis of the isoform *v_2* in a control sample (rs74395342 A;A) demonstrates the presence of two RT-PCR products: one with a size of 408 base pair corresponding to the isoform *v_2*, and one with size of ∼300 base pair whose identity was unknown. Lanes 5 and 6—RT-PCR analysis of the proband's fibroblasts and lung, respectively, demonstrate products longer in sizes than those present in the control sample. Lane 7—RT-PCR analysis of the isoform *v_2* in a control sample (rs74395342 G;G) show similar profile to (A;A) in Lane 4. Lanes M show a 100-base pair DNA ladder. Products from 300 to 600 base pairs are shown. (**B**) Schematic representations of the exonic structures of *NDUFAF6* mRNA isoforms *v_1*–*v_1 0* identified by cDNA sequencing. Individual boxes represent individual exons (e1–e13). Black boxes attached to exon 4 (e4) demonstrate the presence of the additional four base pairs introduced by alternative splicing of exon 4. Open reading frames present in the cDNA isoforms identified in control skin fibroblasts are demonstrated by green and orange colors. Note that some isoform may have two open reading frames. A gray box (e_mut) represents the exonized intronic fragment that contains the c.298-768 T > C mutation and uses the alternative splice donor site created by the chr8:96046951 A > G variant (minor variant of rs74395342) identified in the *NDUFAF6* cDNA isoforms in affected skin fibroblasts. Open reading frames present in these cDNA isoforms are demonstrated by red and blue lines.
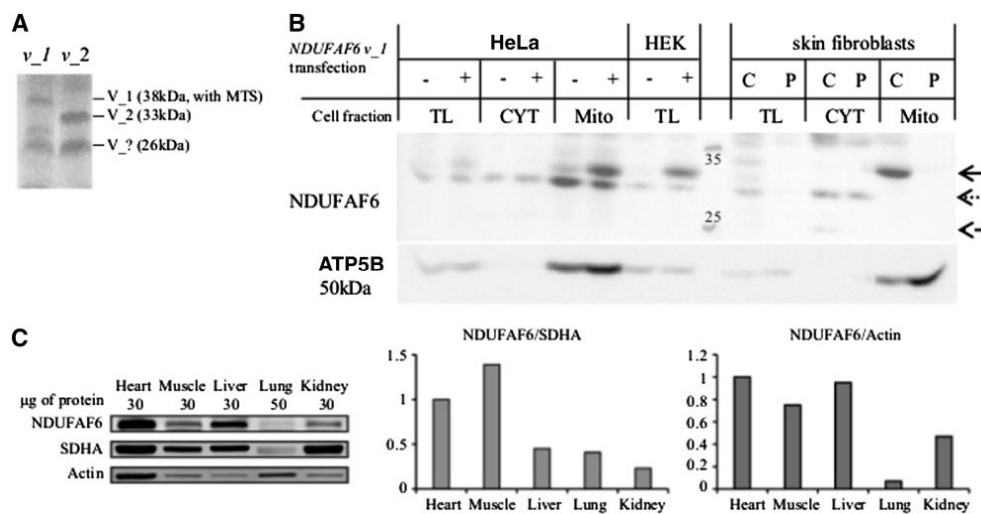

Figure 5. NDUFAF6 analysis. (**A**) *In vitro* translation of cDNA plasmids *v-1* and *v_2* encoding NDUFAF6 isoforms V_1 and V_2, respectively, shows a specific presence of nascent polypeptides of a molecular weights ∼38 and 33 kDa, corresponding to predicted molecular weights of the non-processed precursor of V_1 (e.g. with mitochondrial targeting signal, MTS) and V_2, respectively. Prominent translational products at ∼29 and 26 kDa (V_?) are likely polypetides that are translated from alternative initiation codons. (**B**) Western-blot analysis of NDUFAF6 in total homogenates (TL), cytoplasmic fractions (CYT) and mitochondrial fractions (Mito) prepared from HeLa and HEK cells transiently expressing recombinant human NDUFAF6 V_1 as well as control and affected skin fibroblasts from F2_II.1. Detection with anti-NDUFAF6 antibody (ab150975) shows a specific increase in the amount of the immune-reactive protein of a molecular weight ∼33 kDa corresponding to predicted molecular weight of the processed (e.g. with mitochondrial targeting signal removed) NDUFAF6 isoform V_1 in transiently transfected HeLa and HEK cells. Analysis of the cytoplasmic and mitochondrial fractions demonstrates specific presence of the processed NDUFAF6 V_1 isoform in the mitochondria. In the skin fibroblasts, the amounts of NDUFAF6 V_1 isoform are reduced in total homogenate and mitochondrial fraction from F2_II.1 versus control (arrow). The amounts of the immune-reactive proteins of a molecular weight ∼29 and 26 kDa in the cytoplasmic fraction theoretically corresponding to predicted molecular weights of the cytoplasmic NDUFAF6 isoforms are either comparable or reduced in the proband versus control (dotted and dashed arrows, respectively). Immunodetection of the ATP5B shows efficiency of the cytoplasm/mitochondria fractionation and demonstrate that approximately equal protein amounts have been analyzed in paired samples. (**C**) Western-blot analysis of NDUFAF6 in control human tissues. Detection with anti-NDUFAF6 antibody (ab151096) shows a decreased amount of NDUFAF6 in lung and kidney compared to heart, skeletal muscle and liver. Volumes of tissue lysates corresponding either to 30 μg of total protein (heart, muscle, liver and kidney) or to 50 μg of total protein (lung) were analyzed. The graphs show the relative amounts of NDUFAF6 compared to heart when normalized either to SDHA (left) or to actin (right).

56

and predicted outcome, this analysis revealed loss of the mitochondrial NDUFAF6 isoform V_1 in affected fibroblasts (at ~33 kDa). The amounts of the immune-reactive proteins of a molecular weight ~29 and 26 kDa in the cytoplasmic fraction theoretically corresponding to predicted molecular weights of the cytoplasmic NDUFAF6 isoforms were either comparable or reduced in affected individual F2_II.1 (Fig. 5B). Thus, in the affected individual NDUFAF6 is present in the cytoplasm but not in the mitochondria.

We also performed Western-blot analysis of NDUFAF6 in various control human tissues. In accordance with tissue specific gene expression profiles (see above) there was decreased NDUFAF6 in lung and kidney (41% and 23%, respectively, when normalized to SDHA and compared to heart; and 7% and 47%, respectively, when normalized to actin and compared to heart), (Fig. 5C), which may explain why the kidney and lung are exclusively affected in this condition.

Affected kidney and lung have altered intracellular distribution of NDUFAF6 and ultrastructural characteristics of mitochondrial dysfunction

To assess effects of the aberrant *NDUFAF6* mRNA splicing on expression and intracellular localization of NDUFAF6 isoforms and to evaluate the histopathologic and ultrastructural aspects of this disease, we performed immunohistochemical and immunofluorescence analyses of NDUFAF6 and electron microscopic analysis of kidney and lung from controls and affected individuals (Figs. 6-9).

In the controls (Fig. 6A and B), there was a distinctive granular pattern and concentration of the NDUFAF6 signal in the basal zone of the proximal tubular cells—a site of maximal concentration of mitochondria. In the kidney biopsy of F1_IV.2 (Fig. 6C and D), foci of interstitial and periglomerular fibrosis with small groups of atrophic tubules were detected (Fig. 6C), and increased desquamation and vacuolar degeneration of proximal tubular cells with frequent protrusions of the plasma membranes was present (Fig. 6D). Immunohistochemical staining for the NDUFAF6 protein was reduced in the proximal tubules (Fig. 6C and D) in comparison with controls (Fig. 6A and B). In affected individuals concentration of the NDUFAF6 signal in the basal zone of the proximal tubular cells was not present.

Immunofluorescence detection and colocalization of NDUFAF6 with mitochondrial ATP synthase subunit β (ATPB) and cytoplasmic located heat shock protein 90 (HSP90) (Fig. 7) demonstrated in affected kidney absence of NDUFAF6 staining in mitochondria (Fig. 7G and H) and reduced colocalization signal of NDUFAF6 and HSP90 in the cytoplasm (Fig. 7O and P).

Electron microscopic analysis was performed on the kidney biopsy of F1_V.2 (Fig. 8). Pathologic changes were expressed with maximal intensity in the proximal tubules. The ultrastructural pattern was dominated by the presence of numerous electron lucent vacuoles in the cytoplasm (Fig. 8A and B), microvillous loss and plasma membrane blebbing (Fig. 8B), mitochondrial structural abnormalities and significant signs of autophagy and mitophagy in particular (Fig. 8C–E). Mitochondrial cristae appeared electron dense and thick (Fig. 8C and D). Abnormal configuration or reduction of mitochondrial cristae (Fig. 8C–E), intramitochondrial electron dense inclusions (Fig. 8F) and occasional megamitochondria (Fig. 8F) were detected in tubular epithelial cells.
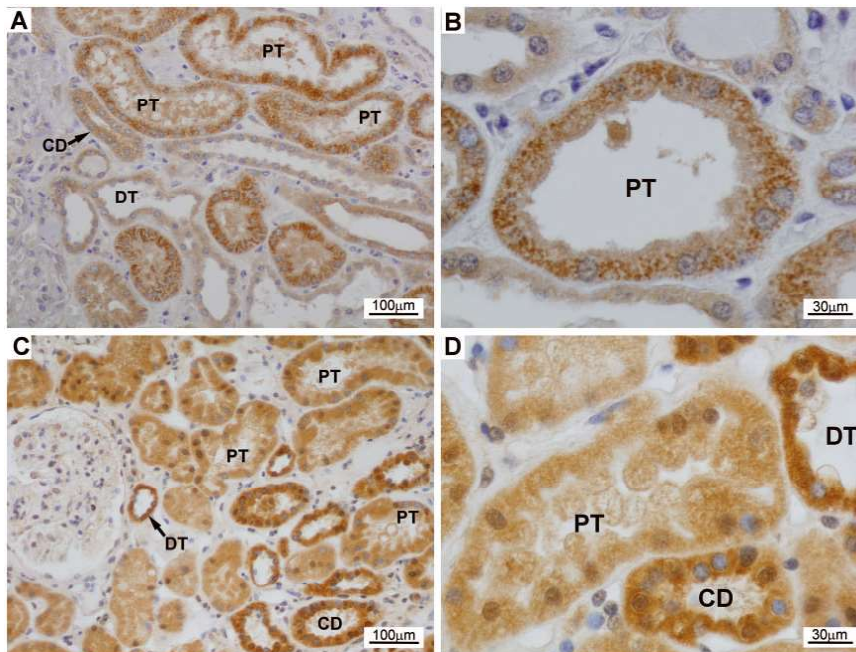

Figure 6. Kidney biopsy from patient F1_IV.2 stained for NDUFAF6 in comparison with control kidney tissue. (**A**) Shows granular staining for NDUFAF6 with maximal intensity in proximal tubular cells beneath their apical zones in control kidney tissue. (**B**) This is a detailed view of a proximal tubule (PT) from the control biopsy. (**C**) This is from an affected kidney and shows reduced and less distinctive staining for NDUFAF6 in proximal tubules without clear cut accentuation in the basal zones of epithelial cells. The signal for NDUFAF6 is strong in distal tubules (DT) and collecting ducts (CD). (**D**) This is a detailed view of the proximal tubule in the affected individual displaying changes compatible with vacuolar degeneration.
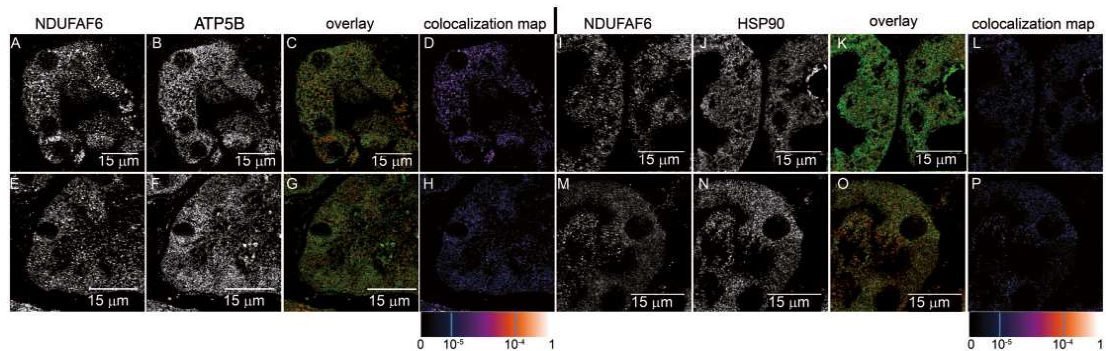
57

Figure 7. Intracellular localization of NDUFAF6 in affected kidney. In control kidney NDUFAF6 is present in finely granular structures (**A** and **I**). Co-staining of NDUFAF6 with (**B**) mitochondrial ATP synthase subunit β (ATP5B) and (**J**) cytoplasmic heat shock protein 90 (HSP90) demonstrate (**C** and **D**) localization of the NDUFAF6 in the mitochondria and (**K** and **L**) in the cytoplasm. In affected kidney NDUFAF6 is present in finely granular structures with reduced and less distinctive staining signal (**E** and **M**). Co-staining with (**F**) ATP5B and (**N**) HSP90 demonstrates (**G** and **H**) loss of localization of NDUFAF6 in mitochondria and (**O** and **P**) reduced colocalization signal of NDUFAF6 and HSP90 in the cytoplasm. The degree of NDUFAF6 colocalization with selected markers is demonstrated by the fluorescent signal overlap (Manders) coefficient values ranging from 0 to 1. The resulting overlap coefficient values are presented as the pseudo color whose scale is shown in the corresponding lookup table.
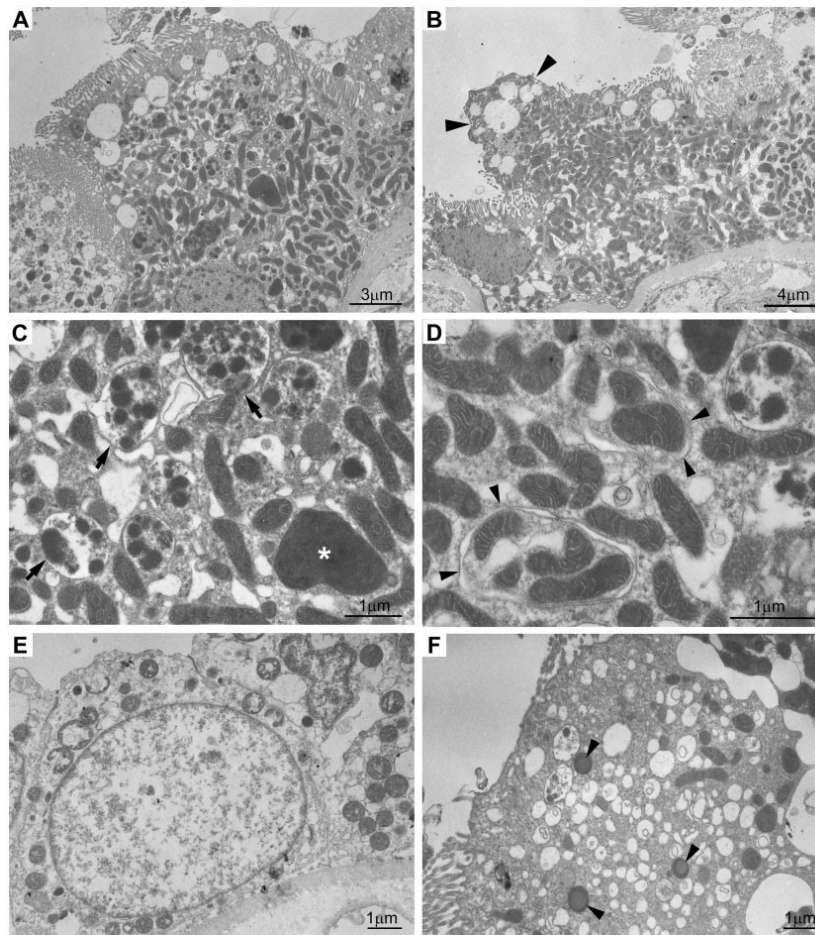

Figure 8. Electron microscopy of tubular epithelial cells in an affected individual F1_V.2. (**A**) Electron lucent vacuoles predominantly in the apical zone and numerous autophagic structures in proximal tubular epithelium. (**B**) proximal tubular epithelial cell contains electron lucent and autophagic vacuoles and also displays partial microvillous loss and plasma membrane blebbing (marked by arrowheads). (**C** and **D**) Higher magnification demonstrates autophagic structures (marked by arrows) and abnormal mitochondria with thick and aberrantly formed electron dense cristae in the cytoplasm of a proximal tubular cell. Megamitochondrion in (**C**) is marked by an asterisk. Structures indicative of mitophagy in (**D**) are marked by arrowheads. (**E**) Irregular mitochondrial swelling with reduction of mitochondrial cristae in collecting duct epithelium. (**F**) Proximal tubular epithelial cell with partial loss of microvilli, prominent vacuolization in the cytoplasm corresponding with severe swelling of organelles and increased number of autophagic structures. Electron dense intramitochondrial inclusions are marked by arrowheads.
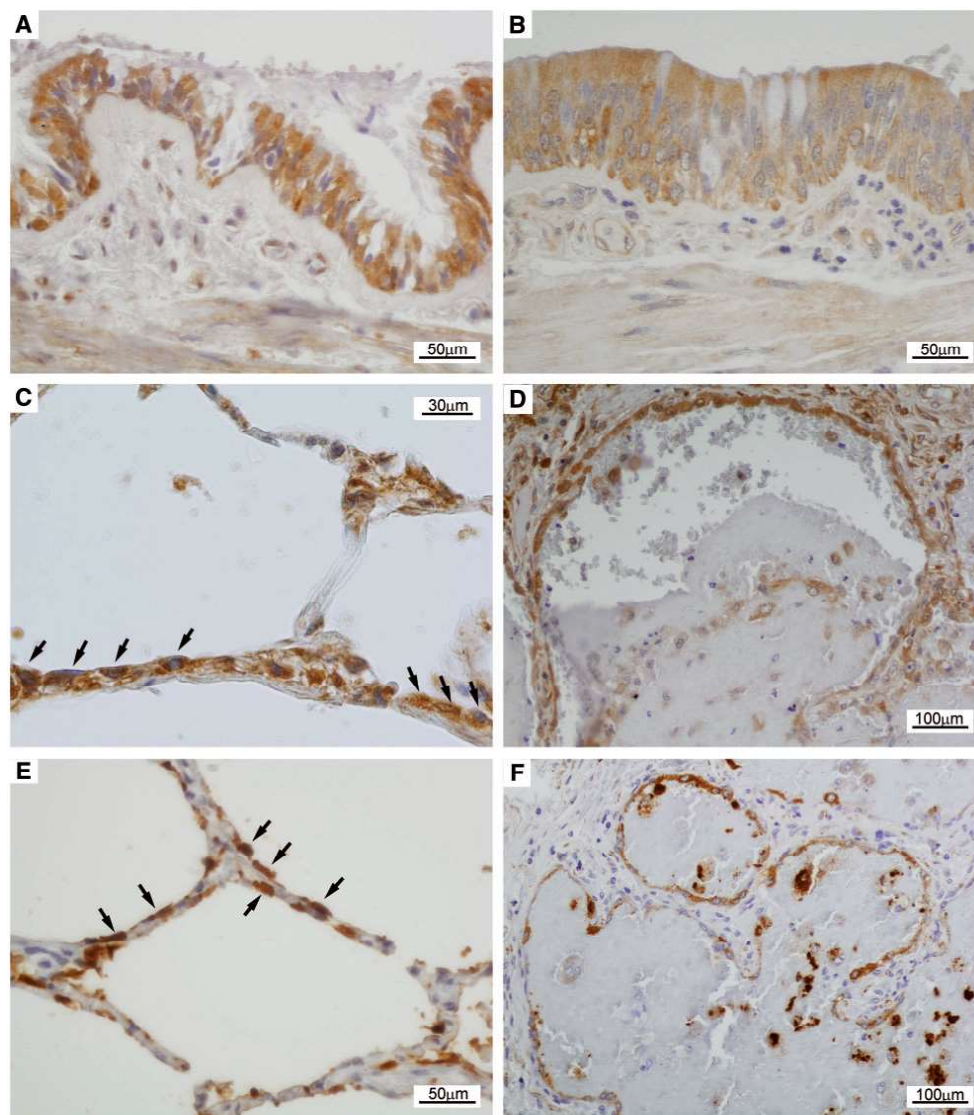
Figure 9. Immunohistochemical detection of NDUFAF6 expression in pulmonary epithelium. (**A** and **B**) NDUFAF6 intracytoplasmic positivity in bronchial respiratory epithelium in a control (A) and affected individual (B) shows reactive epithelial changes and lower NDUFAF6 signal in the affected individual. (**C**) A positive signal for NDUFAF6 is seen in a control in flat alveolar lining cells (marked by arrows) that are positive for cytokeratin 7 (marked by arrows in **E**) and thus considered to be type I pneumonocytes. (**D**) NDUFAF6 positivity is seen in a proband in cuboidal cells lining alveolar spaces that express surfactant protein (**F**) as seen in hyperplastic type II pneumocytes.

Histologic examination of lung samples of family members F1_IV.7, F1_IV.19 and F4_II.2 (Fig. 9) revealed either irregular patchy (F1_IV.19, F4_II.2) or more uniform diffuse (F1_IV.7) interstitial fibrosis. Interstitial inflammatory infiltrate was sparse, consisting of mostly lymphocytes. Acute purulent bronchitis and incipient bronchopneumonia were seen in affected individual F1_IV.7. Intraluminal collection of pigment-laden macrophages was conspicuous in F4_II.2. Hyperplasia of type II pneumonocytes was detected in affected individuals F1_IV.19 and F1_IV.7 using surfactant protein immunohistochemistry (Fig. 9F). Focal calcifications of cartilaginous tissue in bronchial walls were found in F1_IV.19. Secondary pulmonary hypertension changes were most prominent in F1_IV.19. Positive immunohistochemical signal for NDUFAF6 was detected in bronchial and bronchiolar respiratory epithelium, bronchial mucinous glands, alveolar epithelial cells, vascular endothelial cells, smooth muscle cells, fibroblasts and chondrocytes.

In a similar manner to the kidney, immunofluorescence detection and colocalization of NDUFAF6 with Translocase Of Outer Mitochondrial Membrane 20 (TOMM20), (Supplementary Material, Fig. S2), mitochondrial ATP synthase subunit β (ATP5B) and cytoplasmic located heat shock protein 90 (HSP90) (Fig. 10) demonstrated in affected lung the absence of NDUFAF6 staining in mitochondria (Supplementary Material, Figs S2H and L and 10F and I) and reduced colocalization signal of NDUFAF6 and HSP90 in the cytoplasm (Fig. 10O and R).
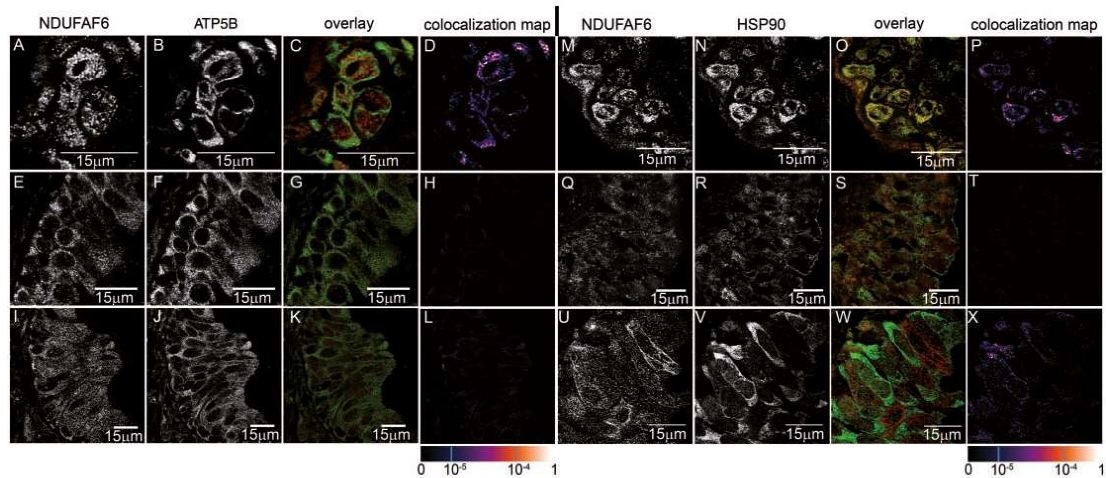
59

Figure 10. Intracellular localization of NDUFAF6 in affected lung. NDUFAF6 is present in control lung (**A** and **M**) in finely granular structures. Co-staining of NDUFAF6 with (**B**) mitochondrial ATP synthase *β* subunit (ATP5B) and (**N**) cytoplasmic heat shock protein 90 (HSP90) demonstrates (**C** and **D**) localization of NDUFAF6 in the mitochondria and (**O** and **P**) in the cytoplasm. In affected lung (**E, I, Q** and **U**), NDUFAF6 is present in finely granular structures with reduced and less distinctive staining signal. Co-staining with ATP5B (**F** and **J**) and HSP90 (**R** and **V**) demonstrates loss of localization of NDUFAF6 in mitochondria (**G, H, K** and **L**) and absent (**S** and **T**) or reduced (**W** and **X**) colocalization signal of NDUFAF6 and HSP90 in the cytoplasm. The degree of NDUFAF6 colocalization with selected markers is demonstrated by the fluorescent signal overlap (Manders) coefficient values that range from 0 to 1. The resulting overlap coefficient values are presented as the pseudo color whose scale is shown in corresponding lookup table.

Affected tissues have defects in mitochondrial respiration and complex I biogenesis

To obtain insight into the molecular and functional consequences of the NDUFAF6 mutation we followed complex I biogenesis, the content of respiratory chain enzymes and oxidative phosphorylation (OXPHOS) activity.

First, we checked the steady state levels of representative subunits for complex I and other OXPHOS components on SDS–PAGE (Fig. 11A). Both in isolated mitochondria from affected lung (F1_IV.19), and whole cells or isolated mitochondria from affected fibroblasts (F2_II.1), we found a profound decrease in the levels of all complex I subunits checked (NDUFA9, NDUFS3 and NDUFB8). Depending on the tissue or particular subunit, the residual content varied between 3% and 63% of control levels when expressed relative to the amount of SDHA. Content of other OXPHOS complexes was either unchanged (complex III, complex V) or displayed slight compensatory increase (complex IV) in fibroblasts. We also performed mass spectrometry label-free quantification of protein content on affected individual versus control fibroblasts (Fig. 11C). Altogether we quantified 3249 proteins, with 512 of them classified as mitochondrial in the Mitocarta 2.0 database (23), obtaining coverage of 44% of the mitoproteome. Similarly to the SDS–PAGE, amounts of 23 out of 24 detected complex I subunits were decreased (17/24 significantly) in fibroblasts from an affected individual (F2_II.1). In contrast, other OXPHOS complexes showed tendency towards increase (not shown).

Next we utilized native electrophoretic techniques (Blue native-BN and Clear native-CN PAGE) to study the native organization of OXPHOS complexes in the inner mitochondrial membrane (Fig. 11B). Using the mild detergent digitonin, we observed most of complex I to be present in several supercomplex forms associated with complex III and complex IV (24). In both the isolated mitochondria from the lung of an affected individual (F1_IV.19), and fibroblasts (whole cells or isolated mitochondria) from another affected individual (F2_II.1), the detected

in-gel activity and amount of complex I were significantly lower than in control samples. For detection of complex I we used an NDUFA9 antibody, as NDUFA9 is one of the subunits that incorporates into the early subassemblies of complex I (25). We did not observe any assembly intermediates of complex I, indicating that subcomplexes with stalled assembly are readily degraded. The absence of complex I in affected individuals also led to a profound increase in the amount of free complex III dimer, especially in fibroblast samples, as it was no longer associated into supercomplexes with complex I. This pattern of an isolated complex I defect and subsequent redistribution of complex III between its supercomplex and free forms is remarkably similar to the pattern observed in the previously described case of an NDUFAF6 mutation presenting as Leigh syndrome (20,26). Thus, while the cytosolic chaperoning function of NDUFAF6 (26) is likely retained in our probands, for proper complex I assembly both cytosolic and mitochondrial NDUFAF6 is required.

The functional impact of complex I deficiency caused by NDUFAF6 mutation was evaluated by high-resolution respirometry (Fig. 11D). Oxygen consumption of digitonin-permeabilized fibroblasts was recorded in the presence of saturating concentrations of substrates feeding electrons to the respiratory chain through complex I (pyruvate + malate + glutamate) and ADP to achieve state 3 respiration. Under these conditions, the affected individual's fibroblasts (F2_II.1) displayed profound respiratory deficiency, with an almost 4-fold decreased respiratory rate compared to control fibroblasts. The defect was partially alleviated by the addition of succinate, which contributes electrons to the respiratory chain through alternative entry at complex II. Nevertheless, the overall state 3 respiratory rate of an affected individual's fibroblasts in the presence of saturating substrate combination was still significantly decreased by 35% compared to controls (Fig. 11D). Expressed in relative terms, the oxidation of complex I-dependent substrates accounted for only 28% of the overall state 3 respiration, whereas in controls complex I substrates respiration contributed 74%. Under FCCP-induced
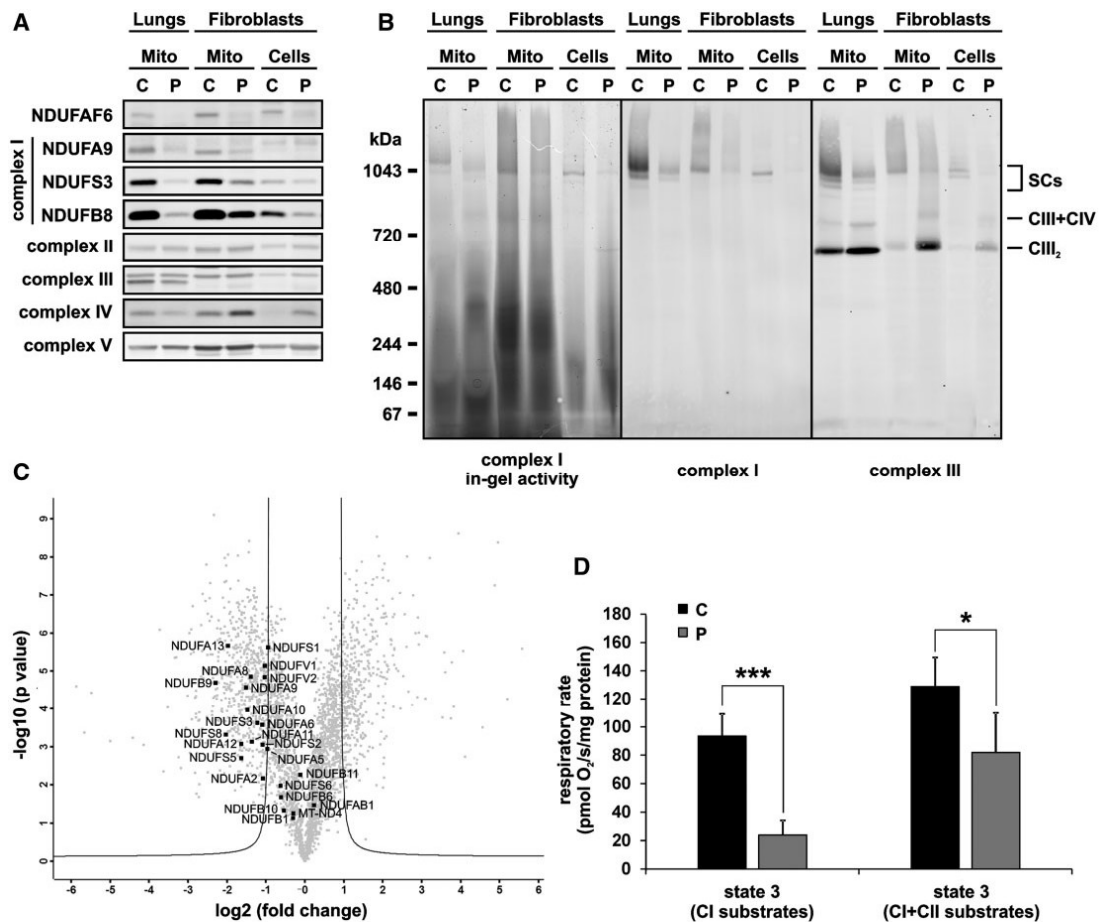
Figure 11. Complex I defect in individuals with the *NDUFAF6* mutation. (**A** and **B**) Isolated mitochondria from the lungs or fibroblasts and the fibroblast whole cell lysate from control (C) and affected proband (P). The lung specimen is from F1_IV.19, and the fibroblast sample from F2_II.1). (A) Samples were separated on SDS–PAGE and incubated with antibodies against NDUFAF6 protein, individual subunits of complex I (NDUFA9, NDUFS3, NDUFB8), complex II subunit SDHA, complex III subunit CORE2, complex IV subunit COX4 and complex V ATP synthase subunit α. (B) Samples were solubilized by digitonin (2 g/g) and analyzed on a 4–13% gradient gel using CNE for complex I in-gel activity and BNE for Western blot. Specific monoclonal antibodies were used for detection of complex I (NDUFA9) and complex III (CORE1). $CIII_2$ is the dimer of complex III; CIII + CIV denotes the supercomplex of complex III and complex IV and SC's denotes various supercomplexes containing complex I, complex III and complex IV. (**C**) Control and proband fibroblasts were analyzed using MS LFQ. Data are expressed as the ratio of affected proband/control sample and visualized using a volcano plot with asymptotes of the hyperbola indicating proteins significantly changed at FDR = 0.01. Proteins on the left (negative) side of the X axis are decreased in the affected proband sample. Complex I associated proteins detected by the MS are highlighted in black. (**D**) Respiratory rates are displayed as mean values of five independent experiments with control (black) and affected individual (gray) fibroblasts. Rates were calculated from measurements in the presence of 10 mM pyruvate + 2 mM malate + 10 mM glutamate + 1 mM ADP (state 3 CI substrates), or the above + 10 mM succinate (state 3 CI + CII substrates); *$P < 0.05$, ***$P < 0.001$.

uncoupled respiration conditions, where the maximum OXPHOS capacity can be determined, the decreased content of complex I also limited the affected individual's fibroblast respiration by 49% compared to controls (not shown).

Altered mitochondrial respiration and complex I biogenesis of fibroblasts from an affected individual were corrected with NDUFAF6 cDNA transfection

To prove the effect of the NDUFAF6 deficiency on mitochondrial respiration and complex I biogenesis we transiently transfected affected fibroblasts with the wild-type mitochondrial NDUFAF6 isoform v_1 cDNA. At the level of protein content (Fig. 12A), we observed an increase in the amount of all examined complex I subunits (NDUFA9, NDUFS3 and NDUFB8). Upon NDUFAF6

transfection, their content in affected fibroblasts increased from ~3–10% to 30–40% of control levels, expressed relative to SDHA. NDUFAF6 transfection did not change the content of representative complex II (SDHA) and complex III (CORE2) subunits. This increase in the steady state content of complex I subunits was also mirrored by an increase in the signal of fully assembled complex I on native electrophoreses (Fig. 12B). NDUFAF6 transfection clearly increased in-gel complex I activity and complex I content, with almost all complex I present in supercomplex forms, as observed also in control cells. While complex III content in the supercomplex area was also significantly higher (Fig. 11B, rightmost panel), there was still a considerable amount of complex III present as free dimer, observed also in affected cells. In agreement with SDS–PAGE, native electrophoresis also showed no changes in complex II content upon transfection, indicating the specificity of NDUFAF6 for complex I assembly.
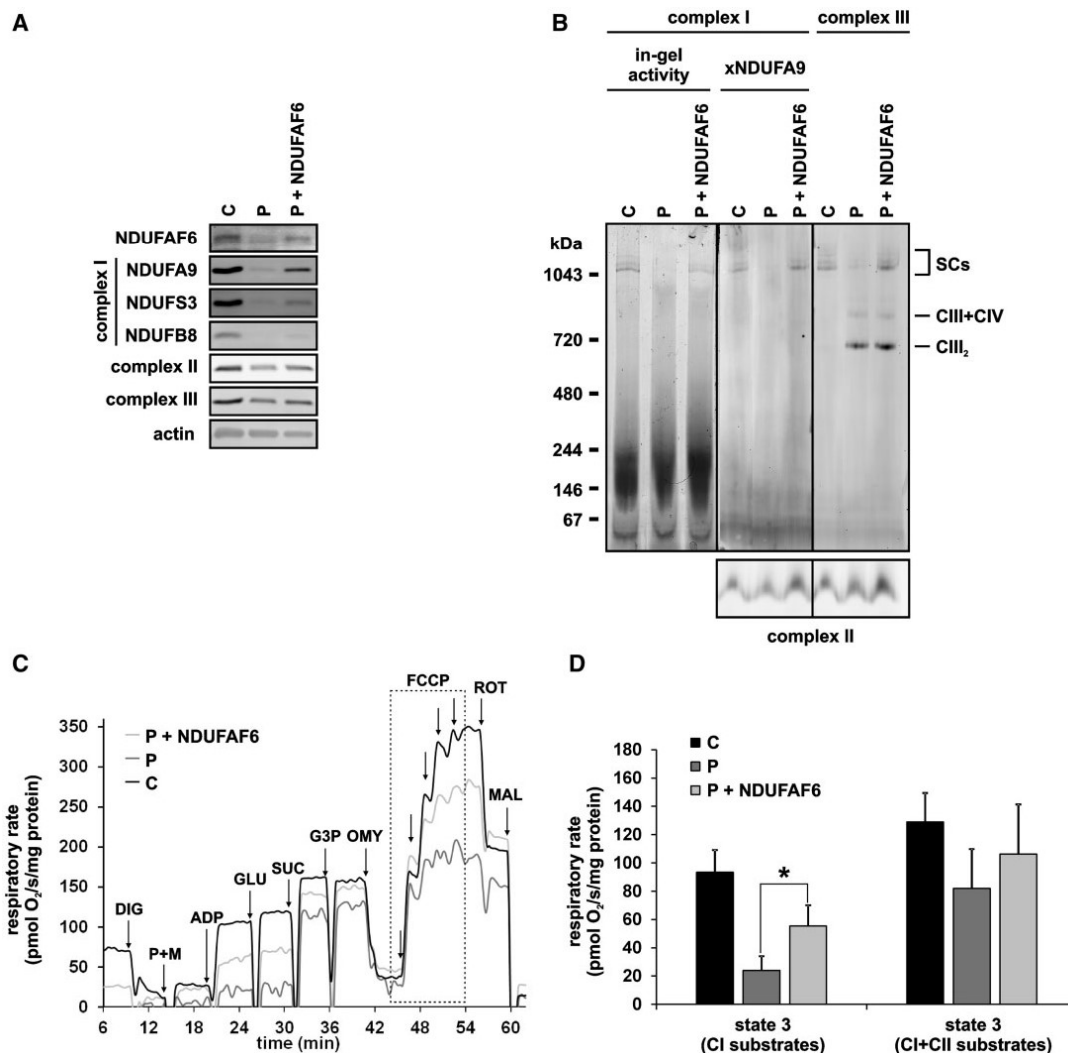
Figure 12. Rescue of the complex I defect by wt *NDUFAF6*. (**A**) SDS–PAGE and Western-blot analysis of the fibroblasts from control (C), affected proband (P) and affected proband transfected with wt *NDUFAF6* (P + NDUFAF6). Antibodies specific to NDUFAF6 protein, complex I subunits (NDUFA9, NDUFS3, NDUFB8), complex II subunit SDHA, complex III subunit CORE2 and actin were used. (**B**) Fibroblasts from control (C), affected proband (P) and affected proband transfected with wt *NDUFAF6* (P + NDUFAF6) were solubilized by digitonin (2 g/g) and analyzed on 4–13% gradient gel using CNE for complex I in-gel activity and BNE for Western blot. Specific monoclonal antibodies were used for detection of complex I (NDUFA9), complex II (SDHA) and complex III (CORE1) native forms. CIII$_2$ denotes the dimer of complex III; CIII + CIV denotes the supercomplex of complex III and complex IV and SC's denotes various supercomplexes containing complex I, complex III and complex IV. (**C**) Oxygen consumption traces of representative complementation experiment with control (black), proband (dark gray) and NDUFAF6-transfected affected proband's fibroblasts (light gray). Rates are normalized to protein content. Additions of 0.05 g/g protein of digitonin (DIG), 10 mM pyruvate + 2 mM malate (P + M), 1 mM ADP (ADP), 10 mM glutamate (GLU), 10 mM succinate (SUC), 10 mM glycerol 3-phosphate (G3P), 500 nM oligomycin (OMY), FCCP (0–300 nM titration), 500 nM rotenone (ROT) and 10 mM malonate (MAL) are indicated by arrows. (**D**) Respiratory rates are displayed as mean values of five independent experiments with control (black) and affected proband's (dark gray) fibroblasts, or two independent experiments with NDUFAF6-transfected fibroblasts from affected individual (light gray). Rates were calculated from measurements in the presence of 10 mM pyruvate + 2 mM malate + 10 mM glutamate + 1 mM ADP (state 3 CI substrates), or the above + 10 mM succinate (state 3 CI + CII substrates); *P < 0.05.

This partial restoration of complex I content after transfection of affected fibroblasts with wtNDUFAF6 was sufficient to functionally correct the complex I defect at the level of respiration with complex I-dependent substrates. As shown by the representative oxygen consumption traces (Fig. 12C), the NDUFAF6-transfected fibroblasts displayed an intermediary phenotype between controls and non-transfected affected cells. Specifically, the NDUFAF6 transfection caused a significant, 2.3-fold increase in state 3 respiration with complex I substrates (Fig. 12D). While we did not observe full correction of the defect, restoration of complex I dependent respiration was in good agreement with the observed increase in complex I content and both mirrored the average transfection efficiency (~40%) of the electroporation system.

Discussion

In this investigation we identified an intronic mutation in *NDUFAF6* as a cause of RFS, chronic kidney failure and progressive pulmonary fibrosis in several families and unrelated

individuals of the Acadian population of eastern Canada. The mutation fully segregates with the phenotype in the expected autosomal recessive mode of inheritance. It is ultra-rare, being present only once in >13 200 genome sequences reported in publicly available databases.

As part of this investigation, we identified several novel mRNA isoforms of *NDUFAF6*, and we showed that the mutation alters their splicing. From the experiments we performed, we were able to predict and prove that the mutation affects the synthesis and intracellular localization of NDUFAF6 isoforms. This is best demonstrated with the mitochondrial isoform V_1, which was not found in affected tissues based on the results of RT-PCR, cDNA sequencing, Western-blot analyses and immuno-histochemical and immunofluorescence studies. These experiments also indicate that the cytoplasmic function of NDUFAF6 (26) may be partially preserved due to the synthesis of truncated NDUFAF6 isoforms that localize in the cytoplasm.

A homozygous mutation in *NDUFAF6*, c.296A > G, that is predicted to result in Gln99Arg substitution in NDUFAF6 was previously identified in two siblings who suffered from persistent lactic acidosis, Leigh syndrome, isolated generalized complex I deficiency and death before age 3 years (13). This phenotype resulted from altered splicing and instability of the v_1 isoform through a mechanism of nonsense mediated decay, whereas the stability and amounts of the v_3 isoform encoding truncated mitochondrial isoform V_3 was unaffected (20). In this case, the expected NDUFAF6 deficiency led to reduced levels of the mature complex I in affected fibroblasts, due to loss of the mitochondrial encoded subunit ND1 and disruption of the initial stages of complex I biogenesis. Effects of the mutation on production of the cytoplasmic isoform V_2 were not studied (20).

We made similar observations in affected fibroblasts and lung from individuals with AVFS. We found a profound decrease in the levels of all complex I subunits that was associated with reduced activity and amount of the mature complex I and an altered pattern of redistribution of complex III between its super-complex and free forms. This was accompanied by profound respiratory deficiency shown by high-resolution respirometry. All these specific abnormalities were restored when affected fibroblasts were transiently transfected with the cDNA encoding wild-type NDUFAF6 isoform V_1.

We believe that these genetic, molecular biologic, immuno-histochemical and biochemical findings firmly established that AVFS is caused by homozygosity for the specific mutation that is composed of the private non-coding mutation c.298-768 T > C (rs575462405) which is in linkage with the population frequent splicing variant c.298-731 A > G (rs74395342). This particular haplotype affects the splicing, synthesis and intracellular distribution of NDUFAF6 isoforms and leads to isolated complex I deficiency.

Fanconi syndrome results from a generalized disturbance in cellular metabolism that affects the primary function of the proximal tubular cell: bulk translocation of electrolytes, organic compounds and macromolecules from the tubular space. As this transport requires a high amount of energy, it is unsurprising that both primary and secondary mitochondrial defects have been identified as causes of the Fanconi syndrome (1,6–9,21,27,28).

Why is it that one mutation (c.296A > G) leads to Leigh syndrome and early death, whereas another mutation (c.298-768 T > C)—or more specifically the haplotype formed by combination of c.298-768 T > C and c.298-731 A > G—leads to specific tubular dysfunction and later in life to chronic kidney failure and pulmonary fibrosis with no other clinical manifestations

characteristic of respiratory chain defects such lactic acidosis, cardiomyopathy, myopathy and neurodegeneration?

The explanation might be that in the case of Leigh syndrome the mutation lead to complete loss of both mitochondrial (20) and cytoplasmic NDUFAF6 isoforms while in the case of AVFS some of the identified mutated mRNA (cDNA) isoforms may produce truncated cytoplasmic proteins that can sustain NDUFAF6 cytoplasmic function, as suggested by RT-PCR, *in vitro* translation, Western blot and immunofluorescence colocalization studies. This would be very similar to investigations with *Drosophila melanogaster* where the complete loss of *Sicily*, a homologue of the human *NDUFAF6*, lead to progressive neurodegeneration and structural mitochondrial abnormalities that are compatible with other forms of severe complex I deficiencies (26). In that study it was shown that the cytoplasmic form of *Sicily* interacts with Hsp90 and prevents degradation of cytosolic complex I subunits. Interestingly, and very similar to AVFS, the neurodegenerative phenotype of the *Sicily* mutants was almost completely rescued by the cytoplasmic form of the *Sicily* itself, with the exception of the mitochondrial structural abnormalities.

In a similar manner, in AVFS the cytoplasmic NDUFAF6 isoforms may interact with HSP90 (as demonstrated by immuno-fluorescence studies) and sustain other functions, thereby preventing development of the myopathic and/or neurodegenerative phenotype. On the other hand, the loss of the mitochondrial NDUFAF6 isoforms may lead to partial complex I deficiency and structural mitochondrial defects that may specifically affect systems and tissues with high energy requirements for endocytosis/membrane transport processes, and over time lead to chronic changes that would manifest only in the cell types that have endogenously lower expression of NDUFAF6 and/or that are increasingly sensitive to excessive production of reactive oxygen species (ROS) (e.g. tubular epithelial cells and type I pneumocytes). This is consistent with histopathologic and ultrastructural evaluation of the kidney from an affected individual, which revealed proximal tubulopathy of mitochondrial origin and slowly progressive chronic tubulointerstitial changes. Investigations of affected lung tissue demonstrated distinctive expression of NDUFAF6 in pulmonary epithelial cells that are targeted in idiopathic pulmonary fibrosis. Mitochondrial dysfunction in these cells (29,30) may disturb the integrity of the alveolar epithelium and provoke hyperplasia of type II pneumocytes and progressive interstitial fibroplasia that are established pathogenetic mechanisms in interstitial pulmonary fibrosis.

In conclusion, we describe a genetically distinct form of Fanconi syndrome. This information may be used in the diagnosis and prevention of this disease in individuals and families of Acadian descent and broadens the spectrum of the clinical presentation of mitochondrial diseases, respiratory chain defects and defects of complex I specifically.

Materials and Methods
Study subjects and clinical examination

An individual affected with proximal renal tubular acidosis (RTA) contacted one of the investigators (AJB) to help identify the genetic cause of this disorder. Further affected individuals were referred by the index case or local nephrologists. After obtaining informed consent, medical records, a blood sample for genetic analysis and other clinical samples were obtained. This investigation was approved by the Wake Forest University

Příloha 1a

School of Medicine, the First Faculty of Medicine of the Charles University, Prague, the Czech Republic and the Moncton Regional Hospital, Moncton, New Brunswick.

Whole exome sequencing

Genomic DNA of all available individuals was extracted from whole blood samples in a standard manner. Whole exome sequencing (WES) was performed using the SOLiD™ 4 (ThermoFisher Scientific, Waltham, MA) and HiSeq 1500 systems (Illumina, San Diego, CA).

SOLiD 4 sequencing

For DNA enrichment, bar-coded DNA libraries and NimbleGen SeqCap EZ Exome v2 (Roche, Madison, WI) were used according to the manufacturer's protocol. DNA sequencing was performed on the captured barcoded DNA library of three affected individuals using the SOLiD™ 4 System at the Institute for Inherited Metabolic Disorders (Prague, Czech Republic) as previously described (31,32). Reads were aligned in color space to the reference genome (hg19) using NovoalignCS version 1.08 (Novocraft, Malaysia) with default parameters. Sequence variants in analyzed samples were identified using the SAMtools package (version 0.1.19) (33). The high confidence variants list was annotated using the ANNOVAR Annotation tool (34) (hg19). Only the sequence variants present in all three affected individuals and having a frequency <0.05 in the dbSNP, 1000 Genomes, Exome Variant Server (http://evs.gs.washington.edu/EVS/) and our internal exome database were prioritized for further analysis. Identified genetic variants were filtered according to the expected autosomal recessive model of the disease and evaluated according to the biological relevance of corresponding genes. Candidate variants were visualized in Integrative Genomics Viewer (IGV)—version 2.3.32 (35).

Illumina sequencing

For DNA enrichment, barcoded DNA libraries and NimbleGen SeqCap EZ Exome v3 (Roche, Madison, WI) were used according to the manufacturer's protocol. DNA sequencing was performed on the captured barcoded DNA library using the Illumina Hiseq 1500 system at the Genomic facility in Motol University Hospital in Prague. The resulting FASTQ files were aligned to the Human Genome Reference (hg19) using Novoalign (3.02.10). Following genome alignment, conversion of SAM format to BAM and duplicate removal were performed using Picard Tools (1.129). The Genome Analysis Toolkit, GATK (3.3) (36) was used for local realignment around indels, base recalibration and variant recalibration and genotyping. Variant annotation were performed with SnpEff (37) and GEMINI (38). Variants with minor allelic frequencies (MAFs) in ESP6500, ExAC and 1000 Genomes databases <0.05 were further evaluated as described above.

CNV prediction

CNV were identified from exome read counts using CoNIFER (0.2.2) (39).

Homozygosity mapping

Runs of homozygosity (ROHs) were identified from genotyping data using the GEMINI framework and the ROH tool (38). Allele frequency was calculated and visualized using TTR R-package

by smooth moving average (SMA) algorithm, where the moving average was set to 8000 in genome dataset.

Whole genome sequencing (WGS)

DNA libraries were prepared using the TruSeq Nano DNA Library Prep kit (Illumina) and sequenced on the Illumina HiSeq X Ten System (Macrogen, Rockvill, MD). Alignment, variant calling, annotation and copy number analysis were done as described (40).

Genotyping

All genetic variants of interest were genotyped by direct Sanger sequencing using the version 3.1 Dye Terminator cycle sequencing kit (ThermoFisher Scientific) with electrophoresis on an ABI 3500XL Avant Genetic Analyzer (ThermoFisher Scientific). Data were analyzed using Sequencing Analysis software (ThermoFisher Scientific).

In silico splice site prediction

For prediction of eventual splicing effects of the identified noncoding variants we used Alamut Mutation Interpretation Software (Interactive Biosoftware, Rouen, France).

Cell culture

Skin fibroblasts were maintained in Dulbecco's modified eagle medium (DMEM), (ThermoFisher Scientific), supplemented with 10% fetal bovine serum (FBS), (ThermoFischer Scientific) and penicillin/streptomycin (Sigma–Aldrich, Prague, Czech Republic).

RNA analysis and cDNA sequencing

Total RNA was isolated from fibroblast cell line pellets or snap-frozen lung specimens using TRIzol solution (ThermoFisher Scientific). RNA concentrations were determined spectrophotometrically at A260 nm by NanoDrop (NanoDrop Technologies, Wilmington, DE), and RNA quality was verified using an Agilent 2100 bioanalyser—RNA Lab-On-a-Chip (Agilent Technologies, Santa Clara, CA). Aliquots of isolated RNA were stored at −80 °C until analysis. The first-strand cDNA synthesis was carried out using an oligo-dT primer and either SuperScript® III Reverse Transcriptase or ThermoScript Reverse Transcriptase (ThermoFisher Scientific) or ProtoScript II First Strand cDNA Synthesis Kit (NEB, Ipswich, MA). *NDUFAF6* cDNA were PCR-amplified from the synthesized first-strand cDNA using oligonucleotide primers (Generi Biotech, Hradec Králové, Czech Republic) designed to span and amplify *NDUFAF6* isoforms *v_1* and *v_3* in parallel and isoform *v_2* separately. The resultant PCR products were analyzed using agarose gel electrophoresis. Individual DNA fragments were extracted from gel slices using PureLink Quick Gel Extraction Kit (ThermoFisher Scientific) and sequenced using the version 3.1 Dye Terminator cycle sequencing kit (ThermoFisher Scientific) with electrophoresis on an ABI 3500XL Avant Genetic Analyzer (ThermoFisher Scientific). Obtained RT-PCR products were also sequenced in parallel using the Illumina HiSeq 1500 system as described for WES and WGS above. The resulting FASTQ files were aligned to the Human Genome Reference (hg19) using TopHat 2.0.12 (41) integrated in the RAP: RNA-Seq Analysis Pipeline (42).

In vitro translation assay

Wild-type NDUFAF6 isoforms *v*_1 and *v*_2 cDNA were synthesized by GenScript (Piscataway, NJ). Protein precursors were synthesized in the presence of ^{35}S-methionine using TNT T7 Quick Coupled Transcription/Translation System (Promega, Madison, WI) with plasmids as a DNA template, according to manufacturer recommendation. Translation products were centrifuged at 13 000*g* for 2 min and supernatant was mixed with SDS sample lysis buffer. Samples were analyzed by SDS–PAGE and radioactivity was detected using Pharos system (Bio-Rad Laboratories; Hercules, CA).

Transient transfection and Western-blot analysis of NDUFAF6

Wild-type NDUFAF6 isoform *v*_1 cDNA was synthesized by GenScript (Piscataway, NJ). HeLa and HEK 293 cells were maintained in DMEM High Glucose medium supplemented with 10% (vol/vol) fetal calf serum (PAA), 100 U/ml penicillin G (Sigma–Aldrich) and 100 μg/ml streptomycin sulfate (PAA Laboratories GmbH, Pashing, Austria). Transfections were carried out using Lipofectamine 3000™ (ThermoFischer Scientific) with either 1.5 or 4 μg DNA for 1.5×10^5 or 8×10^5 cells, respectively.

Cells were harvested either 24 h (for HeLa and HEK 293 cells) or 5 days (for fibroblasts) post-transfection, and mitochondrial and cytoplasmic fraction were prepared using Mitochondria/Cytosol Fractionation Kit (BioVision, Inc., San Francisco, CA).

Control human tissue lysates from muscle (Muscle NB820-59253), liver (Liver NB820-59232) and kidney (Kidney NB820-59231) were purchased from Novus Biologicals (Littleton, CO). Lysates from heart and lung were prepared from frozen autopsy tissues. Briefly, frozen tissue was cut out and homogenized in a Teflon/glass homogenizer in RIPA Buffer (150 mM NaCl, 1% Nonidet NP–40, 1% sodium deoxycholate, 0.1% SDS, 50 mM Tris–HCl, pH 8.0; 10% homogenate), incubated for 30 min at 37 °C and centrifuged for 5 min at 18 000*g* to remove non-lysed proteins.

Denatured protein samples were separated on 13% SDS–PAGE and blotted onto a PVDF membrane. NDUFAF6 was visualized by incubation with rabbit polyclonal antibodies supposedly capable of detecting NDUFAF6 isoforms V_1 and V_2—ab150975 and ab151096 (Abcam, Cambridge) or sc-87001 (Santa Cruz Biotechnology, Heidelberg, Germany), followed by incubation with anti-rabbit IgG-peroxidase antibody—A8924 (Sigma_Aldrich), and detection by SuperSignal West Pico Maximum Sensitivity Substrate (ThermoFisher Scientific). Succinate dehydrogenase complex, subunit A (SDHA) was visualized using mouse monoclonal antibody ab14715 (Abcam). Actin was visualized using mouse monoclonal anti-Actin (Ab-1) antibody CP01-1EA (Calbiochem, CA).

Immunohistochemistry and immunofluorescence analysis

Formaldehyde fixed kidney and lung samples were analyzed. Immunodetection of NDUFAF6 on paraffin sections was performed using the rabbit polyclonal anti-NDUFAF6 antibody sc-87001 (Santa Cruz Biotechnology) diluted 1:200 in 5% BSA, in PBS. Detection of bound primary antibody was achieved using the Dako EnVision+™ Peroxidase Rabbit Kit (Dako, Glostrup, Denmark) with 3,3'-diaminobenzidine as substrate. The specificity of the antigen detection was always ascertained by omission of the primary antibody binding step.

For intracellular localization in kidney and lung, NDUFAF6 was detected with rabbit polyclonal anti-NDUFAF6 antibody diluted 1:300 in 5% BSA, in PBS. Mitochondrial ATP synthase subunit β (ATP5B) and cytoplasmic located heat shock protein 90 (HSP90) were detected with mouse monoclonal anti-ATP5B antibody (ab14730, Abcam) and anti-Hsp90 antibody (ab 79848, Abcam), respectively, both diluted 1:100 in 5% BSA, in PBS. For fluorescence detection, corresponding species specific secondary antibodies Alexa Fluor® 488 and Alexa Fluor® 555 (ThermoFisher Scientific) were used. Slides were mounted in the fluorescence mounting medium ProLong Gold Antifade Mountant with DAPI (ThermoFisher Scientific) and analyzed by confocal microscopy.

Confocal microscopy, image acquisition and analysis

XYZ images were sampled according to Nyquist criterion using a Leica SP8X laser scanning confocal microscope, HC PL Apo objective (63×, N.A.1.40), 405 nm diode/50 mW DMOD Flexible, and 488 and 555 laser lines in 470–670 nm 80 MHz pulse continuum WLL2 (Leica, Wetzlar, Germany). Images were restored using a classic maximum likelihood restoration algorithm in the Huygens Professional Software (SVI, Hilversum, Netherlands). The colocalization maps, employing single pixel overlap coefficient values ranging from 0 to 1, were created in the Huygens Professional Software. The resulting overlap coefficient values are presented as the pseudo color whose scale is shown in the corresponding lookup tables (LUT).

Electron microscopy

Kidney biopsies were fixed with 3% glutaraldehyde in 0.1 M phosphate buffer, post-fixed with 1% OsO$_4$, dehydrated and embedded into Durcupan-Epon mixture. Ultrathin sections were double contrasted with uranyl acetate and lead nitrate and then analyzed using a transmission electron microscope (JEOL 1200 EX).

Isolation of mitochondria

For the analysis of complex I assembly, mitochondria from fibroblast cells were isolated at 4 °C by a hypo-osmotic shock method (43). The freshly harvested cells were disrupted in 10 mM Tris–HCl, pH 7.4, homogenized in a Teflon/glass homogenizer (10% homogenate, w/v) and then sucrose was added to a final concentration of 0.25 M. Mitochondria were sedimented from the 600-g post-nuclear supernatant by 10-min centrifugation at 10 000*g*, washed and resuspended in 0.25 M sucrose, 2 mM EGTA, 40 mM KCl, 20 mM Tris, pH 7.4.

Electrophoresis, Western-blot analysis, in-gel complex I activity

SDS–PAGE was performed on 10% (w/v) polyacrylamide slab minigels (MiniProtean System, Bio-Rad Laboratories) at room temperature. Samples of whole cells or isolated mitochondria were heated for 5 min at 95 °C in a sample lysis buffer [2% (v/v) 2-mercaptoethanol, 4% (w/v) SDS, 50 mM Tris (pH 7.0), 10% (v/v) glycerol]. Separation of native OXPHOS complexes by blue-native (BNE) or clear-native electrophoresis (CNE system) (44) was performed on polyacrylamide gradient (4–13%) minigels at 7 °C. Mitochondrial proteins were solubilized with digitonin at 2 g/g (detergent/protein ratio) for 15 min on ice. The samples were

centrifuged for 20 min at 4 °C and 30 000*g*, and Coomassie Brilliant Blue G dye (Serva Blue G-250, 0.125 g/g detergent) and 5% glycerol were added to the supernatants before electrophoresis. Gels were blotted onto a PVDF membrane (Millipore) and the membrane was blocked in 5% defatted milk in TBS (150 mM NaCl, 10 mM Tris, pH 7.5). The membranes were washed twice in TBST (TBS with 0.1% (v/v) Tween-20) and incubated overnight with the following primary antibodies diluted in TBST: rabbit polyclonal antibody to NDUFAF6 (Abcam ab151096, 1:500), mouse monoclonal antibodies to actin (IgM, Calbiochem CP01-1EA, 1:6000), NDUFA9 (Abcam ab14713, 1:1000), NDUFS3 (Abcam ab14711, 1:1000), NDUFB8 (Abcam ab110242, 1:1000), SDHA (Abcam 1:10 000, ab14715), CORE1 (Abcam ab110252, 1:1000), CORE2 (Abcam ab14745, 1:1000) and a cocktail of monoclonal antibodies to OXPHOS subunits (Abcam ab110412, NDUFA9, SDHA, CORE2, COX4, F_1-α). For a quantitative detection, the infra-red fluorescent secondary antibodies diluted in TBST were used (Alexa Fluor 680 A10038 or A10043, 1:3000, Life Technologies; IRDye 800CW 926-32212 or 926-32213, 1:15 000, Li-Cor Biosciences). The fluorescence was detected using ODYSSEY infra-red imaging system (Li-Cor Biosciences) and the signal was quantified using Aida 3.21 Image Analyzer software. Complex I activity was detected on native gels immediately after electrophoresis according to (44). Briefly, gels were incubated in complex I activity assay buffer (2.5 mg/ml nitrotetrazolium blue, 0.1 mg/ml NADH, 5 mM Tris–HCl, pH 7.4) from 1 h to overnight. The gels were transferred to 5 mM Tris–HCl pH 7.4 and scanned.

LFQ protein mass spectrometry analysis

Cell pellets (affected individual versus control NHDFC fibroblasts) corresponding to 100 μg of protein were solubilized using sodium deoxycholate (1% (w/v) final conc.), reduced with TCEP [tris(2-carboxyethyl)phosphine], alkylated with MMTS (S-methyl methanethiosulfonate), digested sequentially with Lys-C and trypsin and extracted with ethylacetate saturated with water as described (45). Samples were desalted on Empore C18 columns, dried in Speedvac and dissolved in 0.1% TFA + 2% acetonitrile. About 1 μg of peptide digests were separated on 50 cm C18 column using 2.5 h elution gradient and analyzed in a DDA mode on a Orbitrap Fusion Tribrid (Thermo Scientific) mass spectrometer. Resulting raw files were processed in MaxQuant (v. 1.5.3.28) (46) with label-free quantification (LFQ) algorithm MaxLFQ (47). Downstream analysis and visualization was performed in Perseus (v. 1.5.3.1).

Complementation of fibroblasts with wt cDNA

Affected or control fibroblasts were transfected either with vector containing either the wtNDUFAF6 isoform *v*_1 cDNA (in the same manner as used for HeLa and HEK293 cells) or the green fluorescent protein (GFP) (used as a control) using Nucleofector device and NHDF nucleofection kit (VPD-1001, Lonza, Switzerland). For each transfection 3×10^6 cells and 2 μg of DNA was used. Cells were analyzed 5-day post-transfection.

Mitochondrial respiration measurement

Respiration of fibroblasts was measured at 30 °C using Oxygraph-2k (Oroboros, Austria), essentially as described (48). Briefly, freshly harvested cells were suspended in KCl medium (80 mM KCl, 10 mM Tris–Cl, 3 mM MgCl$_2$, 1 mM EDTA, 5 mM potassium phosphate, pH 7.4) and permeabilized with digitonin

(0.05 g/g of protein). Substrates and inhibitors were used at the following concentrations: 10 mM pyruvate, 2 mM malate, 1 mM ADP, 10 mM glutamate, 10 mM succinate, 10 mM glycerol 3-phosphate, 500 nM oligomycin, 100–200 nM FCCP, 1 μM rotenone, 10 mM malonate, 1 μM antimycin A, 2 mM ascorbate, 1 mM TMPD, 0.5 mM KCN. Oxygen consumption was expressed in pmol oxygen/s/mg protein.

Supplementary Material

Supplementary Material is available at *HMG* online.

References

1. Klootwijk, E.D., Reichold, M., Unwin, R.J., Kleta, R., Warth, R. and Bockenhauer, D. (2014) Renal Fanconi syndrome: taking a proximal look at the nephron. *Nephrol. Dial. Transplant.*, **30**, 1456–1460.
2. Bokenkamp, A. and Ludwig, M. (2011) Disorders of the renal proximal tubule. *Nephron Physiol.*, **118**, p1–p6.
3. Kitterer, D., Schwab, M., Alscher, M.D., Braun, N. and Latus, J. (2015) Drug-induced acid-base disorders. *Pediatr. Nephrol.*, **30**, 1407–1423.
4. Hall, A.M., Bass, P. and Unwin, R.J. (2014) Drug-induced renal Fanconi syndrome. *QJM*, **107**, 261–269.
5. Solano, A., Lew, S.Q. and Ing, T.S. (2014) Dent-Wrong disease and other rare causes of the Fanconi syndrome. *Clin. Kidney J.*, **7**, 344–347.
6. Jackson, C.B., Bauer, M.F., Schaller, A., Kotzaeridou, U., Ferrarini, A., Hahn, D., Chehade, H., Barbey, F., Tran, C., Gallati, S., *et al.* (2016) A novel mutation in BCS1L associated with deafness, tubulopathy, growth retardation and microcephaly. *Eur. J. Pediatr.*, **175**, 517–525.
7. Sasarman, F., Thiffault, I., Weraarpachai, W., Salomon, S., Maftei, C., Gauthier, J., Ellazam, B., Webb, N., Antonicka, H., Janer, A., *et al.* (2015) The 3′ addition of CCA to mitochondrial tRNASer(AGY) is specifically impaired in patients with mutations in the tRNA nucleotidyl transferase TRNT1. *Hum. Mol. Genet.*, **24**, 2841–2847.
8. Klootwijk, E.D., Reichold, M., Helip-Wooley, A., Tolaymat, A., Broeker, C., Robinette, S.L., Reinders, J., Peindl, D., Renner, K., Eberhart, K., *et al.* (2014) Mistargeting of peroxisomal

EHHADH and inherited renal Fanconi's syndrome. *N. Engl. J. Med.*, **370**, 129–138.

9. Bowden, S.A., Patel, H.P., Beebe, A. and McBride, K.L. (2013) Successful medical therapy for hypophosphatemic rickets due to mitochondrial complex I deficiency induced de Toni-Debre-Fanconi syndrome. *Case Rep. Pediatr.*, **2013**, 354314.

10. Debray, F.G., Merouani, A., Lambert, M., Brochu, P., Bernard, C., Robinson, B.H. and Mitchell, G.A. (2008) Acute tubular dysfunction with Fanconi syndrome: a new manifestation of mitochondrial cytopathies. *Am. J. Kidney Dis.*, **51**, 691–696.

11. Wornell, P., Crocker, J., Wade, A., Dixon, J. and Acott, P. (2007) An Acadian variant of Fanconi syndrome. *Pediatr. Nephrol.*, **22**, 1711–1715.

12. Crocker, J.F.S., McDonald, A.T.J., Wade, A.W. and Acott, P. (1997) The Acadian variant of Fanconi's syndrome 1643. *Pediatr. Res.*, **41**, 276–276.

13. Pagliarini, D.J., Calvo, S.E., Chang, B., Sheth, S.A., Vafai, S.B., Ong, S.E., Walford, G.A., Sugiana, C., Boneh, A., Chen, W.K., *et al.* (2008) A mitochondrial protein compendium elucidates complex I disease biology. *Cell*, **134**, 112–123.

14. Levey, A.S. and Coresh J. (2006) Using standardized serum creatinine values in the modification of diet in renal disease study equation for estimating glomerular filtration rate. *Ann. Int. Med.*, **145**, 247–254.

15. Cooper, G.M., Stone, E.A., Asimenos, G., Green, E.D., Batzoglou, S. and Sidow, A. (2005) Distribution and intensity of constraint in mammalian genomic sequence. *Genome Res.*, **15**, 901–913.

16. Davydov, E.V., Goode, D.L., Sirota, M., Cooper, G.M., Sidow, A. and Batzoglou, S. (2010) Identifying a high fraction of the human genome to be under selective constraint using GERP++. *PLoS Comput. Biol.*, **6**, e1001025.

17. Kircher, M., Witten, D.M., Jain, P., O'Roak, B.J., Cooper, G.M. and Shendure, J. (2014) A general framework for estimating the relative pathogenicity of human genetic variants. *Nat. Genet.*, **46**, 310–315.

18. Glusman, G., Caballero, J., Mauldin, D.E., Hood, L. and Roach, J.C. (2011) Kaviar: an accessible system for testing SNV novelty. *Bioinformatics*, **27**, 3216–3217.

19. Zurita Rendon, O. and Shoubridge, E.A. (2012) Early complex I assembly defects result in rapid turnover of the ND1 subunit. *Hum. Mol. Genet.*, **21**, 3815–3824.

20. McKenzie, M., Tucker, E.J., Compton, A.G., Lazarou, M., George, C., Thorburn, D.R. and Ryan, M.T. (2011) Mutations in the gene encoding C8orf38 block complex I assembly by inhibiting production of the mitochondria-encoded subunit ND1. *J. Mol. Biol.*, **414**, 413–426.

21. Rotig, A. (2003) Renal disease and mitochondrial genetics. *J. Nephrol.*, **16**, 286–292.

22. (2015) Human genomics. The Genotype-Tissue Expression (GTEx) pilot analysis: multitissue gene regulation in humans. *Science*, **348**, 648–660.

23. Calvo, S.E., Clauser, K.R. and Mootha, V.K. (2016) MitoCarta2.0: an updated inventory of mammalian mitochondrial proteins. *Nucleic Acids Res.*, **44**, D1251–D1257.

24. Acin-Perez, R., Fernandez-Silva, P., Peleato, M.L., Perez-Martos, A. and Enriquez, J.A. (2008) Respiratory active mitochondrial supercomplexes. *Mol. Cell*, **32**, 529–539.

25. Mimaki, M., Wang, X., McKenzie, M., Thorburn, D.R. and Ryan, M.T. (2012) Understanding mitochondrial complex I assembly in health and disease. *Biochim. Biophys. Acta*, **1817**, 851–862.

26. Zhang, K., Li, Z., Jaiswal, M., Bayat, V., Xiong, B., Sandoval, H., Charng, W.L., David, G., Haueter, C., Yamamoto, S., *et al.* (2013) The C8ORF38 homologue Sicily is a cytosolic chaperone for a mitochondrial complex I subunit. *J. Cell Biol.*, **200**, 807–820.

27. Odievre, M.H., Lombes, A., Dessemme, P., Santer, R., Brivet, M., Chevallier, B., Lagardere, B. and Odievre, M. (2002) A secondary respiratory chain defect in a patient with Fanconi-Bickel syndrome. *J. Inherit. Metab. Dis.*, **25**, 379–384.

28. Morris, A.A., Taylor, R.W., Birch-Machin, M.A., Jackson, M.J., Coulthard, M.G., Bindoff, L.A., Welch, R.J., Howell, N. and Turnbull, D.M. (1995) Neonatal Fanconi syndrome due to deficiency of complex III of the respiratory chain. *Pediatr. Nephrol.*, **9**, 407–411.

29. Kim, S.J., Cheresh, P., Jablonski, R.P., Williams, D.B. and Kamp, D.W. (2015) The role of mitochondrial DNA in mediating alveolar epithelial cell apoptosis and pulmonary fibrosis. *Int. J. Mol. Sci.*, **16**, 21486–21519.

30. Patel, A.S., Song, J.W., Chu, S.G., Mizumura, K., Osorio, J.C., Shi, Y., El-Chemaly, S., Lee, C.G., Rosas, I.O., Elias, J.A., *et al.* (2015) Epithelial cell mitochondrial dysfunction and PINK1 are induced by transforming growth factor-beta1 in pulmonary fibrosis. *PloS One*, **10**, e0121246.

31. Park, E.J., Grabinska, K.A., Guan, Z., Stranecky, V., Hartmannova, H., Hodanova, K., Baresova, V., Sovova, J., Jozsef, L., Ondruskova, N., *et al.* (2014) Mutation of Nogo-B receptor, a subunit of cis-prenyltransferase, causes a congenital disorder of glycosylation. *Cell Metab.*, **20**, 448–457.

32. Stranecky, V., Hoischen, A., Hartmannova, H., Zaki, M.S., Chaudhary, A., Zudaire, E., Noskova, L., Baresova, V., Pristoupilova, A., Hodanova, K., *et al.* (2013) Mutations in ANTXR1 cause GAPO syndrome. *Am. J. Hum. Genet.*, **92**, 792–799.

33. Li, H., Handsaker, B., Wysoker, A., Fennell, T., Ruan, J., Homer, N., Marth, G., Abecasis, G. and Durbin, R. (2009) The sequence alignment/Map format and SAMtools. *Bioinformatics*, **25**, 2078–2079.

34. Wang, K., Li, M. and Hakonarson, H. (2010) ANNOVAR: functional annotation of genetic variants from high-throughput sequencing data. *Nucleic Acids Res.*, **38**, e164.

35. Thorvaldsdottir, H., Robinson, J.T. and Mesirov, J.P. (2013) Integrative Genomics Viewer (IGV): high-performance genomics data visualization and exploration. *Brief. Bioinformatics*, **14**, 178–192.

36. McKenna, A., Hanna, M., Banks, E., Sivachenko, A., Cibulskis, K., Kernytsky, A., Garimella, K., Altshuler, D., Gabriel, S., Daly, M., *et al.* (2010) The Genome Analysis Toolkit: a MapReduce framework for analyzing next-generation DNA sequencing data. *Genome Res.*, **20**, 1297–1303.

37. Cingolani, P., Platts, A., Wang le, L., Coon, M., Nguyen, T., Wang, L., Land, S.J., Lu, X. and Ruden, D.M. (2012) A program for annotating and predicting the effects of single nucleotide polymorphisms, SnpEff: SNPs in the genome of *Drosophila melanogaster* strain w1118; iso. *Fly*, **6**, 80–92.

38. Paila, U., Chapman, B.A., Kirchner, R. and Quinlan, A.R. (2013) GEMINI: integrative exploration of genetic variation and genome annotations. *PLoS Comput. Biol.*, **9**, e1003153.

39. Krumm, N., Sudmant, P.H., Ko, A., O'Roak, B.J., Malig, M., Coe, B.P., Quinlan, A.R., Nickerson, D.A. and Eichler, E.E. (2012) Copy number variation detection and genotyping from exome sequence data. *Genome Res.*, **22**, 1525–1532.

40. Davidson, A.E., Liskova, P., Evans, C.J., Dudakova, L., Noskova, L., Pontikos, N., Hartmannova, H., Hodanova, K.,

Příloha 1a

Stranecky, V., Kozmik, Z., *et al.* (2016) Autosomal-dominant corneal endothelial dystrophies CHED1 and PPCD1 are allelic disorders caused by non-coding mutations in the promoter of OVOL2. *Am. J. Hum. Genet.*, **98**, 75–89.

41. Trapnell, C., Pachter, L. and Salzberg, S.L. (2009) TopHat: discovering splice junctions with RNA-Seq. *Bioinformatics*, **25**, 1105–1111.

42. D'Antonio, M., D'Onorio, D., Meo, P., Pallocca, M., Picardi, E., D'Erchia, A.M., Calogero, R.A., Castrignano, T. and Pesole, G. (2015) RAP: RNA-Seq Analysis Pipeline, a new cloud-based NGS web application. *BMC Genomics*, **16**, S3.

43. Bentlage, H.A., Wendel, U., Schagger, H., ter Laak, H.J., Janssen, A.J. and Trijbels, J.M. (1996) Lethal infantile mitochondrial disease with isolated complex I deficiency in fibroblasts but with combined complex I and IV deficiencies in muscle. *Neurology*, **47**, 243–248.

44. Wittig, I., Karas, M. and Schagger, H. (2007) High resolution clear native electrophoresis for in-gel functional assays and fluorescence studies of membrane protein complexes. *Mol. Cell. Proteomics*, **6**, 1215–1225.

45. Masuda, T., Tomita, M. and Ishihama, Y. (2008) Phase transfer surfactant-aided trypsin digestion for membrane proteome analysis. *J Proteome Res.*, **7**, 731–740.

46. Cox, J. and Mann, M. (2008) MaxQuant enables high peptide identification rates, individualized p.p.b.-range mass accuracies and proteome-wide protein quantification. *Nat. Biotechnol.*, **26**, 1367–1372.

47. Cox, J., Hein, M.Y., Luber, C.A., Paron, I., Nagaraj, N. and Mann, M. (2014) Accurate proteome-wide label-free quantification by delayed normalization and maximal peptide ratio extraction, termed MaxLFQ. *Mol. Cell. Proteomics*, **13**, 2513–2526.

48. Pecina, P., Houstkova, H., Mracek, T., Pecinova, A., Nuskova, H., Tesarova, M., Hansikova, H., Janota, J., Zeman, J. and Houstek, J. (2014) Noninvasive diagnostics of mitochondrial disorders in isolated lymphocytes with high resolution respirometry. *BBA Clin.*, **2**, 62–71.

Biallelic loss-of-function variants in *PLD1* cause congenital right-sided cardiac valve defects and neonatal cardiomyopathy

Najim Lahrouchi,[1] Alex V. Postma,[2,3] Christian M. Salazar,[4] Daniel M. De Laughter,[5] Fleur Tjong,[1] Lenka Piherová,[6] Forrest Z. Bowling,[7] Dominic Zimmerman,[1] Elisabeth M. Lodder,[1] Asaf Ta-Shma,[8] Zeev Perles,[8] Leander Beekman,[1] Aho Ilgun,[3] Quinn Gunst,[3] Mariam Hababa,[1] Doris Škorić-Milosavljević,[1] Viktor Stránecký,[6] Viktor Tomek,[9] Peter de Knijff,[10] Rick de Leeuw,[10] Jamille Y. Robinson,[11] Sabrina C. Burn,[12] Hiba Mustafa,[12] Matthew Ambrose,[13] Timothy Moss,[14] Jennifer Jacober,[15] Dmitriy M. Niyazov,[15] Barry Wolf,[16,17] Katherine H. Kim,[16,17] Sara Cherny,[17,18] Andreas Rousounides,[19] Aphrodite Aristidou-Kallika,[20] George Tanteles,[21,22] Bruel Ange-Line,[23,24] Anne-Sophie Denommé-Pichon,[23,24] Christine Francannet,[25] Damara Ortiz,[26] Monique C. Haak,[27] Arend D. J. Ten Harkel,[28] Gwendolyn T.R. Manten,[29] Annemiek C. Dutman,[30] Katelijne Bouman,[31] Monia Magliozzi,[32] Francesca Clementina Radio,[32] Gijs W.E. Santen,[33] Johanna C. Herkert,[31] H. Alex Brown,[11] Orly Elpeleg,[34] Maurice J.B. van den Hoff,[3] Barbara Mulder,[1] Michael V. Airola,[7] Stanislav Kmoch,[6] Joey V. Barnett,[11] Sally-Ann Clur,[35] Michael A. Frohman,[4] and Connie R. Bezzina[1]

[1]Amsterdam UMC, University of Amsterdam, Heart Center, Department of Clinical and Experimental Cardiology, Amsterdam Cardiovascular Sciences, [2]Department of Clinical Genetics, and [3]Department of Medical Biology, Amsterdam UMC, Amsterdam, Netherlands. [4]Department of Pharmacological Sciences and Graduate Program in Molecular and Cellular Pharmacology, Stony Brook University, Stony Brook, New York, USA. [5]Department of Cell and Developmental Biology, Vanderbilt University School of Medicine, Nashville, Tennessee, USA. [6]Research Unit for Rare Diseases, Department of Pediatrics and Adolescent Medicine, 1st Faculty of Medicine, Charles University and General University Hospital, Prague, Czech Republic. [7]Department of Biochemistry and Cell Biology, Stony Brook University, Stony Brook, New York, USA. [8]Department of Pediatric Cardiology, Hadassah, Hebrew University Medical Center, Jerusalem, Israel. [9]Children's Heart Centre, 2nd Faculty of Medicine, Charles University in Prague, Motol University Hospital, Prague, Czech Republic. [10]Department of Human Genetics, Leiden University Medical Centre, Leiden, Netherlands. [11]Department of Pharmacology, Vanderbilt University School of Medicine, Nashville, Tennessee, USA. [12]Department of Obstetrics, Gynecology and Women's Health, [13]Department of Pediatrics, Division of Pediatric Cardiology, and [14]Department of Pediatrics, University of Minnesota, Minneapolis, Minnesota, USA. [15]Department of Pediatrics, Ochsner Clinic, Tulane University, University of Queensland, New Orleans, Louisiana, USA. [16]Division of Genetics, Birth Defects and Metabolic Disorders, Ann and Robert H. Lurie Children's Hospital of Chicago, Chicago, Illinois, USA. [17]Feinberg School of Medicine, Northwestern University, Chicago, Illinois, USA. [18]Division of Cardiology, Ann and Robert H. Lurie Children's Hospital of Chicago, Chicago, Illinois, USA. [19]Makarios Medical Centre, Nicosia, Cyprus. [20]Ultrasound and Fetal Medicine Diagnostic Centre, Nicosia, Cyprus. [21]Cyprus School of Molecular Medicine, Nicosia, Cyprus. [22]Department of Clinical Genetics, The Cyprus Institute of Neurology and Genetics, Nicosia, Cyprus. [23]UMR 1231 INSERM, GAD, Université Bourgogne Franche-Comté, Dijon, France. [24]Unité Fonctionnelle d'Innovation en Diagnostique Génomique des Maladies Rares, FHU-TRANSLAD, Centre Hospitalier Universitaire Estaing (CHU), Dijon Bourgogne, Dijon, France. [25]Service de Génétique Médicale, CHU Estaing, Clermont-Ferrand, France. [26]Medical Genetics Department, UPMC Children's Hospital of Pittsburgh, Pittsburgh, Pennsylvania, USA. [27]Department of Obstetrics and [28]Department of Pediatric Cardiology, Leiden University Medical Centre, Leiden, Netherlands. [29]Department of Obstetrics and [30]Department of Pathology, Isala Women and Children's Hospital, Zwolle, Netherlands. [31]University Medical Center Groningen, Department of Genetics, University of Groningen, Groningen, Netherlands. [32]Genetic and Rare Disease Research Division, Bambino Gesù Children's Hospital IRCCS, Rome, Italy. [33]Department of Human Genetics, Leiden University Medical Center, Leiden, Netherlands. [34]Department of Genetics, Hadassah, Hebrew University Medical Center, Jerusalem, Israel. [35]Department of Pediatric Cardiology, Emma Children's Hospital, Amsterdam UMC, University of Amsterdam, Amsterdam, Netherlands.

Congenital heart disease is the most common type of birth defect, accounting for one-third of all congenital anomalies. Using whole-exome sequencing of 2718 patients with congenital heart disease and a search in GeneMatcher, we identified 30 patients from 21 unrelated families of different ancestries with biallelic phospholipase D1 (*PLD1*) variants who presented predominantly with congenital cardiac valve defects. We also associated recessive *PLD1* variants with isolated neonatal cardiomyopathy. Furthermore, we established that p.I668F is a founder variant among Ashkenazi Jews (allele frequency of ~2%) and describe the phenotypic spectrum of *PLD1*-associated congenital heart defects. PLD1 missense variants were overrepresented in regions of the protein critical for catalytic activity, and, correspondingly, we observed a strong reduction in enzymatic activity for most of the mutant proteins in an enzymatic assay. Finally, we demonstrate that PLD1 inhibition decreased endothelial-mesenchymal transition, an established pivotal early step in valvulogenesis. In conclusion, our study provides a more detailed understanding of disease mechanisms and phenotypic expression associated with PLD1 loss of function.

1

JCI

Introduction

Congenital heart disease is the most common type of birth defect, accounting for one-third of all congenital anomalies, with a worldwide occurrence of 7 per 1000 live births (1). The majority of these defects include abnormalities of valve formation. Right-sided congenital heart disease includes abnormalities of the pulmonary and tricuspid valves, the right ventricle, and the right ventricular outflow tract. Recessive variants in *PLD1*, which encodes phospholipase D1, a signal transduction enzyme that hydrolyses the membrane lipid phosphatidylcholine to generate the lipid second messenger phosphatidic acid (2), were recently associated with severe right-sided congenital cardiac valve defects in 2 small families (3). Although no overt structural cardiac defects were noted, mice lacking PLD1 displayed moderately impaired function of the pulmonary and tricuspid valve on echocardiography (3). However, the functional consequences of PLD1 enzymatic activity and the mechanism by which PLD1 dysfunction leads to congenital valve abnormalities remain unknown.

Using whole-exome sequencing (WES) data from 2718 patients with congenital heart disease and a search in Gene-Matcher (4), we identified 30 patients from 21 unrelated families of different ancestries with biallelic *PLD1* variants. We established that p.I668F is a founder variant among Ashkenazi Jews. We expanded the phenotypic spectrum of *PLD1*-associated congenital heart defects and, for the first time to our knowledge, provide evidence that recessive variants in *PLD1* can also cause neonatal cardiomyopathy in the absence of congenital heart defects. Placement of the missense variants on the 3D crystal structure of PLD1, recently reported by several of the co-authors (5), localized them primarily to sites important for catalytic site integrity. Correspondingly, we uncovered a substantial loss of enzymatic activity through functional analysis. Finally, in line with a loss-of-function mechanism of PLD1, we demonstrate here that PLD1 inhibition decreased endothelial-mesenchymal transition (EndoMT), a pivotal early step in valvulogenesis (6).

Results

PLD1 variants cause congenital valvular defects or neonatal cardiomyopathy in multiple families. To uncover the genetic cause of severe right-sided congenital heart defects in a consanguineous Afghan family with 2 affected siblings (family A, Figure 1A), we performed WES for both parents and one of the affected siblings. In line with the expected recessive inheritance pattern, we identified a homozygous variant, p.R695C, in *PLD1* (GenBank accession number: NM_002662) as the only cosegregating variant. We then searched for additional patients carrying biallelic variants in *PLD1* by performing (a) WES for 75 patients with similar severe right-sided congenital heart defects from the National Registry of Congenital Heart Defects (CONCOR) in the Netherlands (7); (b) analysis of 2643 patients with congenital heart disease trios (i.e., the affected patient and both parents) who underwent WES from the Pediatric Cardiac Genomics Consortium (PCGC) (8, 9); and (c) a search using GeneMatcher (4). In total, we identified 30 patients from 21 unrelated families of different ancestries (Figure 1A, Table 1, and Supplemental Table 1) carrying either homozygous or compound heterozygous *PLD1* variants. All 30 patients were diagnosed with severe congenital heart disease or cardiomyopathy at the fetal or neonatal stage.

Twenty-eight patients from 19 families (families A–S, Figure 1) presented with congenital cardiac valve malformations predominantly affecting the right side of the heart. These defects were characterized by severe tricuspid and/or pulmonary valve abnormalities (27 of 28), hypoplastic right ventricles (16 of 28), and/or hypoplastic pulmonary arteries (11 of 28) (Table 1, Supplemental Table 1, detailed phenotypic descriptions in Supplemental Note 1, and echocardiography in a selection of patients in Supplemental Videos 1–4; supplemental material available online with this article; https://doi.org/10.1172/JCI142148DS1). Five of these 28 patients were diagnosed with Ebstein's anomaly. The extremely thin right ventricular wall in both patients from family A prompted a diagnosis of Uhl's anomaly, a rare heart defect characterized by a congenital partial or complete absence of right ventricular wall myocardium (Figure 1C and ref. 10). Two patients had dilated left ventricles and mitral regurgitation in addition to tricuspid and/or pulmonary valve defects. Six pregnancies were terminated because of a complex heart defect with poor prognosis (gestational age range, 13–22 weeks). One patient underwent an orthotopic heart transplantation at the age of 45 days because of worsening heart function (family S). Four patients survived less than 1 year as a result of their underlying structural heart defect. The majority of live-born infants required surgery in the first days or months of life, most commonly the placement of a Blalock-Taussig shunt and bidirectional Glenn palliation (Table 1).

Of note, 2 patients presented with severe isolated neonatal cardiomyopathy (i.e., in the absence of a structural congenital heart defect), a new finding for this syndrome (families T and U, Figure 1 and Table 1). At 33 weeks of gestation, the patient from family T was found to have persistently reduced fetal movement. A fetal ultrasound revealed hydrops fetalis due to severe cardiomyopathy, and an emergency delivery by caesarean section was performed. Postnatal echocardiography showed severe systolic dysfunction of the left ventricle with severe mitral regurgitation (Supplemental Videos 5 and 6). Despite medical treatment, the child died on the third postnatal day as a result of intractable cardiac failure. The other patient (family U) was a full-term neonate who developed difficulty breathing and bloody vomiting and died on postnatal day 8. The autopsy showed sections of the heart with patchy replacement of the myocardium by histiocytoid cells and occasional plasma cells and eosinophils, a finding most consistent with histiocytoid cardiomyopathy. Both patients were screened for variants in approximately 300 cardiomyopathy-related genes and were found to be negative.

Overall, none of the patients who survived beyond infancy had dysmorphic features, intellectual disability, or notable developmental delays, suggesting that in the context of overt phenotypes, *PLD1* loss of function (see below) is predominantly associated with isolated cardiac disease in humans.

We noted an autosomal-recessive mode of inheritance in all of the families and found that variants in *PLD1* were inherited from each of the unaffected parents. In total, we report 31 *PLD1* variants, of which 21 are missense variants and 10 are expected to result in protein truncation (Supplemental Table 2). Two variants are predicted to affect splicing. Reverse transcription PCR (RT-PCR) analysis of mRNA isolated from a peripheral blood sample from the parents of family E confirmed mis-splicing that
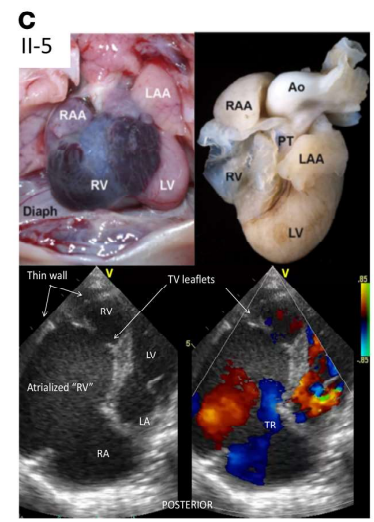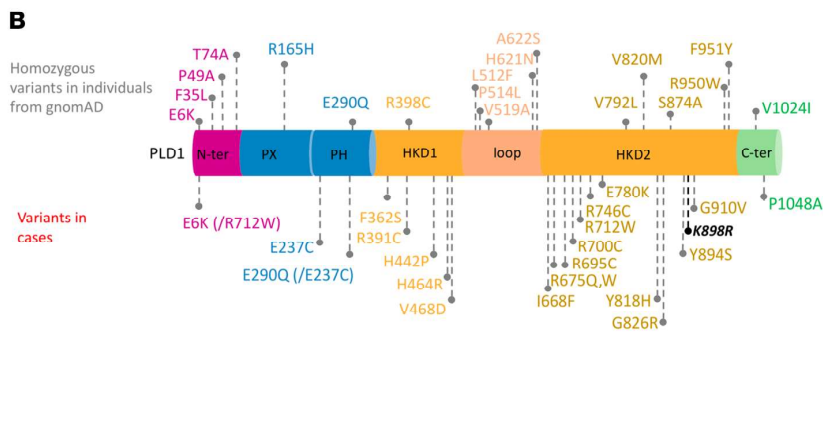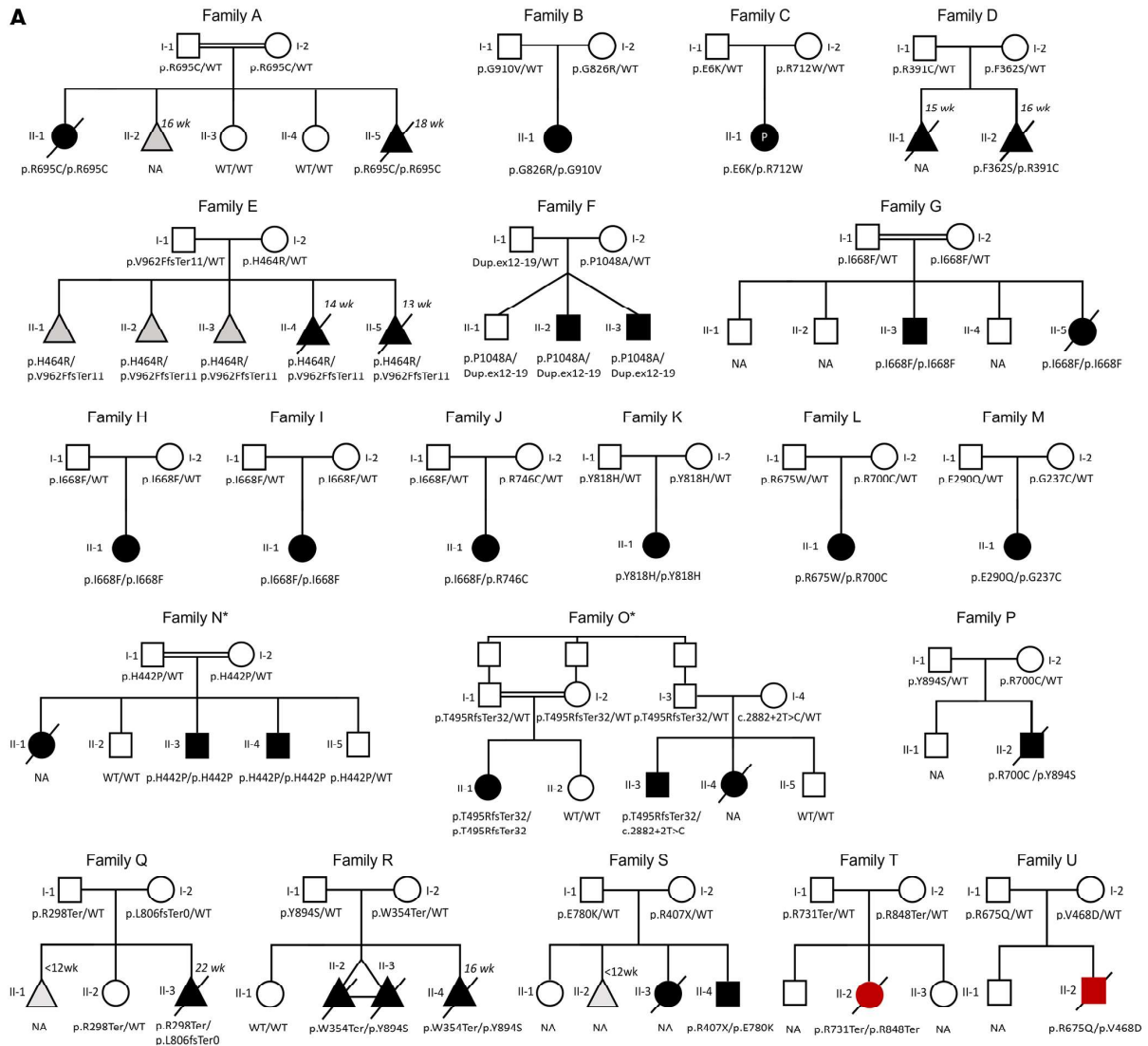
70

The Journal of Clinical Investigation

Figure 1. Recessive variants in *PLD1* cause a spectrum of valvular congenital heart disease and neonatal cardiomyopathy. (**A**) Pedigrees. Solid symbols indicate the affected individuals (black indicates individuals with a congenital heart defect; red indicates individuals with fetal/neonatal cardiomyopathy), and symbols with a slash through them indicate deceased individuals. A double line indicates consanguinity. Males are indicated by squares and females by circles. Solid black triangles with a slash through them indicate fetal death or termination of pregnancy. Gray triangles indicate a miscarriage. Dup, duplication; ex, exon; fs, frame shift; NA, not available; Ter, termination; wk, age in weeks at termination of the pregnancy. #Previously published family (3). Families H–M were identified through analysis of PCGC data, and pedigrees were not available (8, 9). (**B**) PLD1 domain structure and location of pathologic (bottom) and presumptive nonpathologic (top) missense variants. Black indicates an inactive allele (16) used as a baseline control. Gray dots, homozygous missense variants found in gnomAD individuals (11). Statistical comparison of loop variants in patients versus controls was performed using Fisher's exact test ($P = 0.017$). (**C**) Macroscopic appearance of the heart of fetus II-5 from family A. Upper left panel: Position of the heart in the thorax. Note the extremely dilated right ventricle with a thin translucent wall. A sharp demarcation can be seen between the abnormal right ventricular myocardium and normal left ventricular myocardium. Upper right panel: Anterior view of a formalin-fixed heart including large vessels, showing the paper-thin right ventricular wall, which was partially collapsed because of tissue weakness. Bottom panels: Postnatal echocardiograms of child II-1 from family A displaying a thin-walled right ventricle with Ebstein's anomaly of the tricuspid valve and tricuspid regurgitation (see also Supplemental Video 1). This child also had pulmonary atresia. Ao, ascending aorta; Diaph, thoracic diaphragm; LA, left atrium; LAA, left atrial appendage; LV, left ventricle; PT, pulmonary trunk; RAA, right atrial appendage; RV, right ventricle; TV, tricuspid valve; TR, tricuspid regurgitation.

is predicted to result in a truncated PLD1 protein (Supplemental Figure 1). The duplication of exons 13–21 found in family F is predicted to result in a premature stop codon in exon 13. Although 12 of 31 variants were not present in Genome Aggregation Database (gnomAD) (11), the minor allele frequency (MAF) for the others ranged from 0.0008% to 0.16% (Supplemental Table 2). With 2 exceptions, the identified variants were not homozygous in 123,136 exomes and 15,496 genomes from the gnomAD (accessed October 2019; ref. 11), suggesting that homozygosity for these variants is not tolerated. The 2 exceptions are p.E6K and p.E290Q, which were found in compound heterozygosity with p.R712W in family C and p.G237C in family M, respectively. The gnomAD contains 42 predicted loss-of-function *PLD1* variants (expected number, 62); none of them occurs in the homozygous state, suggesting that *PLD1* is intolerant to homozygous loss-of-function variants.

The p.I668F missense variant in PLD1 is a founder variant among Ashkenazi Jews. Given that we found the same homozygous *PLD1* variant, p.I668F, in 3 families, we hypothesized that this was a founder variant. Intriguingly, all 3 families with the homozygous *PLD1* p.I668F congenital heart defect were of Ashkenazi Jewish ancestry, suggesting a novel founder variant. Ashkenazi Jewish descent was self-reported for family G and determined through principal component analysis (PCA) for families H and I, which were recruited through the PCGC and found to cluster with an Ashkenazi Jewish reference population (ref. 12 and Supplemental Figure 2). As expected for a founder variant, all homozygous patients shared p.I668F on the background of a common haplotype spanning approximately 881 kb (chr3:171087469–171969077, hg19). Using the Gamma method (13), we estimated the age of

the p.I668F founder variant at 46 generations (95% CI, 15–154 generations). Assuming a 20-year generational span, a common ancestor with this haplotype would have lived approximately 920 years ago (CI: 300–3080 years). Interestingly, p.I668F has a MAF of approximately 2% among the Ashkenazi Jewish subpopulation in gnomAD and is rare among the other populations (0.004%–0.14%; ref. 11).

Missense variants in PLD1 lead to reduced enzymatic activity. Placement of the 21 missense variants described above onto the PLD1 structure revealed that they largely clustered in the highly conserved HxKxxxxD (HKD) domains and the C-terminal region (Figure 1B) that are critical for enzymatic activity (14). In contrast, 18 presumed nondeleterious *PLD1* missense variants found homozygously in the general population (according to gnomAD, ref. 11; MAF range: 0.001%–18%) were distributed along the entire length of the protein, including in the N-terminus, PX and PH domains, and loop regions that are dispensable for catalytic activity (14). Of note, while 5 of 18 variants that were found in the homozygous state in gnomAD resided in the loop region of PLD1, none of the patients carried a variant in the PLD1 loop region (Figure 1B, $P = 0.017$).

To test their effect on PLD1 enzymatic activity, we engineered the disease-associated missense variants into an HA-tagged WT PLD1 expression vector (15) and transfected them into HEK293 cells. Western blot analysis showed levels of expression of the mutant proteins that were comparable to the levels seen for WT PLD1 and PLD1-p.K898R, a previously identified catalytically inactive variant (Supplemental Figure 3 and ref. 16). Enzymatic activity was assessed using an in vitro cellular transphosphatidylation assay in the presence of PMA, which activates PKC, a potent stimulator of PLD1 activity (15, 17). PLD1-p.K898R (16) was used as a baseline control (Supplemental Figure 4). We observed a strong to dramatic reduction in PLD1 enzymatic activity for 17 of the 19 variants tested, leading to the prediction that patients carrying biallelic *PLD1* variants will generally have less than 25% residual PLD1 activity in comparison with individuals with WT *PLD1* alleles (Figure 2A). Of note, the 2 variants that occurred in the homozygous state in individuals from gnomAD (i.e., p.E6K and p.E290Q) and compound heterozygously in the patients did not affect PLD1 enzymatic activity as measured in this assay.

Since an intact C-terminus is required for enzymatic activity (5, 14), we expected that all of the variants resulting in premature termination of PLD1 protein, such as p.R731Ter/p.R848Ter in the patient with isolated cardiomyopathy from family T, would fully eliminate PLD1 activity. Of note, the other patient who presented with isolated cardiomyopathy (family U) was compound heterozygous for 2 missense variants (p.V468D/p.R675Q) that resulted in drastically reduced catalytic activity (2.7% compared with WT). Thus, residual PLD1 enzymatic activity of variants from patients presenting with isolated cardiomyopathy was similar to that of patients who presented with structural cardiac malformations.

PLD1 disease–associated variants localize to sites important for catalytic activity. Some of us recently reported the crystal structure for a catalytically functional PLD1 protein (representing ~60% of the protein, ref. 5) that encompasses most of the disease-associated variants reported in this study. Figure 2B shows the placement of 18 of the 21 disease-associated missense variants

72

Table 1. Clinical characteristics of patients with biallelic *PLD1* variants

Family	Patient	*PLD1* variant (cDNA)	*PLD1* variant (AA)	PLD1 function (%)	Ethnicity/origin	Sex	Status	Age	TVD	PVD	HRV	PAH	MVD	Cardiomyopathy	Surgery/procedures (age)
Congenital heart defect															
Family A	II-1	c.2083C>T/c.2083C>T	p.R695C/p.R695C	5.7	Afghan	F	Deceased	11 mo	+	+	+	–	–	–	BTS (11 mo)
Family A	II-5	c.2083C>T/c.2083C>T	p.R695C/p.R695C	5.7	Afghan	F	TOP	18 wk	+	+	–	+	–	–	None (TOP)
Family B	II-1	c.2729C>T/c.2476G>A	p.C910V/p.C826R	2.8	Dutch	F	Alive	40 yr	+	+	–	+	–	–	BTS, BGP, VSD, and ASD closure, Fontan
Family C	II-1	c.16C>A/c.2134C>T	p.E6K/p.R712W	74.9	Bangladeshi	M	Alive	37 wk	–	+	–	–	–	–	NA
Family D	II-1	c.1085T>C/c.1171C>T	p.F362S/p.R391C	17.3	Cypriot	M	TOP	15 wk	+	+	+	–	–	–	None (TOP)
Family D	II-2	c.1085T>C/c.1171C>T	p.F362S/p.R391C	17.3	Cypriot	F	TOP	16 wk	+	+	+	+	–	–	None (TOP)
Family E	II-4	c.1391A>G/c.3000+2T>A	p.H464R/p.V962FsTer1	1.1	Czech	M	TOP	14 wk	+	+	–	–	–	–	None (TOP)
Family E	II-5	c.1391A>G/c.3000+2T>A	p.H464R/p.V962FsTer1	1.1	Czech	M	TOP	13 wk	+	NA	–	NA	–	–	None (TOP)
Family F	II-1	c.3142C>G/intragenic_duplication	p.P1048A/intragenic_duplication	0.7	Latino	M	Alive	11 mo	–	–	–	–	–	–	–
Family F	II-2	c.3142C>G/intragenic_duplication	p.P1048A/intragenic_duplication	0.7	Latino	M	Alive	11 mo	–	+	–	–	–	–	Balloon dilation PV (4 mo)
Family F	II-3	c.3142C>G/intragenic_duplication	p.P1048A/intragenic_duplication	0.7	Latino	M	Alive	11 mo	+	+	+	–	–	LVNC	BGP, atrial septectomy and ligation of PDA (6 mo)
Family G	II-1	c.2002A>T/c.2002A>T	p.I668F/p.I668F	20.3	Ashkenazi Jewish	M	Alive	5 yr	+	+	+	+	–	–	BTS and BGP awaiting Fontan TCPC procedure
Family G	II-5	c.2002A>T/c.2002A>T	p.I668F/p.I668F	20.3	Ashkenazi Jewish	F	Deceased	7 d	+	+	+	+	–	–	None (deceased)
Family H	II-1	c.2002A>T/c.2002A>T	p.I668F/p.I668F	20.3	Ashkenazi Jewish	F	NA	NA	+	+	–	–	–	–	NA
Family I	II-1	c.2002A>T/c.2002A>T	p.I668F/p.I668F	20.3	Ashkenazi Jewish	F	NA	NA	+	+	+	–	–	–	NA
Family J	II-1	c.2002A>T/c.2236C>T	p.I668F/p.R746C	18.1	European	M	NA	NA	+	+	+	–	–	NA	–
Family K	II-1	c.2452T>C/c.2452T>C	p.Y818H/p.Y818H	42.1	East Asian	F	NA	NA	+	–	+	–	–	–	NA
Family L	I-1	c.2023C>T/c.2098C>T	p.R675W/p.R700C	5.7	East Asian	F	NA	NA	–	+	+	+	–	–	NA
Family M	II-1	c.709G>T/c.868G>C	p.G237C/p.E290Q	75.5	European	M	NA	NA	–	–	–	+	–	–	–
Family N[A]	II-1	c.1325A>C/c.1325A>C	p.H442P/p.H442P	7.1	Middle Eastern	F	Deceased	12 mo	+	+	–	–	+	–	–
Family N[A]	II-3	c.1325A>C/c.1325A>C	p.H442P/p.H442P	7.1	Middle Eastern	M	Alive	25 yr	+	+	+	–	–	–	CS (3 yr), BGP (5 yr), VSD closure, 1.5 ventricle repair (22 yr)
Family N[A]	II-4	c.1325A>C/c.1325A>C	p.H442P/p.H442P	7.1	Middle Eastern	M	Alive	20 yr	+	+	+	+	–	–	BTS (2 wk), BGP (1 yr), Fontan (16 yr)
Family O[A]	II-1	c.1482_1483del/c.2882+2T>C	p.T495RfsTer32/c.2882+2T>C	0	Middle Eastern	F	Alive	5 yr	–	–	–	+	–	–	MV repair (8 mo)
Family O[A]	II-3	c.1482_1483del/c.2882+2T>C	p.T495RfsTer32/c.2882+2T>C	0	Middle Eastern	M	Alive	20 yr	+	–	–	–	–	–	–
Family O[A]	II-4	c.1482_1483del/c.2882+2T>C	p.T495RfsTer32/c.2882+2T>C	0	Middle Eastern	F	Deceased	21 d	+	+	+	–	–	–	CS (5d)
Family P	II-1	c.2098C>T/c.A2681A>C	p.R700C/p.Y894S	p.R700C (9.6%) p.Y894S Not tested	Mixed Caucasian	M	Deceased	23 d	+	+	–	+	–	–	–
Family Q	II-1	c.1062C>A/c.2681A>C	p.W354Ter/p.Y894S	p.Y894S Not tested	French	F	Fetal death	16 wk	+	+	+	–	–	–	–
Family R	II-3	c.892C>T/c.2415delC	p.R298Ter/p.L806fsTer0	0	Dutch	F	TOP	19 wk	+	+	+	+	–	–	None (TOP)
Family S	II-4	c.1219C>T/c.2338G>A	p.R407X/p.E780K	p.E780K Not tested	Hispanic	M	Alive	15 mo	+	+	+	+	–	–	Cardiac transplantation
Neonatal cardiomyopathy															
Family T	II-2	c.2542A>T/c.2191A>T	p.R848Ter/p.R731Ter	0	Dutch	M	Deceased	3 d	–	–	–	–	–	DCM	–
Family U	II-2	c.1403T>A/c.2024G>A	p.V468D/p.R675Q	2.5	Latino	M	Deceased	8 d	–	–	–	–	–	Histiocytoid CMP	–

For a more detailed phenotype description see Supplemental Table 1. AA, amino acid; ASD, atrial septal defect; BTS, Blalock-Taussig shunt; BGP, bidirectional Glenn procedure; CMP, cardiomyopathy; CS, central shunt; DCM, dilated cardiomyopathy; HRV, hypoplastic right ventricle; LVNC, left ventricular noncompaction cardiomyopathy; MV, mitral valve; MVD, mitral valve defect; NA, not available; PAH, pulmonary artery hypoplasia; PDA, persistent ductus arteriosus; PVD, pulmonary valve defect; TOP, termination of pregnancy; TVD, tricuspid valve defect; TCPC, total cavopulmonary connection; VSD, ventricular septal defect. F, female; M, male; TCPC, total cavopulmonary connection; VSD, ventricular septal defect. [A]Previously published family (3). Families H–M were identified through analysis of PCCC data (8, 9). +, indicates that the phenotype was present; –, indicates that the phenotype was absent. Variants were annotated on transcript NM_002662.

reported here on the 3D structure (see also Supplemental Videos 7–24). Placement of the remaining 3 variants was not assessed, as these were located in the N-terminal (p.E6K) and PH domain regions (p.E237C and p.E290Q) of the PLD1 protein, which were not included in the crystal structure (5). Strikingly, the majority of the missense variants clustered near sites critical for catalytic activity, which is consistent with the observed reduction of PLD1 enzymatic activity for these variants.

We categorized these variants into 3 groups according to their predicted disruptive effects (Figure 2B). The first class of variants affect the active site of PLD1. These variants either alter a residue directly involved in catalysis (p.H464) or are located within the active site (p.G826, p.Y894, and p.G910), thus affecting catalysis. The second class of variants stabilize elements that form the binding site for the membrane lipid phosphatidylinositol-4,5-bisphosphate [PI(4,5)P$_2$], which is a required cofactor for PLD1 activity (5, 15). These residues include p.R695, which was mutated in the index family (family A) of our study, as well as p.H442, p.R712, and p.R746. Mutation of these residues are predicted to alter the PI(4,5)P$_2$ binding site and decrease PLD1 activity. The majority and remaining ones fall into a third class of variants that are distributed throughout the catalytic domain. The mutated residues are buried within the correctly folded structure and are involved in interactions with neighboring residues. These variants would destabilize local interaction networks presumably necessary for proper folding or create new unfavorable interactions. A notable example is the p.I668F founder variant in Ashkenazi Jews. For this variant, substitution with the larger phenylalanine side chain is predicted to create steric clashes with nearby residues that form part of the substrate-binding pocket (Supplemental Video 12). These clashes would alter the shape of the pocket, thus diminishing PLD1 activity.

Only 3 of the variants that we identified in the patients were found outside the catalytic domain. These were located at either the extreme N-terminus (p.E6K) or within the PH domain (p.G237C and p.E290Q), which is required for proper localization of PLD1 to the plasma membrane. As discussed above, both p.E6K (family C) and p.E290Q (family M) seem to be tolerated in the homozygous state and were associated with disease only in combination with p.R712W or p.G237C, respectively. Furthermore, these 2 variants retained full PMA-stimulated enzymatic activity (Figure 2A). In contrast, a 50% reduction of activity was observed with p.G237C. We predict that this variant may affect membrane binding, as this is the main function of the PH domain (18), and p.G237 is near 2 residues, C240 and C241, which are posttranslationally modified by palmitoylation to anchor PLD1 to membranes and are functionally required for PLD1's role in regulating exocytosis (18–20).

We also assessed the location of the 18 variants found homozygously in the general population of individuals in gnomAD (11) and found that only 7 of these variants localized to the catalytic domain (Figure 1B and Supplemental Table 3). In contrast to the disease-associated missense variants above that are embedded at sites critical for catalysis, these residues all lie on the periphery of the protein, with their side chains facing outward and having few, if any, interactions with other residues (Supplemental Figure 5). This underscores the importance of evaluating amino acid substitutions in the setting of the 3D structure. In addition, the disease-associated missense variants were more often predicted to be deleterious and affected residues that were more conserved across species (Supplemental Figure 6). Taken together, the disease-associated variants reported here primarily located to sites critical for catalysis and correspondingly exhibited major loss of enzymatic activity.

PLD1 is required for endocardial cell endothelial-mesenchymal transition in atrioventricular cushion explants. Structural atrioventricular (AV) valve defects are the cardinal malformation in patients with PLD1 loss of function. In the embryonic heart, a pivotal early step in valvulogenesis occurs when a subpopulation of endocardial cells overlaying the provalvular cardiac cushions undergoes endothelial-mesenchymal transition (EndoMT) (6). These mesenchymal cells seed the cushions leading to remodeling of the extracellular matrix and contribute to development of the valves and cardiac septa.

To date, many important EndoMT genes have been identified using an in vitro collagen gel assay system (Supplemental Figure 7), in which chick embryo AV cushions (AVCs) are excised, transfected, and explanted endocardial side down onto a collagen pad (21). The explant myocardium compacts and beats while the endocardial cells spread out and form a surface monolayer. Some of the endocardial cells eventually undergo EndoMT, seeding the collagen gel with mesenchymal cells. The spatial specificity observed in vivo, where the AVC, but not the ventricular endocardium, undergoes EndoMT, is reproduced in this in vitro assay (21). We used this assay to investigate the involvement of *PLD1* in EndoMT by incubating chick embryo AVC explants with 1-butanol, which suppresses the generation of phosphatidic acid by PLD1, and 3-butanol, which does not suppress phosphatidic acid formation, as a control compound. We observed normal levels of invasion in 3-butanol–treated explants compared with vehicle-incubated controls (our unpublished observations). However, 1-butanol incubation significantly reduced the number of transformed cells compared with the 3-butanol–treated controls (Figure 3A), suggesting that PLD1 function is involved in EndoMT in vitro.

We then confirmed the role of PLD1 using PLD small-molecule inhibitors (22). PLD1 inhibition dramatically reduced the number of transformed cells, whereas no reduction was seen using an inhibitor of PLD2, the other classic member of the PLD superfamily (Figure 3, B and C). Similarly, siRNA constructs targeting chick PLD1 significantly decreased the number of transformed cells compared with a scrambled control (Figure 3D). We used an siRNA targeting TGF-βR3, which is required for EndoMT in AVCs (23), as a positive control. Finally, PLD1 inhibition did not decrease endocardial cell proliferation or increase cell death (Supplemental Figure 8, C and D, and Supplemental Methods, Note 2). Together, these data indicate that *PLD1* is required for EndoMT, a pivotal early step in valvulogenesis, and suggest that abnormal EndoMT may underlie, at least in part, the cardiac structural malformations in patients with loss-of-function biallelic *PLD1* variants.

Discussion

We established an international cohort of 30 patients from 21 unrelated families of different ancestries with autosomal-
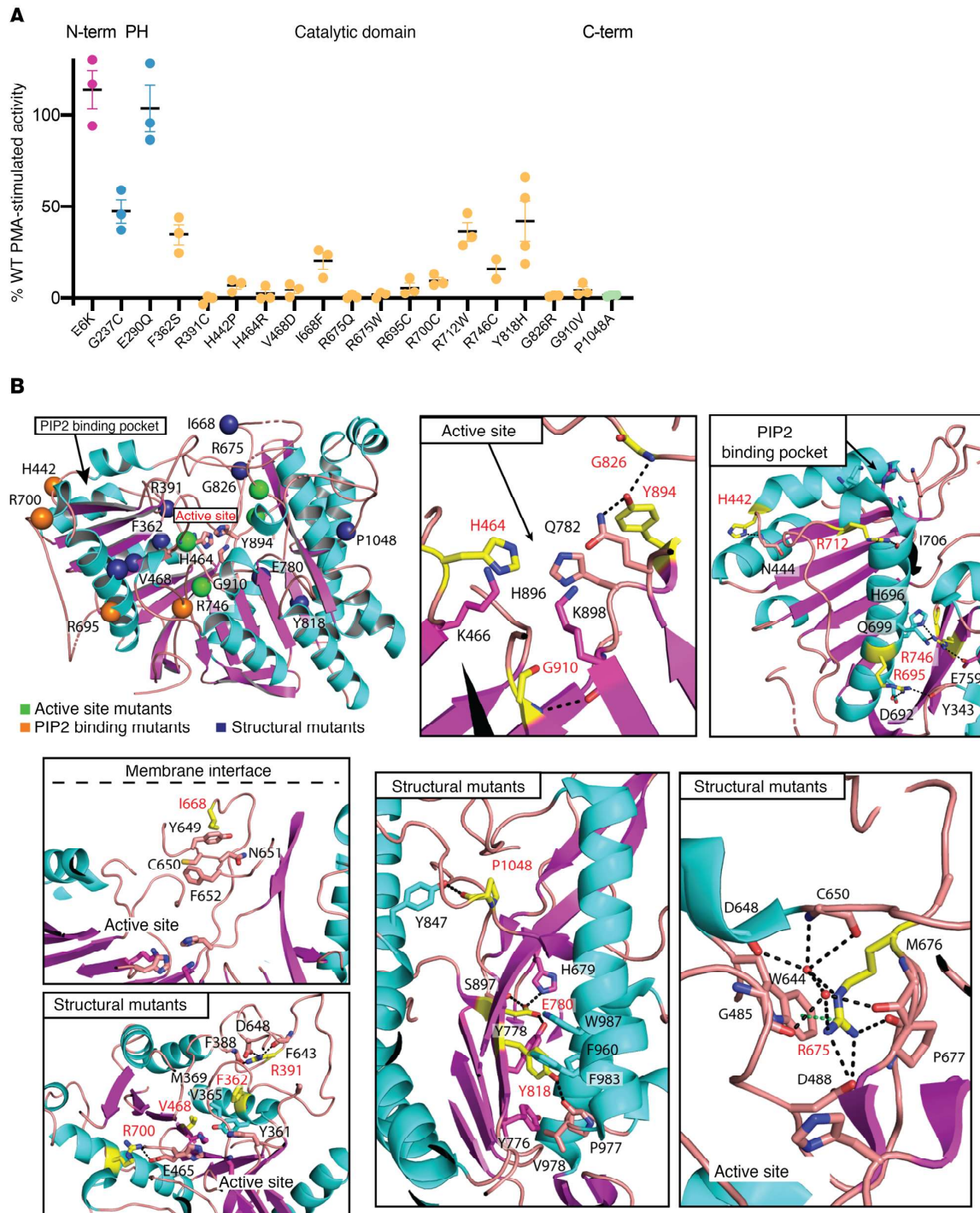
74

Figure 2. Activity of pathogenic PLD1 variants and their placement on the 3D protein structure. (**A**) Activity of missense PLD1 variants above the K898R negative control as normalized to the WT PLD1 positive control. Data points represent independent experiments performed in duplicate and averaged. Error bars represent the SEM. Magenta, N-terminus; blue, PH-domain; yellow, catalytic domain; green, C-terminus N-term, N-terminus; C-term, C-terminus. (**B**) Placement of missense variants on the PLD1 catalytic domain crystal structure. α Helices are shown in cyan, and β strands are shown in magenta. Spheres indicate pathogenic missense mutations: green spheres indicate active site variants; orange spheres indicate PI(4,5)P$_2$–binding (PIP2-binding) mutants; and blue spheres indicate structural mutants. Insets show close-ups of WT residue interactions potentially disrupted by pathogenic variants. Pathogenic residues are represented by yellow sticks; black dashed lines indicate hydrogen bonds; and green dashed lines indicate cation-pi interaction. See Supplemental Videos 7–24 for rotatable presentations and a depiction of the impact of mutations on local structure.
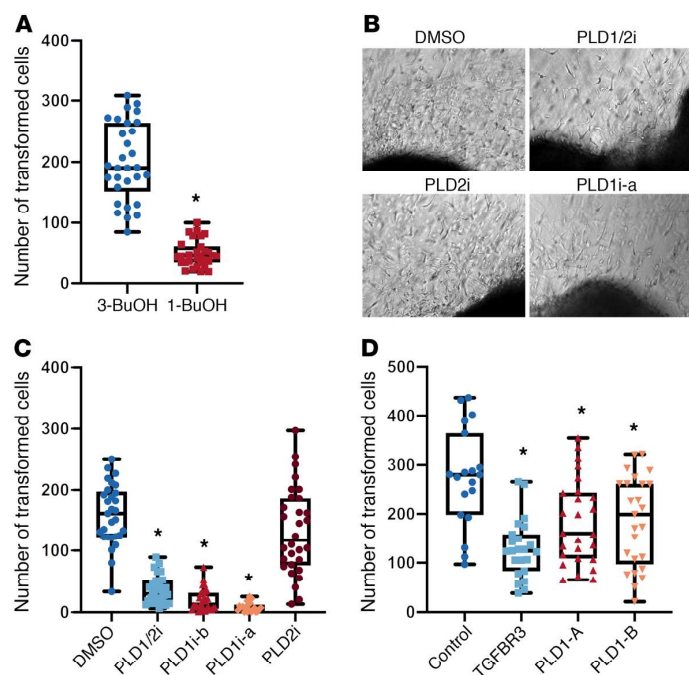
75

Figure 3. PLD1 is required for EndoMT in AVC explants in vitro. The role of PLD1 in EndoMT was determined using a collagen gel assay by incubating Hamburger-Hamilton (HH) stage 16 chick AV canal cushion explants on collagen gels for 48 hours with chemical (**A**), small-molecule inhibitors (**B** and **C**) of PLD, or an siRNA (**D**). The number of cells undergoing EndoMT per explant was counted for each condition over 3 separate experiments. (**A**) HH16 AVC explants were incubated with either 0.6% normal butanol (1-BuOH), which inhibits PLD generation of phosphatidic acid, or tertiary butanol (3-BuOH), which does not inhibit phosphatidic acid production. $n = 30$ explants for each condition. (**B**) Representative photomicrographs of AVC explants on collagen gels incubated with 5 μM doses of small-molecule inhibitors of PLD1i-a (VU0359595), PLD2i (VU0285655-1), and PLD1/2i (VU0155056, which inhibits both PLD1 and PLD2), or with DMSO. (**C**) HH16 AVC explants ($n = 30$ for each condition) were incubated with small-molecule PLD inhibitors or DMSO. PLD1/2i (VU0155056) inhibits both PLD1 and PLD2 (*$P = 2.9 \times 10^{-17}$ compared with control); PLD1i-B (VU0155069) selectively inhibits PLD1 (*$P = 3.9 \times 10^{-20}$ compared with control); PLD2i (VU0285655-1, *$P = 0.28$ compared with control); and PLD1i-a (VU0359595, *$P = 1.4 \times 10^{-21}$ compared with control). (**D**) HH16 AVC explants were incubated with siRNAs targeting *TGFBR3* (*$P = 2.5 \times 10^{-6}$ compared with control), 2 different regions of *PLD1-A* (*$P = 5.7 \times 10^{-3}$ compared with control) and *PLD1-B* (*$P = 0.011$ compared with control), or a scrambled siRNA (control). Control explants ($n = 19$) were GC content–matched, randomized siRNA constructs with no homology to any known chick gene. *TGFBR3* ($n = 23$) was an siRNA targeting a gene known to be required for EndoMT in vitro. PLD1-A ($n = 26$) and PLD1-B ($n = 25$) were independent constructs targeting different regions of PLD1. All P values were calculated using the Student's t test, and Bonferroni's correction was used to correct for multiple testing. Error bars represent the SEM.

recessive variants in *PLD1*. This allowed us to expand the phenotypic spectrum of *PLD1*-associated congenital heart defects and, for the first time to our knowledge, provide evidence that recessive variants in *PLD1* can also cause neonatal cardiomyopathy in the absence of congenital heart defects. We demonstrated that the identified missense variants cause a drastic reduction in the catalytic activity of *PLD1*. By means of pharmacological inhibition of *PLD1* and by siRNA knockdown of *PLD1* in chick embryo AVC explants, we demonstrated that *PLD1* was required for EndoMT, an established pivotal early step in valvulogenesis.

Patients with autosomal-recessive variants in *PLD1* predominantly presented with nonsyndromic congenital cardiac valve malformations, primarily affecting the right side of the heart. Specifically, most patients were diagnosed with tricuspid and/or pulmonary valve abnormalities in combination with a hypoplastic right ventricle and hypoplastic pulmonary arteries. While this is in line with the previous report on 2 families with individuals who had PLD1-related autosomal-recessive congenital heart disease (3), in this study, we also identified 5 patients with autosomal-recessive variants in *PLD1* who were diagnosed with Ebstein's anomaly. Of note, thus far, the genetic underpinnings of Ebstein's anomaly have remained obscure, with only variants in 2 genes, *MYH7* (24) and *NKX2*-5 (25), being associated with this defect through a candidate-based approach. We further expanded the phenotypic spectrum of *PLD1*-related disease, as we also identified 2 patients with *PLD1* biallelic variants who were diagnosed with severe neonatal cardiomyopathy in the absence of congenital heart defects. Similar to the congenital heart disease cases, both patients with cardiomyopathy carried biallelic variants in *PLD1* that are expected to result in severe loss of enzymatic activity. The mechanism underlying this pleiotropic effect of *PLD1* loss of function, resulting in either valvular heart defects or isolated cardiomyopathy, is currently unknown. It may comprise compensatory mechanisms entailing, among others, modulatory genetics factors, conditions in utero, and stochastic factors. The identification of bialellic *PLD1* variants in additional patients with cardiomyopathy in the future will provide further support of causality for this specific phenotype and may enable insights into the underlying mechanism.

Our study robustly implicates recessive genetic variation in *PLD1* as a cause of severe cardiac disease. It is expected that consideration of *PLD1* as a disease gene will enable reproductive counseling and preimplantation genetic screening in affected families. Although not all parents or siblings carrying a *PLD1* variant in the heterozygous state underwent echocardiography, none of them was reported to be clinically affected, suggesting that heterozygous carriers are not at risk for severe congenital heart disease or cardiomyopathy. Notably, in 3 families of Ashkenazi Jewish ancestry, congenital heart defects were caused by homozygosity for the same *PLD1* variant, namely p.I668F, which has a MAF of approximately 2% in this ethnic group. By means of haplotype analysis, we demonstrated that in these 3 families, this variant was inherited from a common ancestor, establishing it as a founder variant in this ethnic group. As this variant is estimated to occur homozygously in up to approximately 1 of 2500 births among Ashkenazi Jews, this finding has clinical implications for assessing the risk of congenital heart defects among individuals of this ancestry (12). As a comparison, a recessive founder variant in *GDF1* (MAF of ~0.9% in the Ashkenazi Jewish subpopulation in gnomAD) was recently found to account for approximately 5% of severe congenital heart defects in Ashkenazi Jews (9). Carriership testing

for these variants could potentially be used in population-based preconception and prenatal carrier screening to assess the risk of congenital heart defects among descendants of Ashkenazi Jews.

We showed that *PLD1* missense variants localized primarily to sites important for catalytic site integrity on the 3D crystal structure of *PLD1*. Concordantly, we demonstrated that 17 of 19 missense variants led to a drastic reduction in the catalytic activity of PLD1 in an enzymatic assay. Two missense variants, p.E6K (in family C) and p.E290Q (in family M), found in the compound heterozygous state with other variants, showed full PMA-stimulated enzymatic activity. The exact role of these 2 variants in determining the congenital heart defect phenotype in combination with the mutant allele in *trans* is unclear. Both variants were found once in the homozygous state in approximately 140,000 individuals included in gnomAD (11), which could suggest that these variants do not contribute to the disease or that they are associated with a less severe loss-of-function defect. It should be noted, however, that our enzymatic assay relied on PMA-induced PKC activation of PLD1, and one could hypothesize that these variants might impact stimulation through a different activator (e.g., PLD1 is also stimulated by the Arf and Rho small GTPases at distinct sites on the PLD1 protein, ref. 16) or could alter the subcellular localization or interaction of PLD1 with a downstream effector. Furthermore, we cannot exclude the possibility that the 2 individuals homozygous for these variants in gnomAD were clinically affected, as phenotypic information was not available.

The observation that 10 of 31 variants identified are expected to result in protein truncation suggests that a loss-of-function mechanism underlies the observed cardiac defects. This is further supported by the observations that PLD1 enzymatic activity is drastically reduced by the missense variants and that either pharmacological inhibition or siRNA knockdown of PLD1 in AVC explants inhibited EndoMT. Mechanisms whereby loss of PLD1 activity leads to right-sided AV valve defects could entail established crosstalk between PLD1 signaling and TGF-β signaling (26). In the developing heart, TGF-β signaling is crucial for the EndoMT that generates the mesenchyme of the cardiac cushions essential for valve formation (27, 28). In the adult heart, loss of PLD1 can lead to a reduction in TGF-β signaling activity in the context of myocardial infarction (MI) (29), suggesting that PLD1 acts upstream of TGF-β signaling. The hearts subjected to myocardial infarction had decreased NF-κB signaling, which is known to be induced by TGF-β (30), and is required for EndoMT in vitro (31). Intriguingly, NF-κB signaling driven by PLD activity can form an autoregulatory loop that promotes PLD1 expression (32). Downstream mechanisms may also involve sonic hedgehog (Shh) expression, which can be stimulated by TGF-β signaling (33, 34). Shh maintains secondary heart field cell proliferation, a requirement for normal arterial pole formation (35). Inhibition of Shh signaling at this developmental stage leads to pulmonary atresia. Thus, a reduction in TGF-β and SSh signaling resulting from loss-of-function *PLD1* variants might underlie the arterial pole defects seen in affected patients.

In the endocardial cushions, EndoMT provides the mesenchymal cells and remodeled matrix essential for the formation of both left and right heart structures, with the inflow cushions contributing to the mitral and tricuspid valves and the outflow cushions

contributing to the pulmonary and aortic valves. This "sidedness" offers unique environments with respect to cell populations, extracellular matrix, and hemodynamics, where the mesenchymal cells are instructed in the formation of left- and right-specific structures. These differing contexts may underlie the susceptibility of the right side of the heart to loss of PLD1 activity. In this scenario, cells contributing to the right side of the heart may be less able in this environment to compensate for the disruption of EndoMT in the common cushions. Although no overt structural cardiac defects were noted, mice lacking PLD1 (36) displayed impaired function of the pulmonary and tricuspid valves on echocardiography (3). The mechanism behind the apparent discrepancy in phenotypic severity in humans versus mice is unknown. A potential explanation might involve a compensatory mechanism through upregulation of genes that are able to offset the diminished or loss of function of the mutated PLD1 (37, 38).

In conclusion, we have expanded the phenotypic spectrum of *PLD1*-associated congenital heart defects and provide evidence that recessive variants in *PLD1* can also cause neonatal cardiomyopathy in the absence of congenital heart defects. We show that p.I668F is a recessive founder variant among the Ashkenazi Jews. We demonstrated that missense variants in *PLD1* predominantly resulted in a strong enzymatic loss of function and that PLD1 is implicated in EndoMT, an established pivotal early step in valvulogenesis, providing a possible mechanism whereby loss of PLD1 function may have led to the cardiac defects observed in the patients studied here. Together, these data provide an increased understanding of disease mechanisms and phenotypic expression associated with genetic defects in *PLD1*.

Methods

Case recruitment and DNA sequencing. The index patient in family A was enrolled at the Amsterdam UMC in Amsterdam, the Netherlands. Family B was identified among 75 unrelated patients with severe right-sided valvular congenital heart disease (i.e., tricuspid atresia or stenosis, Ebstein's anomaly, or pulmonary atresia) from the National Registry and DNA bank of congenital heart defects (CONCOR) (7) in the Netherlands. We subsequently used GeneMatcher (4) and an analysis of 2643 congenital heart disease trios (i.e., the affected patient and both parents) from the PCGC who underwent WES (8, 9) to identify other patients with biallelic variants in *PLD1*. Details on case recruitment and next-generation sequencing methods for each family can be found in the Supplemental Methods. Genetic variants were submitted to the NCBI's ClinVar database (www.ncbi.nlm.nih.gov/clinvar/), and the following accession number was obtained: SUB9058450.

cDNA analysis of the c.3000+2T>A PLD1 splicing variant and the proband carrying p.G826R/p.G910V. Total RNA was isolated from PBMCs using TRIzol solution (Thermo Fisher Scientific). RNA concentrations were determined spectrophotometrically at A260 nm by NanoDrop (NanoDrop Technologies), and RNA quality was verified using an Agilent 2100 Bioanalyzer – RNA Lab-On-a-Chip (Agilent Technologies). Aliquots of isolated RNA were stored at −80°C until analysis. First-strand cDNA synthesis was carried out using an oligo-dT primer and SuperScript III Reverse Transcriptase (Thermo Fisher Scientific). *PLD1* cDNA was PCR amplified from the synthesized first-strand cDNA using oligonucleotide primers (Generi Biotech) designed to span and amplify the variant-bearing PLD1

77

sequence. The resultant PCR products were analyzed using agarose gel electrophoresis. Individual DNA fragments were extracted from gel slices using the PureLink Quick Gel Extraction Kit (Thermo Fisher Scientific) and sequenced by direct Sanger sequencing as described above. The p.G826R/p.G910V cDNA was subcloned into pcDNA3.1 (Invitrogen, Thermo Fisher Scientific) and Sanger sequenced to determine whether the variants were on the same strand.

Plasmid constructs, cell line, and transfections. We purchased a human *PLD1* cDNA clone (BC068976) set in a pGEM-T plasmid (Sino Biological). The clone was fully sequence verified and contained no nucleotide changes. Variants were introduced using site-directed mutagenesis (Q5, New England BioLabs), and the mutant constructs were fully verified by sequencing. Next, the WT and mutant cDNA clones were subcloned into a pcDNA3.1(+) vector for expression and sequence verified. The COS7 cells were cultured according to standard methods. Transfections were performed using polyethylenimine (PEI) in a plasmid to a PEI ratio of 1:4.

In vitro cellular PLD activity. Enzymatic activity was measured on the basis of the ability of PLD1 to catalyze a transphosphatidylation reaction using 1-butanol to generate phosphatidylbutanol (39). Human embryonic kidney 293T (HEK293T) cells were incubated overnight in a 6-well plate and transfected in full media the next day with PLD1 expression plasmids using Fugene (Promega). After overnight transfection for 12–16 hours, the cells were labeled with [^{3}H]-palmitate (ART 129, American Radiolabeled Chemicals) and cultured for 24 hours. The radiolabeled media were then replaced with Opti-MEM and the cells cultured for 1–2 hours prior to the addition of 0.3% butanol and 100 nM PMA. After 30 minutes, cold methanol was added to stop the reaction, and the lipids were extracted and dried using a speed vacuum and then resuspended in chloroform/methanol (19:1) containing 50 μg nonradiolabeled phosphatidylbutanol (Avanti Polar Lipids) to enable location of the labeled enzymatic product on TLC plates (LK5DF, Whatman, MilliporeSigma). The plates were then developed as previously described (39), and the lipids were visualized using iodine flakes (MilliporeSigma) and scraped into 5 mL scintillation fluid for quantification. In these studies, we used PLD1-K898R as a baseline control. K898 is located in the second of 2 highly conserved HKD motifs (Figure 1B and ref. 15) that constitute key functional elements of the 2 halves of the assembled core catalytic site (16, 40, 41). A representative experiment showing the production of phosphatidylbutanol (PtdBut) by the WT allele and the absence of its production by the fully inactive K898R allele is shown in Supplemental Figure 4. A limited amount of PtdBut production was observed in the K898R sample, which derives from the small amounts of endogenous WT PLD1 and PLD2 present in the cell line used for the transfections. The percentage of activity of mutant proteins was determined in comparison with the overexpressed WT PLD1 activity after subtraction from the baseline activity observed with the fully inactive K898R mutant allele.

Western blot analysis. HEK293T cells were transfected with 2.5 μg mutant HA-tagged PLD1 or WT PLD1 per well in a 6-well plate using Fugene (Promega). After 24–48 hours, the cells were collected in 60 L homogenization buffer (1 mM DTT, 1 mM EDTA, and 0.1 mM PMSF in PBS) per well and sonicated using a microtip sonicator at the lowest setting. Lysate (10 μL) plus 10 μL SDS-PAGE loading buffer containing 8 M urea were combined and loaded onto an acrylamide gel for electrophoresis and transfer onto a nylon membrane. The PLD1 protein generated from the transfected expression vector was detected

using a monoclonal anti-HA antibody (3F10, MilliporeSigma), followed by secondary goat anti–rat antisera coupled to an infrared dye (IR800, Thermo Fisher Scientific). Images were recorded and bands quantitated using the Odyssey CLx System (LI-COR).

In vitro collagen gel assay. Collagen gel assays (see ref. 21) with siRNA or small molecule additions were performed as described previously (42). siRNA-knockdown experiments have been described elsewhere (43). Briefly, AVCs were excised from stage 16 chick embryo hearts and collected in M199 medium (Mediatech) at room temperature for each experimental condition. For transfection, 4 μL siPORT NeoFX (Ambion) was incubated in a final volume of 100 μL M199 for 10 minutes at room temperature. Next, the appropriate final concentration (for 300 μL total volume) of the siRNA was added to a final volume of 100 μL. These 2 tubes were mixed and incubated for 15 minutes at room temperature to allow complexes to form. The 200 μL mixture was then added to the 100 μL containing AVCs, and this solution was incubated at 37°C, 5% CO_2 for 45 minutes. Explants were then placed endothelial side down on collagen gels (1.86 mg/mL) and incubated under the same conditions for 48 hours prior to fixation (0.8% formaldehyde, 0.05% glutaraldehyde for 5 minutes at room temperature). Controls for siRNA toxicity were randomized genomic DNA base pair composition-matched (%GC base pair matched) constructs that did not correspond to any sequence in the chick genome. The following antisense strand siRNAs were used: PLD1-A, antisense strand siRNA, AUGGUGUA-CACGUUGAGGCtt and PLD1-B, antisense strand siRNA, CUUAG-CGUUCACAUACCACtt. The positive control was an siRNA targeting *Tgfbr3* (44). For experiments using small-molecule inhibitors, AVCs were harvested and placed endothelial side down on collagen gels in the presence of the indicated molecule concentrations. Explants were incubated for 48 hours prior to fixation as above. After incubation, EndoMT was quantified by counting the number of cells with mesenchymal morphology that invaded the collagen gel.

PCA to define the ancestry of PCGC congenital heart disease cases. PCAs were performed in PLINK 2.0 (45) on the WES PCGC cases, as previously described (46), using data from the 1000 Genomes populations (Phase 3v5) and on the Ashkenazi Jewish individuals from the NCBI's Gene Expression Omnibus (GEO) database (GEO GSE23636; ref. 12) as a reference. To increase the genetic overlap with the WES PCGC cases and the 1000 Genomes populations, we performed genome-wide imputation using Eagle2 phasing, Minimac3, and the Haplotype reference consortium (HRCr1.1) panel implemented on the Michigan Imputation Server for the data set for Ashkenazi Jewish individuals. After imputation, we performed stringent genetic quality control using hard genotype calls after imputation (genotype probability >0.9) and restricted to variants with an imputation score above 0.8. We excluded variants with a genotype missingness greater than 0.01, a Hardy-Weinberg equilibrium test at a *P* value of less than 0.05, a phenotype-biased missing test at a *P* value of less than 0.05, and a MAF of less than 0.05. Downstream analyses were conducted in R, version 3.4.3.

Haplotype analysis and variant dating. Haplotypes were generated using WES data. Estimation of the p.I668P variant age was conducted using the Gamma method (13). This method uses the genetic length of ancestral haplotypes shared between individuals carrying the variant and has as a major advantage that it can be reliably applied to small samples with high-density SNP data.

78

Statistics. All error bars represent the SEM. Comparisons between 2 groups were performed using the 2-tailed Student t test for normally distributed continuous variables, the Mann-Whitney U test for non-normally distributed continuous variables, and the χ^2 or Fisher's exact test, as suitable, for categorical variables. A P value of less than 0.05 was considered significant. For multiple comparisons, Bonferroni's correction for multiple testing was applied. Statistical analyses were performed with GraphPad Prism (version 7.02, GraphPad Software) and R (version 4.0.0).

Study approval. The study protocol was approved by the local IRBs where the patients were followed, and signed informed consent was obtained from the patients or their parents. The IRBs' institutions and locations are as follows: family A: Amsterdam UMC, Amsterdam, the Netherlands; family B: National Registry and DNA bank of congenital heart defects, the Netherlands; family C: Bambino Gesù Children's Hospital IRCCS, Rome, Italy; family D: The Cyprus Institute of Neurology and Genetics, Nicosia, Cyprus; family E: Charles University and General University Hospital, Prague, Czech Republic; family F: University of Minnesota, Minneapolis, Minnesota, USA; family G, N, and O: Hebrew University Medical Center, Jerusalem, Israel. family P: UPMC Children's Hospital of Pittsburgh, Pittsburgh, Pennsylvania, USA; family Q: Université Bourgogne-Franche Comté, Dijon, France; family R: University of Groningen, University Medical Center Groningen, Groningen, the Netherlands; family S: D Ann & Robert H. Lurie Children's Hospital of Chicago, Illinois, USA; family T: Leiden University Medical Center, Leiden, the Netherlands; and family U: Ochsner Clinic Foundation, New Orleans, Louisiana, USA. Families H–M were recruited to the Congenital Heart Disease Network Study of the Pediatric Cardiac Genomics Consortium (CHD GENES: ClinicalTrials.gov identifier NCT01196182), and the study protocol was approved by the local IRB.

Author contributions

CRB, MAF, and NL designed and supervised the study. NL and MAF compiled results, wrote the manuscript, and prepared all the figures. NL, VS, and DZ performed sequencing data analysis. NL, SAC, FT, DSM, ATS, ZP, JYR, SCB, HM, MA, TM, JJ, DMN, AR, AAK, GT, BAL, ADJTH, CF, DO, GTRM, ACD, KB, MM, FCR, MH, MCH, ADJTH, BM, SK, GWES, JCH, VT, OE, BW, ASDP, KHK, and SC recruited patients and gathered detailed clinical information for the study. NL and SAB reviewed and summarized patients' characteristics. PDK and RDL performed multiplex PCR sequencing followed by NGS in patient 1 from family A. ACD performed the autopsy of a patient. CMS performed the Western blots and PLD activity and localization assays. NL, AVP, and EML performed haplotype analyses. NL performed PCAs. MH and QG assessed PLD1-knockout hearts. MAF was involved in experimental design and manuscript preparation. MVA and FZB analyzed the PLD1-mutant structural data. DMDL, JYR, and JVB performed and analyzed the explant assays. SK and LP performed RT-PCR analysis of mRNA. LB and AI generated PLD1-mutant plasmids. All the authors read and agreed on the final draft of the manuscript. The order of the co–first authors was assigned on the basis of their relative contributions to the study.

Address correspondence to: Connie R. Bezzina or Najim Lahrouchi, Amsterdam UMC, AMC Heart Center, Department of Clinical and Experimental Cardiology, Meibergdreef 9, 1105 AZ Amsterdam, Netherlands. Phone: 31.20.566.5403; Email: c.r.bezzina@amsterdamumc.nl (CRB); n.lahrouchi@amsterdamumc.nl (NL). Or to: Michael A Frohman, Department of Pharmacological Sciences, 438 CMM, Stony Brook University, Stony Brook, New York 11794, USA. Phone: 631.632.1476; Email: Michael.Frohman@stonybrook.edu.

1. Dolk H, et al. Congenital heart defects in Europe: prevalence and perinatal mortality, 2000 to 2005. *Circulation*. 2011;123(8):841–849.
2. Nelson RK, Frohman MA. Physiological and pathophysiological roles for phospholipase D. *J Lipid Res*. 2015;56(12):2229–2237.
3. Ta-Shma A, et al. Congenital valvular defects associated with deleterious mutations in the *PLD1* gene. *J Med Genet*. 2017;54(4):278–286.
4. Sobreira N, et al. GeneMatcher: a matching tool for connecting investigators with an interest in the same gene. *Hum Mutat*. 2015;36(10):928–930.
5. Bowling FZ, et al. Crystal structure of human PLD1 provides insight into activation by PI(4,5)P$_2$ and RhoA. *Nat Chem Biol*. 2020;16(4):400–407.
6. Barnett JV, Desgrosellier JS. Early events in valvulogenesis: a signaling perspective. *Birth Defects Res Part C Embryo Today Rev*. 2003;69(1):58–72.
7. Vander Velde ET, et al. CONCOR, an initiative towards a national registry and DNA-bank of patients with congenital heart disease in the Netherlands: rationale, design, and first results. *Eur J Epidemiol*. 2005;20(6):549–557.
8. Gelb B, et al. The Congenital Heart Disease Genetic Network Study: rationale, design, and early results. *Circ Res*. 2013;112(4):698–706.

9. Jin SC, et al. Contribution of rare inherited and de novo variants in 2,871 congenital heart disease probands. *Nat Genet*. 2017;49(11):1593–1601.

10. van der Palen RLF, et al. Uhl's anomaly: clinical spectrum and pathophysiology. *Int J Cardiol*. 2016;209:118–121.

11. Karczewski KJ, et al. The mutational constraint spectrum quantified from variation in 141,456 humans. *Nature*. 2020;581(7809):434–443.

12. Bray SM, et al. Signatures of founder effects, admixture, and selection in the Ashkenazi Jewish population. *Proc Natl Acad Sci U S A*. 2010;107(37):16222–16227.

13. Gandolfo LC, et al. Dating rare mutations from small samples with dense marker data. *Genetics*. 2014;197(4):1315–1327.

14. Sung TC, et al. Structural analysis of human phospholipase D1. *J Biol Chem*. 1999;274(6):3659–3666.

15. Hammond SM, et al. Human ADP-ribosylation factor-activated phosphatidylcholine-specific phospholipase D defines a new and highly conserved gene family. *J Biol Chem*. 1995;270(50):29640–29643.

16. Sung TC. Mutagenesis of phospholipase D defines a superfamily including a trans-Golgi viral protein required for poxvirus pathogenicity. *EMBO J*. 1997;16(15):4519–4530.

17. Sung TC, et al. Structural analysis of human phospholipase D1. *J Biol Chem*. 1999;274(6):3659–3666.

18. Du G, et al. Regulation of phospholipase D1 subcellular cycling through coordination of multiple membrane association motifs. *J Cell Biol*. 2003;162(2):305–315.

19. Vitale N, et al. Phospholipase D1: a key factor for the exocytotic machinery in neuroendocrine cells. *EMBO J*. 2001;20(10):2424–2434.

20. Sugars JM, et al. Fatty acylation of phospholipase D1 on cysteine residues 240 and 241 determines localization on intracellular membranes. *J Biol Chem*. 1999;274(42):30023–30027.

21. DeLaughter DM, et al. What chick and mouse models have taught us about the role of the endocardium in congenital heart disease. *Birth Defects Res A Clin Mol Teratol*. 2011;91(6):511–525.

22. Lavieri RR, et al. Design, synthesis, and biological evaluation of halogenated N-(2-(4-oxo-1-phenyl-1,3,8-triazaspiro[4.5]decan-8-yl)ethyl) benzamides: discovery of an isoform-selective small molecule phospholipase D2 inhibitor. *J Med Chem*. 2010;53(18):6706–6719.

23. Bassing CH, et al. A transforming growth factor beta type I receptor that signals to activate gene expression. *Science*. 1994;263(5143):87–89.

24. Postma AV, et al. Mutations in the sarcomere gene MYH7 in Ebstein anomaly. *Circ Cardio vasc Genet*. 2011;4(1):43–50.

25. Benson DW, et al. Mutations in the cardiac transcription factor NKX2.5 affect diverse cardiac developmental pathways. *J Clin Invest*. 1999;104(11):1567–1573.

26. Piazza GA, et al. Lysophosphatidic acid induction of transforming growth factors α and β: modulation of proliferation and differentiation in cultured human keratinocytes and mouse skin. *Exp Cell Res*. 1995;216(1):51–64.

27. Xu J, et al. TGF-β-induced epithelial to mesenchymal transition. *Cell Res*. 2009;19(2):156–172.

28. Gise A von, Pu WT. Endocardial and epicardial epithelial to mesenchymal transitions in heart development and disease. *Circ Res*. 2012;110(12):1628.

29. Schönberger T, et al. Pivotal role of phospholipase D1 in tumor necrosis factor-α-mediated inflammation and scar formation after myocardial ischemia and reperfusion in mice. *Am J Pathol*. 2014;184(9):2450–2464.

30. Sakurai H, et al. Functional interactions of transforming growth factor β-activated kinase 1 with IκB kinases to stimulate NF-κB activation. *J Biol Chem*. 1999;274(15):10641–10648.

31. DeLaughter DM, et al. Spatial transcriptional profile of the chick and mouse endocardial cushions identify novel regulators of endocardial EMT in vitro. *J Mol Cell Cardiol*. 2013;59:196–204.

32. Kang DW, et al. Autoregulation of phospholipase D activity is coupled to selective induction of phospholipase D1 expression to promote invasion of breast cancer cells. *Int J Cancer*. 2011;128(4):805–816.

33. Javelaud D, et al. TGF-β/SMAD/GLI2 signaling axis in cancer progression and metastasis. *Cancer Res*. 2011;71(17):5606–5610.

34. Dennler S, et al. Induction of sonic hedgehog mediators by transforming growth factor-β: Smad3-dependent activation of Gli2 and Gli1 expression in vitro and in vivo. *Cancer Res*. 2007;67(14):6981–6986.

35. Dyer LA, Kirby ML. Sonic hedgehog maintains proliferation in secondary heart field progenitors and is required for normal arterial pole formation. *Dev Biol*. 2009;330(2):305–317.

36. Elvers M, et al. Impaired α(IIb)β(3) integrin activation and shear-dependent thrombus formation in mice lacking phospholipase D1. *Sci Signal*. 2010;3(103):ra1.

37. El-Brolosy MA, et al. Genetic compensation triggered by mutant mRNA degradation. *Nature*. 2019;568(7751):193–197.

38. Ma Z, et al. PTC-bearing mRNA elicits a genetic compensation response via Upf3a and COMPASS components. *Nature*. 2019;568(7751):259–263.

39. Morris AJ, et al. Measurement of phospholipase D activity. *Anal Biochem*. 1997;252(1):1–9.

40. Leiros I, et al. The first crystal structure of a phospholipase D. *Structure*. 2000;8(6):655–667.

41. Dixon JE, Stuckey JA. Crystal structure of a phospholipase D family member. *Nat Struct Biol*. 1999;6(3):278–284.

42. Townsend TA, et al. Endocardial cell epithelial-mesenchymal transformation requires Type III TGFβ receptor interaction with GIPC. *Cell Signal*. 2012;24(1):247–256.

43. Townsend TA, et al. Transforming growth factor-beta-stimulated endocardial cell transformation is dependent on Par6c regulation of RhoA. *J Biol Chem*. 2008;283(20):13834–13841.

44. Townsend TA, et al. BMP-2 and TGFβ2 shared pathways regulate endocardial cell transformation. *Cells Tissues Organs*. 2011;194(1):1–12.

45. Chang CC, et al. Second-generation PLINK: rising to the challenge of larger and richer datasets. *Gigascience*. 2015;4(1):7.

46. Belkadi A, et al. Whole-exome sequencing to analyze population structure, parental inbreeding, and familial linkage. *Proc Natl Acad Sci U S A*. 2016;113(24):6713–6718.

80

Genetic architecture of recent-onset dilated cardiomyopathy in Moravian region assessed by whole-exome sequencing and its clinical correlates

Anna Chaloupka[a], Lenka Piherova[b], Ilga Grochova[a], Jana Binova[c], Jan Krejci[a], Lenka Spinarova[a], Viktor Stranecky[b], Stanislav Kmoch[b], Milos Kubanek[c]

Aims. Recent-onset dilated cardiomyopathy (RODCM) is a disease of heterogeneous aetiology and clinical outcome. In this pilot study, we aimed to assess its genetic architecture and correlate genotype with left ventricular reverse remodelling (LVRR).
Patients and Methods. In this multi-centre prospective observational study, we enrolled 83 Moravian patients with RODCM and a history of symptoms of less than 6 months, for whole-exome sequencing (WES). All patients underwent 12-month clinical and echocardiographic follow-up. LVRR was defined as an absolute increase in left ventricular ejection fraction > 10% accompanied by a relative decrease of left ventricular end-diastolic diameter > 10% at 12 months.
Results. WES identified at least one disease-related variant in 45 patients (54%). LVRR occurred in 28 patients (34%), most often in carriers of isolated titin truncated variants, followed by individuals with a negative, or inconclusive WES and carriers of other disease-related variants (56% vs. 42% vs. 19%, P=0.041).
Conclusion. A substantial proportion of RODCM cases have a monogenic or oligogenic genetic background. Carriers of non-titin disease-related variants are less likely to reach LVRR at 12- months than other individuals. Genetic testing could contribute to better prognosis prediction and individualized treatment of RODCM.

Key words: dilated cardiomyopathy, familial cardiomyopathy, next generation sequencing, genetic architecture, cardiac remodelling

[a]1st Internal Clinic of Cardio-angiology, St. Anne's University Hospital and Faculty of Medicine, Masaryk University, Brno, Czech Republic
[b]Research Unit for Rare Diseases, Department of Paediatrics and Adolescent Medicine, 1st Faculty of Medicine, Charles University, Prague, Czech Republic
[c]Department of Cardiology, Institute for Clinical and Experimental Medicine, Prague, Czech Republic.
Corresponding author: Anna Chaloupka, e-mail: anna.chaloupka@fnusa.cz

INTRODUCTION

Dilated cardiomyopathy (DCM) is a prevalent disease leading to chronic heart failure (CHF). It has a heterogeneous aetiology including genetic, inflammatory, toxic and metabolic causes[1,2]. The clinical diagnosis of DCM is based on the presence of left ventricular (LV) systolic dysfunction in the absence of abnormal loading conditions or significant coronary artery disease sufficient to cause global systolic impairment[2,3]. In routine practice, the aetiology of DCM remains often unexplained due to incomplete assessment of family history or recognition of clinical red-flags, suggesting genetic etiology[4]. In addition, potentially reversible causes of DCM like myocarditis and toxic injury may be undiagnosed due to insufficient accuracy of non-invasive diagnostic tools to confirm myocarditis, or concealed history of alcohol, or drug abuse[5,6].

An ultimate diagnostic and prognostic challenge are patients with recent-onset DCM (RODCM) who may have variable clinical outcomes ranging from complete recovery of LV systolic dysfunction to rapid progression to end-stage CHF or sudden cardiac death[7]. Importantly, left ventricular reverse remodelling (LVRR), defined as a partial improvement of LV systolic function accompanied by reduction of LV volumes, has been identified as a marker of favourable prognosis in RODCM (ref.[8-10]). LVRR may indicate either the beneficial effect of pharmacotherapy, disappearance of myocardial toxic or inflammatory insult. Due to the permanent character of myocardial damage, LVRR should be less prevalent in genetic forms of DCM (ref.[7,11]).

Tremendous advances have been made in understanding the genetic basis of DCM over the last 30 years. To date, hundreds of mutations in more than 40 genes encoding proteins with various cellular functions have been identified as causing DCM (ref.[12-14]). The predominating molecular cause seem to be truncating titin variants, responsible for almost a quarter cases of familial DCM (ref.[14]). Most familial forms of DCM are monogenic disorders, most commonly with autosomal dominant inheritance[15,16]. Some genotypes like mutations of *LMNA*, *PLN*, and *RBM20* have been associated with severe forms of CHF and / or malignant ventricular arrhythmias[17-19]. Cardiomyopathy gene panels are usually used in clinical settings to screen the most common disease-causing genes. Discovery of next-generation sequencing (NGS) enables us to screen whole protein-coding genome (exome) in a timely and cost-effective way and thus substantially increase mutation detection in both sporadic and familial cases of DCM (ref.[20]). Recognition of the genetic com-

ponent, particularly in patients with RODCM or their asymptomatic relatives, could improve risk stratification and thus diagnostic and therapeutic management.

The above formed the motivation for deciding to assess the genetic architecture of RODCM with whole-exome sequencing (WES), and to study the genotype-phenotype correlates. Specifically, we wanted to analyse the relationship between the results of WES and left ventricular reverse remodelling. The analysis was designed as a pilot study of the first WES results derived from a large project of WES in RODCM.

MATERIALS AND METHODS

Patients and study design

Patients were recruited in the Department of 1st Internal Cardio-angiology, St. Anne's University Hospital in Brno, Czech Republic. This multi-centre prospective observational study was approved by the Institutional Ethics Committee at all respective participating institutions and all patients signed the written informed consent. All clinical, genomic data and samples were independently anonymized and stored in secured local databases according to the provisions of the Czech data protection authority (www.uoou.cz) and in accordance with Act 373/2011 Sb (§28-29). We prospectively enrolled 83 con-

Table 1. Patient characteristics.

Variable	Baseline (n=83)	12-month follow-up (n=83)
Age [years]	48 (40-56)	-
Gender (males/females)	68 (82%)	-
	15 (18%)	
Arterial hypertension	33 (40%)	-
Diabetes mellitus	10 (12%)	-
Positive family history of DCM	14 (17%)	-
NYHA class	I – 3 (4%)	I – 22 (26%)
	II – 40 (48%)	II – 44 (53%)
	III – 39 (47%)	III – 17 (21%)
	IV – 1 (1%)	IV – 0 (0%)
Systolic BP [mmHg]	120 (115-130)	128 (115-145)
Diastolic BP [mmHg]	80 (75-87)	87 (80-95)
Heart rate [bpm]	80 (69-90)	70 (60-80)
Sinus rhythm	82 (99%)	80 (96%)
QRS duration [ms]	100 (80-120)	108 (100-129)
LVEDD [mm]	65 (60-70)	61 (55-67)
LVEDV [mL]	214 (179-260)	187 (153-237)
LVEF [%]	25 (17-30)	35 (27-45)
E/Em	13 (10-19)	9 (7-11)
Left atrium (PLAX) [mm]	45 (42-49)	42 (37-46)
RVEDD (PLAX) [mm]	34 (30-38)	32 (28-35)
TAPSE [mm]	18 (16-21)	21 (18-24)
RV Sm [cm/s]	10 (9-12)	13 (11-15)
ACEi	63 (76%)	73 (88%)
ARB	6 (7%)	10 (12%)
Equivalent dose of ACEi or ARB ≥ 50%	25 (30%)	39 (47%)
Beta-blockers	74 (89%)	83 (100%)
Equivalent dose of betablockers ≥ 50%	14 (17%)	27 (32%)
Aldosterone receptor blockers	58 (70%)	66 (79%)
Furosemide	62 (75%)	70 (84%)
Furosemide ≥ 40 mg daily	45 (54%)	46 (55%)
Sodium [mmol/L]	140 (138-142)	141 (139-142) (n=68)
Creatinine [μmol/L]	86 (76-98)	81 (75-91) (n=70)
NT-proBNP [ng/mL]	1664 (751-3232)	446 (109-779) (n=69)

Patient characteristics at baseline and 12-month follow-up. Continuous variables are shown as median and IQR, discrete variables as absolute and relative frequency.
DCM – dilated cardiomyopathy, NYHA class – New York Heart Association class, BP – blood pressure, LVEDD – left ventricular end-diastolic diameter, LVEDV – left ventricular end-diastolic volume, LVEF – left ventricular ejection fraction, PLAX – parasternal long axis, RVEDD – right ventricular end-diastolic diameter, TAPSE – tricuspid annular plane systolic excursion, RV Sm – right ventricular Sm wave, ACEi – angiotensin converting enzyme inhibitor, ARB – angiotensin receptor blocker.

2

secutive patients with recent-onset DCM, specified by a history of heart failure of less than 6 months. DCM was defined in accordance with the ESC definition by the presence of LV dilatation (LVEDD 33mm/m in men and 32 mm/m in women) and LV systolic dysfunction (LVEF < 45%) in the absence of abnormal loading conditions (hypertension, valve disease) or coronary artery disease sufficient to cause global systolic impairment[2]. Other inclusion criteria were age ≥ 18 years and signed informed consent. DCM was considered familial when at least 2 genetically related first-degree relatives were diagnosed with DCM, or in cases of premature sudden cardiac death or CHF in a first-degree relative. Exclusion criteria, except for the already mentioned hypertension, valvular disease and coronary artery disease encompassed proven myocarditis or specific antibiotic, antiviral or immunosuppressive therapy, post-tachycardic, toxic, metabolic or endocrine aetiology, and specific therapy affecting natural ventricular remodelling such as resynchronization therapy and ventricular assist devices.

Initial patient assessment included 3-generation family history, physical examination, ECG, echocardiographic examination, routine blood tests, and collection of 5 mL of noncoagulated peripheral venous blood for molecular genetic testing. All patients received standard heart failure pharmacotherapy. Equivalent doses of angiotensin converting enzyme inhibitors, angiotensin receptor blockers and beta-blockers were expressed as a percentage of the maximum recommended daily dose according to the latest ESC guidelines[1]. All patients were followed-up by clinical examination, ECG, echocardiography and routine blood tests at 12 months, to assess cardiac remodelling. Echocardiography was performed by experienced operators in accordance with the guidelines of the American Society of echocardiography[21,22] – M-mode, 2D images and Doppler recordings were obtained using a Vivid E9 (GE Healthcare, Chalfont St Giles, UK). The LVEF was assessed using Simpson's biplane method.

Patients with a positive genetic screening were invited for genetic counselling by a clinical geneticist and their first-degree relatives were invited for clinical cardiology assessment – ECG, echocardiography, and after signing an informed consent, a gene-specific genetic testing, in line with current recommendations[23]. Table 1 describes the study group characteristics.

Next-generation sequencing (NGS)

Genomic DNA was extracted from peripheral blood samples (EDTA blood) using a standard Qiagen SPE extraction kits. Exome sequencing was performed using 1 µg of DNA from affected individuals. For DNA enrichment of barcoded DNA libraries were used SeqCap EZ MedExome Target Enrichment Kit (Roche, Madison, USA) according to the manufacturer's protocol. DNA sequencing was performed on the captured barcoded DNA library using the Illumina Hiseq 2500 system at the Genomic facility in Motol University Hospital in Prague. The resulting FASTQ files were aligned to the Human Genome Reference (hg19) using Novoalign (3.02.10).

Following genome alignment, conversion of SAM format to BAM and duplicate removal were performed using Picard Tools (1.129). The Genome Analysis Toolkit, GATK (3.3) (ref.[24]) was used for local realignment around indels, base recalibration and variant recalibration and genotyping.

Variant annotation and classification

Variant annotation was performed with SnpEff (ref.[25]) and GEMINI (ref.[26]). Only the sequence having a frequency lower than 0.0005 in the dbSNP, ExAC (http://exac.broadinstitute.org/), gnomAD (http://gnomad.broadinstitute.org/) and our internal exome database were prioritized for further analysis. Identified genetic variants were filtered according to the expected autosomal dominant model of the disease and evaluated according to the biological relevance of the corresponding genes. Candidate variants were visualized in Integrative Genomics Viewer (IGV) – version 2.3.32 (ref.[27]).

Standard variant classification[28] was adopted according to the guidelines for the interpretation of sequence variants[29] dividing variants into 5 groups as 1. Benign, 2. Likely benign, 3. Variants of uncertain significance, 4. Likely pathogenic and 5. Pathogenic. Mutation Taster tool (www.mutationtaster.org) (ref.[30]) was used to evaluate the disease-causing potential of the sequence variants and only variants in group 5. pathogenic, 4. likely pathogenic, and selected 3. variants of unknown significance where Mutation Taster predicted pathogenic variant were considered to be disease-related, the remaining variants were classified as non-significant.

Cardiology assessment and gene-specific testing in first-degree relatives

All patients with positive genetic results were invited by letter for genetic counselling by a clinical geneticist and their first-degree relatives were invited for clinical cardiology assessment – ECG, echocardiography, and after signing an informed consent, a gene-specific genetic testing using Sanger sequencing method to study segregation in families.

Statistical analysis

Categorical data were expressed as percentages and compared using the chi-squared test and Fisher's exact test. Continuous variables were expressed as means (SD) or medians and interquartile range. They were compared using the Student t-test for paired or unpaired data, and by the non-parametric Mann-Whitney test, or Wilcoxon test where appropriate. For all tests, a probability value of $P<0.05$ was considered significant. The data were analysed using statistical software SPSS (Chicago, Illinois, USA) for Windows, version 17.0.

### Genotype-phenotype association analysis

Patients with RODCM were characterized by age, gender, family history of DCM, concomitant diseases, NYHA class, blood pressure and ECG characteristics, pharmacotherapy, laboratory results, and echocardiog-

3

raphy parameters at baseline and at 12-month follow-up. Whole-exome sequencing was carried out for all subjects. LVRR was defined as an absolute increase in left ventricular ejection fraction (LVEF) > 10% accompanied by a relative decrease of left ventricular end-diastolic diameter (LVEDD) >10% at 12-month follow-up. Association with genetic causes and specific gene mutations was examined.

RESULTS

Clinical and genetic screening for familial DCM

In our well-defined cohort of 83 consecutive patients with RODCM (for patient characteristics see Table 1) we found a positive family history of DCM in 14 patients (17%), while 69 patients (83%) appeared to be sporadic
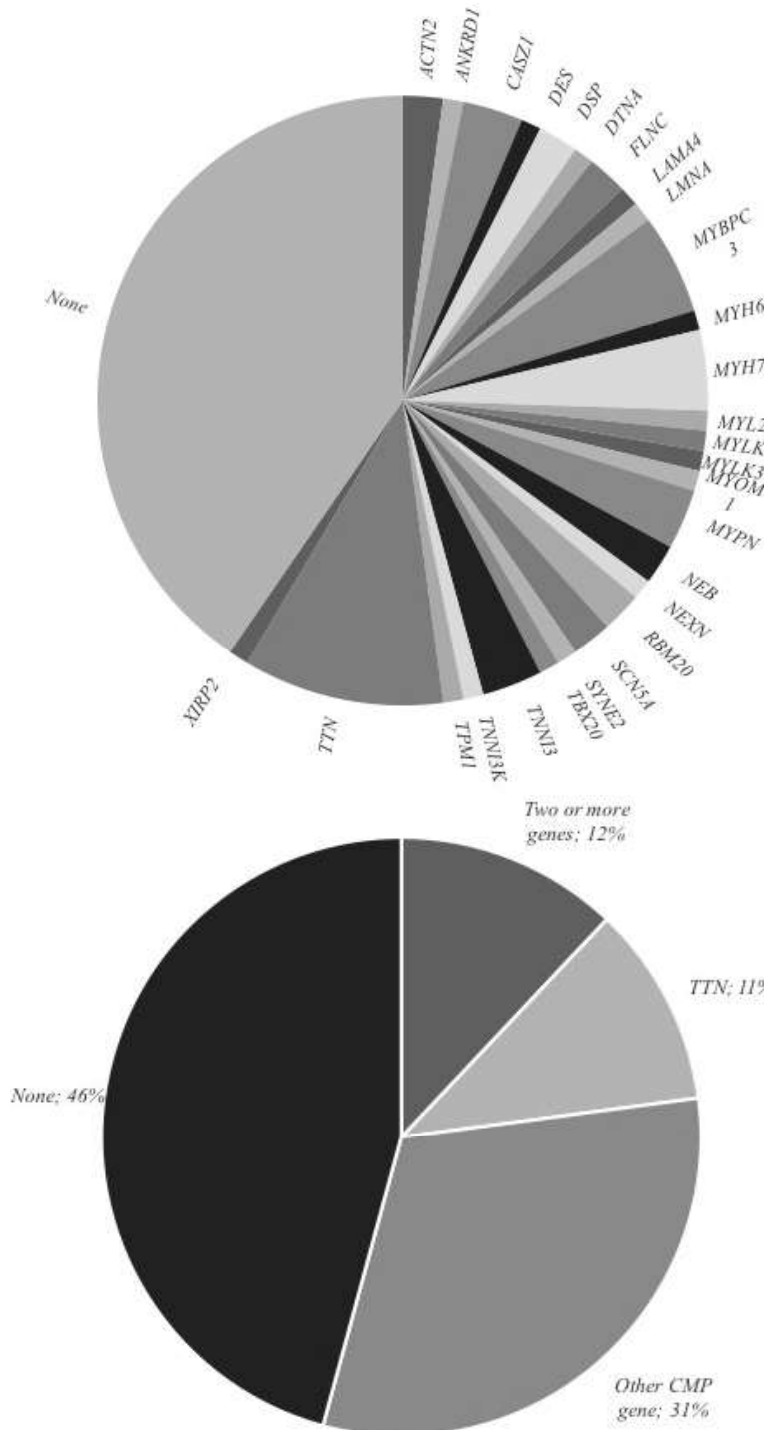
Panel A
Panel A shows gene variant distribution. Only genes with disease-related variants shown, the variants classified as non-conclusive, or where no variants were found are labelled as "None". Abbreviations: *ACTN2* – alpha-actinin 2, *ANKRD1* – ankyrin repeat domain 1, *CASZ1* – castor zinc finger 1, *DES* – desmin, *DSP* – desmoplakin, *DTNA* – dystrobrevin alpha, *FLNC* – filamin C, *LAMA4* – laminin subunit alpha 4, *LMNA* – lamin A/C, *MYBPC3* – myosin binding protein C, *MYH6* – myosin heavy chain 6, *MYH7* – myosin heavy chain 7, *MYL2* – myosin light chain 2, *MYLK* – myosin light chain ligase, *MYLK3* – myosin light chain kinase 3, *MYOM1* – myomesin 1, *MYPN* – myopalladin, *NEB* – nebulin, *NEXN* – nexilin, *RBM20* – RNA-binding protein 20, *SCN5A* – type V voltage-gated cardiac Na channel, *SYNE2* – nesprin, *TBX20* – T-box 20, *TNNI3* – Cardiac troponin I3, *TNNI3K* – Cardiac troponin I3 interacting kinase, *TPM1*- alpha-tropomyosin, *TTN* – titin, *XIRP2* – Xin Actin Binding Repeat Containing 2

Panel B
Panel B illustrates the percentage of RODCM patients divided into 4 categories according to identified variants – none/non-conclusive "*None*", only titin (*TTN*) variant "*TTN*", only other cardiomyopathy-related gene variant "*Other CMP gene*", and ≥ 2 identified disease-related gene variants "*Two or more genes*". Eight patients had variants in 2 genes (*MYPN + MYOM1, MYPN + MYH6, TNNI3 + LAMA4, TNNI3 + MYL2, CASZ1 + TTN, CASZ1 + SCN5A, RBM20 + ACTN2 and DES + LMNA*). In one patient we identified 2 rare variants in *NEB* gene and 1 variant in *DTNA* gene.
Abbreviations: *TTN* – titin, CMP – cardiomyopathy, *ACTN2* – alpha-actinin 2, 1, *CASZ1* – castor zinc finger 1, *DES* – desmin, *DTNA* – dystrobrevin alpha, *LAMA4* – laminin subunit alpha 4, *LMNA* – lamin A/C, *MYH6* – myosin heavy chain 6, *MYL2* – myosin light chain 2, *MYOM1* – myomesin 1, *MYPN* – myopalladin, *NEB* – nebulin, *RBM20* – RNA-binding protein 20, *SCN5A* – type V voltage-gated cardiac Na channel, *TNNI3* – Cardiac troponin I3, *TTN* – titin

Fig. 1. A, B. Gene distribution in RODCM.

4

Příloha 1a

Table 2. Left ventricular reverse remodelling and results of WES.

	Exom negative or non-conclusive (n=38)	Isolated titin truncating mutation (n=9)	Other variant or combination (n=36)	P
12 months Δ LVEF absolute (percent points)	16 (6-23)	15 (9-34)	6 (3-15)	0.036 *
12 months Δ LVEDD relative (%)	-7.7 (-13.4 to 3.7)	-11.3 (-18.9 to -7.1)	-1.5 (-12 to 1.7)	0.086
12 months Δ LVEF > 10 points (n= 44; 53%)	24 (63%)	7 (78%)	13 (36%)	0.019 *
12 months Δ LVEDD < -10% (n= 34; 41%)	18 (47%)	6 (67%)	10 (28%)	0.058
12 months Δ LVEF > 10 points and Δ LVEDD < -10% (n=28; 34%)	16 (42%)	5 (56%)	7 (19%)	0.041*

Relationship between results of whole-exome sequencing and LVRR
n – number, ΔLVEF absolute – absolute change of left ventricular ejection fraction, Δ LVEDD relative – relative change of left ventricular end-diastolic diameter

cases. WES suggested much stronger genetic determination of RODCM than the family history itself. NGS genetic testing uncovered disease-causing pathogenic variants in 45 patients (54%) and only 38 patients (46%) had non-conclusive, or negative genetic result.

Whole-exome sequencing data (WES)

As expected, the gene spectrum of identified variants in RODCM was quite wide (Fig. 1) comprising a total of 28 different genes, with the majority of truncating variants in titin (*TTN*) gene which was found in 10 (12%) patients. Other known cardiomyopathy genes were identified in 26 (31%) of all patients, with most variants in sarcomeric genes – cardiac myosin binding-protein C (*MYBPC3*), beta-myosin heavy chain 7 (*MYH7*), cardiac troponin I3 (*TNNI3*). Other rare variants included genes coding proteins in various myocyte compartments – sarcomere (*MYH6, TPM1, TNNI3K, MYL2, MYL3, MYLK, MYOM1*), Z-disc (*ACTN2, MYPN, NEXN, NEB, ANKRD1*), cytoskeleton (*DES, FLNC*), desmosomes (*DSP*), nuclear envelope (*LMNA, SYNE2*), nucleus (*RBM20, CASZ1, TBX20*), ion channels (*SCN5A*), dystrophin complex (*DTNA*), and extracellular matrix (*LAMA4*). Some of the pathogenic gene variants affected genes which were not previously described as typical DCM genes but were annotated to other cardiomyopathies or affect heart development. A large number of studies suggest the additive effect of several mutations in different genes in a single patient, sometimes dubbed as oligogenic inheritance[28]. In our cohort, 10 patients (12%) had pathogenic variants in ≥ 2 genes.

Fig. 1. A and B pie chart shows gene distribution in RODCM.

Cardiology assessment and gene-specific testing in first-degree relatives

The clinical and genetic cascade screening in families is still ongoing. To date, the family response rate is 23 (48%) for genetic testing and 18 (37.5%) for cardiology assessment. In total, we already assessed 47 first-degree relatives genetically and 35 clinically, the mean was 2 first-degree relatives per patient. Sanger sequencing uncovered 13 (48.1%) family members with positive segregation of the disease-causing variant, all of them were asymptomatic and none of them met the DCM echocardiographic criteria, even though we were able to detect mild changes as grade I diastolic dysfunction and non-specific ECG abnormalities (early repolarization, negative T waves). Cardiology assessment uncovered only 1 patient (2.9%) with DCM who was previously diagnosed and treated, and the gene-specific testing results of this patient are not available yet). In addition, 16 (45.7%) of asymptomatic first-degree relatives showed mild echocardiographic and ECG abnormalities which may precede the development of the disease.

Development of clinical and echocardiographic characteristics at 12 months

We observed a significant improvement in several important clinical characteristics at 12 months of follow-up. Both subjective (NYHA class $P < 0.001$) and objective (NT-proBNP level, $P<0.001$) markers of heart failure improved significantly in the whole cohort (Table 1). Left ventricular echocardiographic parameters also showed significant improvement (LVEF, $P<0.001$) and LVEDD, $P<0.001$) (Table 1).

Genetic prediction of reverse remodelling

We found a moderate association between the development of left ventricular echocardiographic parameters at 12 months and WES results in our recent-onset DCM patient cohort. Individuals with a negative or non-conclusive WES result had a higher occurrence of LVRR and more favourable changes of LVEF and LVEDD than patients with non-titin disease-related variants (Table 2). Interestingly, 9 carriers of isolated titin truncating variants achieved similar or even better improvement in LVEF and LVEDD (LVRR prevalence in 56% of cases) compared to individuals with negative or non-conclusive WES. (Table 2). Table 3 describes the other baseline variables and their relationship to 12-month LVRR. Interestingly, female gen-

5

Table 3. Left ventricular reverse remodelling and baseline patient characteristics.

| Variable | Prediction of 12 months ΔLVEF > 10 points and Δ LVEDD < -10% | | *P*-value |
	Positive pts (n=28 pts)	Negative pts (n=55 pts)	
Age [years]	46 (38-54)	49 (44-57)	0.200
Gender	18 (64%)	50 (91%)	
(males / females)	18 (64%)/10 (36%)	50 (91%)/5 (9%)	0.003 **
Arterial hypertension	15 (53%)	18 (33%)	0.067
Diabetes	2 (7%)	8 (14%)	0.126
Positive family history of DCM	3 (11%)	11 (20%)	0.285
NYHA class	I - 1 (4%)	I - 2 (4%)	0.116
	II - 9 (32%)	II - 31 (56%)	
	III - 17 (44%)	III - 22 (40%)	
	IV - 1 (4%)	IV - 0 (0%)	
Systolic BP [mmHg]	120 (110-132)	124 (116-130)	0.477
Diastolic BP [mmHg]	80 (75-85)	80 (75-87)	0.659
Heart rate [bpm]	83 (70-100)	80 (69-88)	0.156
QRS [ms]	90 (80-100)	100 (80-132)	0.225
LBBB	6 (21%)	16 (29%)	0.318
LVEDD [mm]	63 (59-71)	65 (60-70)	0.370
LVEF [%]	23 (16-25)	25 (17-30)	0.339
E/Em	13 (8-17)	13 (10-19)	0.878
Left atrium (PLAX) [mm]	45 (40-49)	45 (42-49)	0.518
RVEDD [mm]	33 (28-38)	35 (31-39)	0.347
TAPSE [mm]	18 (17-20)	18 (15-23)	0.774
RV Sm [cm/s]	10 (8-11)	11 (9-12)	0.092
ACEi	22 (78%)	41 (65%)	0.685
ARB	5 (18%)	1 (2%)	0.348
Equivalent dose of ACEi or ARB ≥ 50%	8 (28%)	17 (31%)	0.444
Beta-blockers	25 (89%)	49 (66%)	0.978
Equivalent dose of betablockers ≥ 50%	6 (21%)	8 (14%)	0.309
Aldosterone receptor blockers	19 (71%)	39 (68%)	0.482
Furosemide ≥ 40 mg daily	12 (43%)	33 (60%)	0.106
Sodium [mmol/L]	140 (138-142)	140 (138-143)	0.375
Creatinine [μmol/L]	78 (63-91)	88 (78-100)	0.018 *
NT-proBNP [ng/mL]	2053 (1087-3741)	1298 (745-2801)	0.134

Association between baseline patient variables and LVRR (ΔLVEF > 10% and ΔLVEDD < -10%)

n – number, pts – patients, ΔLVEF – change of left ventricular ejection fraction, Δ LVEDD – change of left ventricular end-diastolic diameter, DCM – dilated cardiomyopathy, NYHA class – New York Heart Association class, BP – blood pressure, LBBB – left bundle branch block, LVEDD – left ventricular end-diastolic diameter, LVEDV – left ventricular end-diastolic volume, LVEF – left ventricular ejection fraction, PLAX – parasternal long axis, RVEDD – right ventricular end-diastolic diameter, TAPSE – tricuspid annular plane systolic excursion, RV Sm – right ventricular Sm wave, ACEi – angiotensin converting enzyme inhibitor, ARB – angiotensin receptor blocker

der and a lower baseline creatinine serum levels predicted LVRR.

DISCUSSION

To the best of our knowledge, our project is the first study correlating prospective genotyping and clinical follow-up in RODCM. The main results of this pilot analysis can be summarized as follows: firstly, more than half of RODCM cases has a monogenic or oligogenic genetic background. Secondly, carriers of non-titin disease-related variants are less likely to reach LVRR at 12 months as compared with remaining individuals.

Clinical and genetic screening to detect genetic cause of DCM

A positive family history of DCM is reported in 10 to 20% of cases[15,20]. Echocardiographic screening in first-degree relatives may uncover LV enlargement and / or LV systolic dysfunction in almost one third of the relatives. A quarter of these relatives with abnormal echocardiography later develop symptomatic cardiomyopathy[20]. Most cases of familial DCM have an autosomal dominant mode of inheritance sometimes with incomplete penetrance and variable expressivity[15]. This exposes the relatives to risk of major adverse cardiovascular events, which could be prevented. Therefore, recent guidelines recommend obtaining a family history of at least 3 generations and

clinical screening in first-degree relatives in all patients with unexplained cardiomyopathy[15]. Genetic testing in unexplained DCM is a recommendation level A. Our data suggest genetic determination in a substantial proportion of unselected patients with recent-onset dilated cardiomyopathy and thus support the recommendation of genetic testing.

Genetic architecture of RODCM and its reversibility

Whole-exome genetic screening in our RODCM cohort revealed disease-related variants in 28 different genes with predominance of truncating variants of *TTN* (12%). Since our study group contained mainly sporadic cases of DCM, this is in agreement with previous studies showing that truncating variants of *TTN* contribute to 12-18% of sporadic cases and 20-25% of familial cases of DCM (ref.[14,19-20]). Truncating variants in cardiac long isoform of *TTN* can be detected also in 0.5% of healthy general population and were previously associated with larger left ventricular volumes in their carriers. Animal studies suggested that these *TTN* variants lead to increased fragility to metabolic insults or volume overload, which may trigger evolution of DCM (ref.[31]). This was confirmed in 2 landmark clinical trials showing increased prevalence of truncating *TTN* variants in alcoholic and peripartum cardiomyopathy reaching values of 9.9% and 15%, respectively[32,33]. Both alcoholic and peripartum cardiomyopathy are known as relatively reversible diseases. There are few retrospective studies showing a marked reversibility also in dilated cardiomyopathy due to truncating variants of *TTN* suggesting the role of other contributing factors in this disease as pressure or volume overload or a toxic insult[34,35].

Non-titin gene variants involved in the pathophysiology of our RODCM cases were extremely heterogeneous with a predominance of sarcomeric genes. The most common were variants of cardiac myosin binding protein C3 (*MYBPC3*) and cardiac beta myosin heavy chain (*MYH7*) accounting for 4 to 6% of cases. Interestingly, in this real-life cohort of RODCM patients, we found very few variants of genes associated with a poor outcome of dilated cardiomyopathy like *LMNA*, *DES*, *RBM20* and *FLNC* (ref.[19]). There is limited evidence regarding the occurrence of LVRR in non-titin mutation carriers with the exception of laminopathies. The available studies in laminopathies have documented the absence of LVRR and poor prognosis[34-36]. Further studies are needed to assess LVRR and prognosis in non-titin mutation carriers with RODCM.

Study limitations

We performed this pilot study to develop the methodology of genomic and clinical data analysis in individuals with RODCM. The relatively small sample size limits the applicability of the data and precludes conclusions regarding association between genotype and hard clinical outcomes as mortality and morbidity. One of the general limitations of WES compared to predefined gene panels is the difficulty in interpretation of the results. In clinical settings it is advisable to assess WES only if f the family size is large enough for segregation analysis[23]. We are aware of incomplete clinical and genetic screening in af-

fected families, which could improve interpretation of pathogenicity in detected variants. The main reason was the relatively poor participation of families in the genetic and clinical screening, presumably due to often long travel distances. However, this screening is still ongoing and will hopefully bring in more relatives in the near future.

CONCLUSION

This pilot study is a first whole-exome sequencing study describing the genetic architecture of recent-onset dilated cardiomyopathy in the Moravian region. We discovered that a substantial proportion of RODCM cases have a monogenic or oligogenic genetic background. We found that carriers of non-titin disease-related variants were less likely to reach left ventricular reverse remodelling at 12 months compared to the remaining individuals. This could be seen as a negative prognostic marker of disease development. Further studies are needed to assess the relationship between genotype and hard clinical outcomes in RODCM. We believe that genetic testing could contribute to prognostic evaluation and even individualized treatment of RODCM in the near future.

ABBREVIATIONS

ECG, Electrocardiography; CHF, Heart failure; DCM, Dilated cardiomyopathy; ICD, Implantable cardioverter-defibrillator; LV, Left ventricular; LVEDD, Left ventricular end-diastolic diameter; LVEF, Left ventricular ejection fraction; LVRR, Left ventricular reverse remodelling; NGS, Next-generation sequencing; NYHA, New York Heart Association; RODCM, Recent onset dilated cardiomyopathy; SD, Standard deviation; WES, Whole exome sequencing.

Author contributions: AC: data collection, data interpretation, manuscript writing and literature search; MK: study design, study organization, statistical analysis, data interpretation, drafting of the manuscript; LP: next-generation genetic testing, data interpretation, drafting of the manuscript; JB: data collection and interpretation, drafting of the manuscript; VS: analysis of genomic data, data interpretation; SK: analysis of genomic data, data interpretation, drafting of the manuscript; IG: genetic counselling, data collection, gene-specific genetic testing; JK: data collection, study organization.
Conflict of interest statement: None declared.

REFERENCES

1. Yancy CW, Jessup M, Bozkurt B, Butler J, Casey DE, Drazner MH, Fonarow GC, Geraci SA, Horwich T, Januzzi JL, Johnson MR, Kasper EK, Levy WC, Masoudi FA, McBride PE, McMurray JJV, Mitchell JE, Peterson PN, Riegel B, Sam F, Stevenson LW, Tang WHW, Tsai EJ,

Wilkoff BL. 2013 ACCF/AHA guideline for the management of heart failure: executive summary: a report of the American College of Cardiology Foundation/American Heart Association Task Force on practice guidelines. Circulation 2013;128(16):1810-52.

2. Elliott P, Andersson B, Arbustini E, Bilinska Z, Cecchi F, Charron P, Dubourg O, Kühl U, Maisch B, McKenna WJ, Monserrat L, Pankuweit S, Rapezzi C, Seferovic P, Tavazzi L, Keren A. Classification of the cardiomyopathies: a position statement from the European Society Of Cardiology Working Group on Myocardial and Pericardial Diseases. Eur Heart J 2008;29(2):270-6.

3. Pinto YM, Elliott PM, Arbustini E, Adler Y, Anastasakis A, Böhm M, Duboc D, Gimeno J, de Groote P, Imazio M, Heymans S, Klingel K, Komajda M, Limongelli G, Linhart A, Mogensen J, Moon J, Pieper PG, Seferovic PM, Schueler S, Zamorano JL, Caforio ALP, Charron P. Proposal for a revised definition of dilated cardiomyopathy, hypokinetic non-dilated cardiomyopathy, and its implications for clinical practice: a position statement of the ESC working group on myocardial and pericardial diseases. Eur Heart J 2016;37(23):1850-8.

4. Rapezzi C, Arbustini E, Caforio ALP, Charron P, Gimeno-Blanes J, Heliö T, Linhart A, Mogensen J, Pinto Y, Ristic A, Seggewiss H, Sinagra G, Tavazzi L, Elliott PM. Diagnostic work-up in cardiomyopathies: bridging the gap between clinical phenotypes and final diagnosis. A position statement from the ESC Working Group on Myocardial and Pericardial Diseases. Eur Heart J 2013;34(19):1448-58.

5. Šramko M, Kubánek M, Tintěra J, Kautznerová D, Weichet J, Malušková J, Franeková J, Kautzner J. Utility of combination of cardiac magnetic resonance imaging and high-sensitivity cardiac troponin T assay in diagnosis of inflammatory cardiomyopathy. Am J Cardiol 2013;111(2):258-64.

6. Bozkurt B, Colvin M, Cook J, Cooper LT, Deswal A, Fonarow GC, Francis GS, Lenihan D, Lewis EF, McNamara DM, Pahl E, Vasan RS, Ramasubbu K, Rasmusson K, Towbin JA, Yancy C, American Heart Association Committee on Heart Failure and Transplantation of the Council on Clinical Cardiology; Council on Cardiovascular Disease in the Young; Council on Cardiovascular and Stroke Nursing; Council on Epidemiology and Prevention; and Council on Quality of Care and Outcomes Research. Current Diagnostic and Treatment Strategies for Specific Dilated Cardiomyopathies: A Scientific Statement From the American Heart Association. Circulation 2016;134(23):e579-646.

7. Givertz MM, Mann DL. Epidemiology and natural history of recovery of left ventricular function in recent onset dilated cardiomyopathies. Curr Heart Fail Rep 2013;10(4):321-30.

8. Merlo M, Pyxaras SA, Pinamonti B, Barbati G, Di Lenarda A, Sinagra G. Prevalence and prognostic significance of left ventricular reverse remodeling in dilated cardiomyopathy receiving tailored medical treatment. J Am Coll Cardiol 2011;57(13):1468-76.

9. Kubanek M, Sramko M, Maluskova J, Kautznerova D, Weichet J, Lupinek P, Vrbska J, Malek I, Kautzner J. Novel predictors of left ventricular reverse remodeling in individuals with recent-onset dilated cardiomyopathy. J Am Coll Cardiol 2013;61(1):54-63.

10. Krejci J, Hude P, Ozabalova E, Mlejnek D, Zampachova V, Svobodova I, Stepanova R, Spinarova L. Improvement of left ventricular systolic function in inflammatory cardiomyopathy: What plays a role? Biomed Pap Med Fac Univ Palacky Olomouc Czechoslov 2016;160(4):524-32.

11. Merlo M, Pyxaras SA, Pinamonti B, Barbati G, Di Lenarda A, Sinagra G. Prevalence and prognostic significance of left ventricular reverse remodeling in dilated cardiomyopathy receiving tailored medical treatment. J Am Coll Cardiol 2011;57(13):1468-76.

12. Hershberger RE, Hedges DJ, Morales A. Dilated cardiomyopathy: the complexity of a diverse genetic architecture. Nat Rev Cardiol 2013;10(9):531-47.

13. Hershberger RE, Norton N, Morales A, Li D, Siegfried JD, Gonzalez-Quintana J. Coding sequence rare variants identified in MYBPC3, MYH6, TPM1, TNNC1, and TNNI3 from 312 patients with familial or idiopathic dilated cardiomyopathy. Circ Cardiovasc Genet 2010;3(2):155-61.

14. Herman DS, Lam L, Taylor MRG, Wang L, Teekakirikul P, Christodoulou D, Conner L, DePalma SR, McDonough B, Sparks E, Teodorescu DL, Cirino AL, Banner NR, Pennell DJ, Graw S, Merlo M, Di Lenarda A, Sinagra G, Bos JM, Ackerman MJ, Mitchell RN, Murry CE, Lakdawala NK, Ho CY, Barton PJR, Cook SA, Mestroni L, Seidman JG, Seidman CE. Truncations of titin causing dilated cardiomyopathy. N Engl J Med 2012;366(7):619-28.

15. Hershberger RE, Givertz MM, Ho CY, Judge DP, Kantor PF, McBride KL, Morales A, Taylor MRG, Vatta M, Ware SM. Genetic Evaluation of Cardiomyopathy-A Heart Failure Society of America Practice Guideline. J Card Fail 2018;24(5):281-302.

16. Lopes LR, Elliott PM. Genetics of heart failure. Biochim Biophys Acta 2013;1832(12):2451-61.

17. Taylor MRG, Fain PR, Sinagra G, Robinson ML, Robertson AD, Carniel E, Di Lenarda A, Bohlmeyer TJ, Ferguson DA, Brodsky GL, Boucek MM, Lascor J, Moss AC, Li WLP, Stetler GL, Muntoni F, Bristow MR, Mestroni L, Familial Dilated Cardiomyopathy Registry Research Group. Natural history of dilated cardiomyopathy due to lamin A/C gene mutations. J Am Coll Cardiol 2003;41(5):771-80.

18. van Rijsingen IAW, van der Zwaag PA, Groeneweg JA, Nannenberg EA, Jongbloed JDH, Zwinderman AH, Pinto YM, Dit Deprez RHL, Post JG, Tan HL, de Boer RA, Hauer RNW, Christiaans I, van den Berg MP, van Tintelen JP, Wilde AAM. Outcome in phospholamban R14del carriers: results of a large multicentre cohort study. Circ Cardiovasc Genet 2014;7(4):455-65.

19. Kayvanpour E, Sedaghat-Hamedani F, Amr A, Lai A, Haas J, Holzer DB, Frese KS, Keller A, Jensen K, Katus HA, Meder B. Genotype-phenotype associations in dilated cardiomyopathy: meta-analysis on more than 8000 individuals. Clin Res Cardiol Off J Ger Card Soc 2017;106(2):127-39.

20. Baig MK, Goldman JH, Caforio AL, Coonar AS, Keeling PJ, McKenna WJ. Familial dilated cardiomyopathy: cardiac abnormalities are common in asymptomatic relatives and may represent early disease. J Am Coll Cardiol 1998;31(1):195-201.

21. Lang RM, Bierig M, Devereux RB, Flachskampf FA, Foster E, Pellikka PA, Picard MH, Roman MJ, Seward J, Shanewise JS, Solomon SD, Spencer KT, Sutton MSJ, Stewart WJ, Chamber Quantification Writing Group, American Society of Echocardiography's Guidelines and Standards Committee, European Association of Echocardiography. Recommendations for chamber quantification: a report from the American Society of Echocardiography's Guidelines and Standards Committee and the Chamber Quantification Writing Group, developed in conjunction with the European Association of Echocardiography, a branch of the European Society of Cardiology. J Am Soc Echocardiogr Off Publ Am Soc Echocardiogr 2005;18(12):1440-63.

22. Quiñones MA, Otto CM, Stoddard M, Waggoner A, Zoghbi WA, Doppler Quantification Task Force of the Nomenclature and Standards Committee of the American Society of Echocardiography. Recommendations for quantification of Doppler echocardiography: a report from the Doppler Quantification Task Force of the Nomenclature and Standards Committee of the American Society of Echocardiography. J Am Soc Echocardiogr Off Publ Am Soc Echocardiogr 2002;15(2):167-84.

23. Pinto YM, Elliott PM, Arbustini E, Adler Y, Anastasakis A, Böhm M, Duboc D, Gimeno J, de Groote P, Imazio M, Heymans S, Klingel K, Komajda M, Limongelli G, Linhart A, Mogensen J, Moon J, Pieper PG, Seferovic PM, Schueler S, Zamorano JL, Caforio ALP, Charron P. Proposal for a revised definition of dilated cardiomyopathy, hypokinetic non-dilated cardiomyopathy, and its implications for clinical practice: a position statement of the ESC working group on myocardial and pericardial diseases. Eur Heart J 2016;37(23):1850-8.

24. McKenna A, Hanna M, Banks E, Sivachenko A, Cibulskis K, Kernytsky A, Garimella K, Altshuler D, Gabriel S, Daly M, DePristo MA. The Genome Analysis Toolkit: a MapReduce framework for analyzing next-generation DNA sequencing data. Genome Res 2010;20(9):1297-303.

25. Cingolani P, Platts A, Wang LL, Coon M, Nguyen T, Wang L, Land SJ, Lu X, Ruden DM. A program for annotating and predicting the effects of single nucleotide polymorphisms, SnpEff: SNPs in the genome of Drosophila melanogaster strain w1118; iso-2; iso-3. Fly (Austin) 2012;6(2):80-92.

26. Paila U, Chapman BA, Kirchner R, Quinlan AR. GEMINI: integrative exploration of genetic variation and genome annotations. PLoS Comput Biol 2013;9(7):e1003153.

27. Thorvaldsdóttir H, Robinson JT, Mesirov JP. Integrative Genomics Viewer (IGV): high-performance genomics data visualization and exploration. Brief Bioinform 2013;14(2):178-92.

28. Burke MA, Cook SA, Seidman JG, Seidman CE. Clinical and Mechanistic Insights Into the Genetics of Cardiomyopathy. J Am Coll Cardiol 2016;68(25):2871-86.

8

29. Richards S, Aziz N, Bale S, Bick D, Das S, Gastier-Foster J, Grody WW, Hegde M, Lyon E, Spector E, Voelkerding K, Rehm HL. Standards and Guidelines for the Interpretation of Sequence Variants: A Joint Consensus Recommendation of the American College of Medical Genetics and Genomics and the Association for Molecular Pathology. Genet Med Off J Am Coll Med Genet [Internet] 2015 May [cited 2018 Jul 30];17(5):405–24. Available from: https://www.ncbi.nlm.nih.gov/pmc/articles/PMC4544753/

30. Schwarz JM, Cooper DN, Schuelke M, Seelow D. MutationTaster2: mutation prediction for the deep-sequencing age. Nat Methods 2014;11(4):361-2.

31. Akinrinade O, Ollila L, Vattulainen S, Tallila J, Gentile M, Salmenperä P, Koillinen H, Kaartinen M, Nieminen MS, Myllykangas S, Alastalo T-P, Koskenvuo JW, Heliö T. Genetics and genotype-phenotype correlations in Finnish patients with dilated cardiomyopathy. Eur Heart J 2015;36(34):2327-37.

32. Schafer S, de Marvao A, Adami E, Fiedler LR, Ng B, Khin E, Rackham OJL, van Heesch S, Pua CJ, Kui M, Walsh R, Tayal U, Prasad SK, Dawes TJW, Ko NSJ, Sim D, Chan LLH, Chin CWL, Mazzarotto F, Barton PJ, Kreuchwig F, de Kleijn DPV, Totman T, Biffi C, Tee N, Rueckert D, Schneider V, Faber A, Regitz-Zagrosek V, Seidman JG, Seidman CE, Linke WA, Kovalik J-P, O'Regan D, Ware JS, Hubner N, Cook SA. Titin-truncating variants affect heart function in disease cohorts and the general population. Nat Genet 2017;49(1):46-53.

33. Ware JS, Amor-Salamanca A, Tayal U, Govind R, Serrano I, Salazar-Mendiguchía J, García-Pinilla JM, Pascual-Figal DA, Nuñez J, Guzzo-Merello G, Gonzalez-Vioque E, Bardaji A, Manito N, López-Garrido MA, Padron-Barthe L, Edwards E, Whiffin N, Walsh R, Buchan RJ, Midwinter W, Wilk A, Prasad S, Pantazis A, Baski J, O'Regan DP, Alonso-Pulpon L, Cook SA, Lara-Pezzi E, Barton PJ, Garcia-Pavia P. Genetic Etiology for Alcohol-Induced Cardiac Toxicity. J Am Coll Cardiol 2018;71(20):2293-302.

34. Ware JS, Li J, Mazaika E, Yasso CM, DeSouza T, Cappola TP, Tsai EJ, Hilfiker-Kleiner D, Kamiya CA, Mazzarotto F, Cook SA, Halder I, Prasad SK, Pisarcik J, Hanley-Yanez K, Alharethi R, Damp J, Hsich E, Elkayam U, Sheppard R, Kealey A, Alexis J, Ramani G, Safirstein J, Boehmer J, Pauly DF, Wittstein IS, Thohan V, Zucker MJ, Liu P, Gorcsan J, McNamara DM, Seidman CE, Seidman JG, Arany Z, IMAC-2 and IPAC Investigators. Shared Genetic Predisposition in Peripartum and Dilated Cardiomyopathies. N Engl J Med 20161;374(3):233-41.

35. Jansweijer JA, Nieuwhof K, Russo F, Hoorntje ET, Jongbloed JDH, Lekanne Deprez RH, Postma AV, Bronk M, van Rijsingen IAW, de Haij S, Biagini E, van Haelst PL, van Wijngaarden J, van den Berg MP, Wilde AAM, Mannens MMAM, de Boer RA, van Spaendonck-Zwarts KY, van Tintelen JP, Pinto YM. Truncating titin mutations are associated with a mild and treatable form of dilated cardiomyopathy. Eur J Heart Fail 2017;19(4):512-21.

36. Tobita T, Nomura S, Fujita T, Morita H, Asano Y, Onoue K, Ito M, Imai Y, Suzuki A, Ko T, Satoh M, Fujita K, Naito AT, Furutani Y, Toko H, Harada M, Amiya E, Hatano M, Takimoto E, Shiga T, Nakanishi T, Sakata Y, Ono M, Saito Y, Takashima S, Hagiwara N, Aburatani H, Komuro I. Genetic basis of cardiomyopathy and the genotypes involved in prognosis and left ventricular reverse remodeling. Sci Rep 2018;8(1):1998.

9

Příloha 1a

Article

Desminopathy: Novel Desmin Variants, a New Cardiac Phenotype, and Further Evidence for Secondary Mitochondrial Dysfunction

Miloš Kubánek [1,*], Tereza Schimerová [1,2], Lenka Piherová [3], Andreas Brodehl [4],
Alice Krebsová [1], Sandra Ratnavadivel [4], Caroline Stanasiuk [4], Hana Hansíková [5],
Jiří Zeman [5], Tomáš Paleček [6], Josef Houštěk [7], Zdeněk Drahota [7], Hana Nůsková [7],
Jana Mikešová [7], Josef Zámečník [8], Milan Macek Jr. [9], Petr Ridzoň [10], Jana Malusková [11],
Viktor Stránecký [3], Vojtěch Melenovský [1], Hendrik Milting [4] and Stanislav Kmoch [3]

[1] Department of Cardiology, Institute for Clinical and Experimental Medicine, 14021 Prague, Czech Republic;
    nedt@ikem.cz (T.S.); krea@ikem.cz (A.K.); vome@ikem.cz (V.M.)
[2] Institute of Physiology, First Faculty of Medicine, Charles University, 11636 Prague, Czech Republic
[3] Research Unit for Rare Diseases, Department of Pediatrics and Adolescent Medicine, First Faculty of
    Medicine, Charles University, 11636 Prague, Czech Republic; Lenka.Piherova@lf1.cuni.cz (L.P.);
    Viktor.Stranecky@lf1.cuni.cz (V.S.); skmoch@lf1.cuni.cz (S.K.)
[4] Erich and Hanna Klessmann Institute, Heart and Diabetes Center NRW, University Hospital of the
    Ruhr-University Bochum, 32545 Bad Oeynhausen, Germany; ABrodehl@hdz-nrw.de (A.B.);
    SRatnavadivel@hdz-nrw.de (S.R.); CStanasiuk@hdz-nrw.de (C.S.); HMilting@hdz-nrw.de (H.M.)
[5] Department of Pediatrics and Adolescent Medicine, First Faculty of Medicine, Charles University and
    General University Hospital in Prague, 12108 Prague, Czech Republic; Hana.Hansikova@lf1.cuni.cz (H.H.);
    jzem@lf1.cuni.cz (J.Z.)
[6] 2nd Department of Medicine–Department of Cardiovascular Medicine, First Faculty of Medicine, Charles
    University and General University Hospital in Prague, 12108 Prague, Czech Republic;
    Tomas.Palecek@lf1.cuni.cz
[7] Institute of Physiology, Czech Academy of Sciences, 11720 Prague, Czech Republic;
    josef.houstek@fgu.cas.cz (J.H.); zdenek.drahota@fgu.cas.cz (Z.D.); h.nuskova@dkfz-heidelberg.de (H.N.);
    jana.mikesova@uochb.cas.cz (J.M.)
[8] Department of Pathology and Molecular Medicine, Second Faculty of Medicine, Charles University, 11636
    Prague, Czech Republic; josef.zamecnik@lfmotol.cuni.cz
[9] Department of Biology and Medical Genetics, Second Faculty of Medicine, Charles University, 11636 Prague,
    Czech Republic; milan.macek.jr@lfmotol.cuni.cz
[10] Department of Neurology, Thomayer's Hospital, 14059 Prague, Czech Republic; petr.ridzon@ftn.cz
[11] Department of Pathology, Institute for Clinical and Experimental Medicine, 14021 Prague, Czech Republic;
    Institute for Clinical and Experimental Medicine, 14021 Prague, Czech Republic; jana.maluskova@ikem.cz
*   Correspondence: milos.kubanek@ikem.cz; Tel.: +42-0236-055-047; Fax: +42-0236-052-989

check for
updates

Abstract: Background: The pleomorphic clinical presentation makes the diagnosis of desminopathy difficult. We aimed to describe the prevalence, phenotypic expression, and mitochondrial function of individuals with putative disease-causing desmin (DES) variants identified in patients with an unexplained etiology of cardiomyopathy. **Methods:** A total of 327 Czech patients underwent whole exome sequencing and detailed phenotyping in probands harboring DES variants. **Results:** Rare, conserved, and possibly pathogenic DES variants were identified in six (1.8%) probands. Two DES variants previously classified as variants of uncertain significance (p.(K43E), p.(S57L)), one novel DES variant (p.(A210D)), and two known pathogenic DES variants (p.(R406W), p.(R454W)) were associated with characteristic desmin-immunoreactive aggregates in myocardial and/or skeletal biopsy samples. The individual with the novel DES variant p.(Q364H) had a decreased myocardial expression of desmin with absent desmin aggregates in myocardial/skeletal muscle biopsy and presented with familial left ventricular non-compaction cardiomyopathy (LVNC), a relatively novel

phenotype associated with desminopathy. An assessment of the mitochondrial function in four probands heterozygous for a disease-causing DES variant confirmed a decreased metabolic capacity of mitochondrial respiratory chain complexes in myocardial/skeletal muscle specimens, which was in case of myocardial succinate respiration more profound than in other cardiomyopathies. **Conclusions:** The presence of desminopathy should also be considered in individuals with LVNC, and in the differential diagnosis of mitochondrial diseases.

1. Introduction

Desminopathy (OMIM # 601409) represents a group of autosomal inherited disorders caused by pathogenic variants in the disease-causing desmin (*DES*) gene, encoding the major muscle specific intermediate filament protein desmin (OMIM: #125660) [1]. Desmin is the major component of intermediate filaments in cardiac, skeletal, and smooth muscle cells, with a particularly high content in Purkinje fibers and diaphragmatic muscle cells [1]. Consequently, cardiomyopathy, cardiac conduction disease, and progressive skeletal myopathy are the most common clinical presentations of desminopathy. It may occur as an isolated cardiac disease or in variable combinations and with different onsets. As summarized in a meta-analysis [1], 49%, 60%, and 74% of individuals harboring a pathogenic *DES* variant develop cardiomyopathy, cardiac conduction disease, and skeletal myopathy, respectively. The most common form of myocardial involvement is dilated cardiomyopathy (DCM) [1–3], followed by restrictive (RCM) [4–7], arrhythmogenic (ACM) and hypertrophic cardiomyopathy (HCM), and arrhythmogenic cardiomyopathy pattern [8–11]. On the other hand, there is low evidence regarding an association between desminopathy and left ventricular noncompaction cardiomyopathy (LVNC). Importantly, intermediate filaments are essential not only for cellular integrity, organization, and differentiation, but also for a signal transduction and adequate mitochondrial function [12]. Accordingly, several experimental [12–14] and clinical [15,16] studies have proven a secondary mitochondrial dysfunction in desminopathy, which in one case even mimicked mitochondrial disease [16].

The pleomorphic clinical presentation makes the diagnosis of desminopathy challenging. Fortunately, massively parallel sequencing (MPS) utilizing either cardiomyopathy panels and/or even whole exome sequencing (WES) aid in the diagnosis of desminopathy regardless of its clinical presentation. Hereby, we aimed to describe the prevalence of desminopathy and their phenotypes in a large representative cohort of patients with cardiomyopathy of unexplained etiology using WES.

2. Materials and Methods

A representative cohort of 327 Czech patients with an unexplained etiology of cardiomyopathy underwent WES between September 2015 and June 2017. The cohort consisted mainly of cases with familial and sporadic DCM (81%), LVNC (13%), and less frequently of RCM (6%) or ACM (6%). Rare and possibly pathogenic missense *DES* variants were identified in 6 (1.8%) index patients from 6 different families (Figure 1).
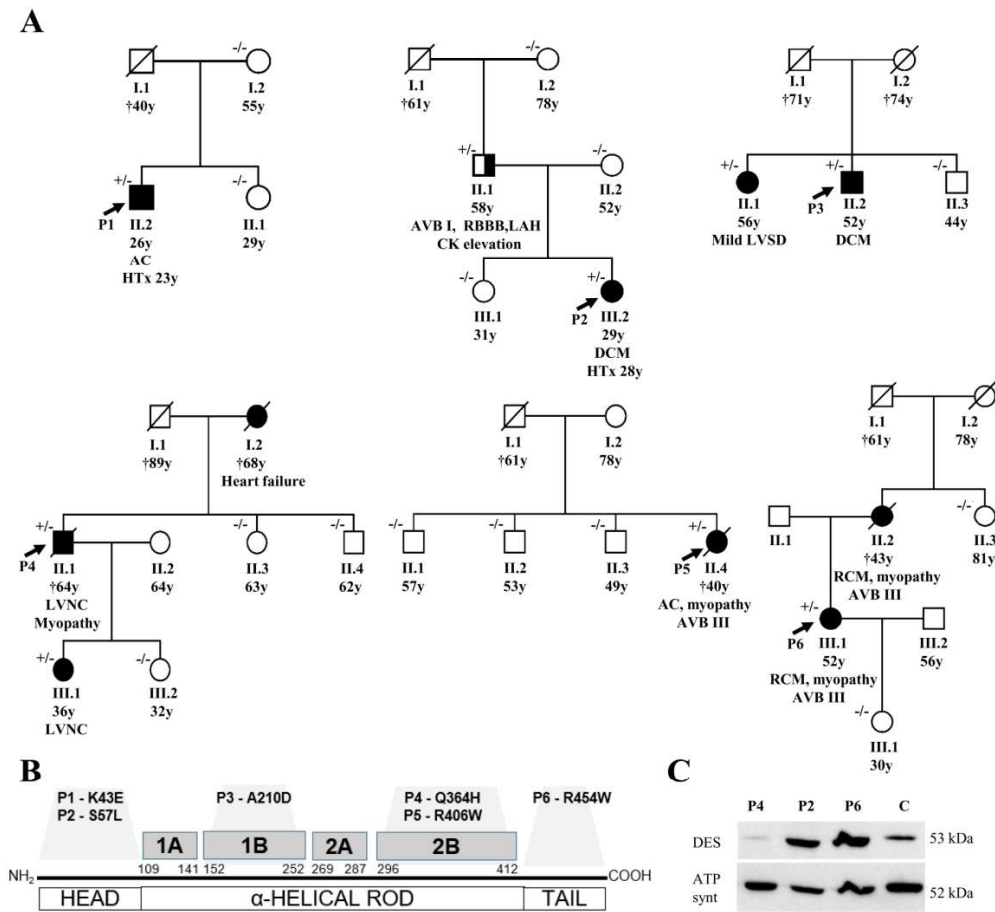
Příloha 1a

Figure 1. (**A**) shows pedigrees of the affected families and segregation of desmin variants (+/− heterozygous status, −/− wild type). In the fourth family (with P4) we also assessed a segregation of the rare variant of *MYH7* (NM_000257.3), c.4679G > C, p.(Arg1560Pro), which was present just in P4 (II/1) and absent in II/3, II/4, III/1, and III/2. (**B**) summarizes the structure of the desmin gene with localization of the detected variants. (**C**) illustrates the detection of desmin by western blot in myocardial samples (P2, P4, P6, control sample; 30ug protein aliquots) with an obvious reduction of signal in P4 with left ventricular non-compaction cardiomyopathy (*DES*-p.(Q364H)). Abbreviations: AC = arrhythmogenic cardiomyopathy, AVB = atrioventricular block, DCM = dilated cardiomyopathy, DES = desmin, HTx = heart transplantation, LAH = left anterior hemiblock, LVNC = left ventricular non-compaction cardiomyopathy, LVSD = left ventricular systolic dysfunction, RBBB = right bundle branch block, and RCM = restrictive cardiomyopathy.

2.1. Clinical Description of Studied Patients and of Their Families

Comprehensive clinical, laboratory, and electrophysiological data of all index cases were collected. Two probands of them (P2, P4) also underwent cardiovascular magnetic resonance imaging (Siemens Trio scanner, Siemens Medical Solutions, Erlangen, Germany) as described previously [17]. All available relatives undertook cardiologic screening, which included physical examination, electrocardiography, and echocardiography as well as a collection of blood samples for genetic analysis. Patients with suspected disease-causing *DES* variants were subjected to a detailed neurologic assessment, measurement of serum creatine phosphokinase, nerve conductance, and electromyography of two muscles (left vastus medialis and left deltoid muscle), as reported previously [17].

The study was approved by the Institutional Review Board´s representing all clinical collaborators (Institute for Clinical and Experimental Medicine and Thomayer´s Hospital; 1st Faculty of Medicine of the Charles University and General Faculty Hospital; both Prague) and was conducted in accordance with the principles of the Declaration of Helsinki. Written informed consent was obtained from all probands.

2.2. Genetic Analysis and Detection of Variants

To detect causal genetic variants, WES was performed according to internationally accepted guidelines [18]. Full technical details are provided in the Supplementary Materials. The criteria for classifying variants as putative disease-causing variants included their rare occurrence (≤0.05% among control samples), changes in predicted amino acid sequences, conservation across different species (http://www.ncbi.nlm.nih.gov/BLAST/), segregation within the family, and previously reported pathogenicity in databases.

Exons with identified variants of the *DES* gene were PCR amplified (Table S1) from genomic DNA of all available individuals from the analyzed families and sequenced using the version 3.1 Dye Terminator cycle sequencing kit with electrophoresis on an ABI 3500XL Avant Genetic Analyzer (both ThermoFisher Scientific; Waltham, MA, USA). Data were analyzed using Sequencing Analysis software version 6.0 (both ThermoFisher Scientific; USA) and the segregation of the candidate *DES* variants with the phenotype was evaluated.

2.3. In Vitro Analysis of DES Variants

As many but not all pathogenic *DES* variants cause an abnormal cytoplasmic desmin aggregation, we constructed for the identified *DES* variants expression plasmids by site-directed mutagenesis (Agilent Technologies, Santa Clara, CA, USA) according to the manufacturer's instructions. Desmin encoding parts of all plasmids were verified by Sanger sequencing (Macrogen, Amsterdam, Netherlands). The plasmid pmRuby-N1-DES and pmRuby-N1-DES-p.(Y122C) have been previously described [19,20]. Previously reported variant DES-p.(Y122C) was used as a positive control forming abnormal cytoplasmic aggregates [20]. HT1080 cells, which do not express endogenous desmin and cardiomyocytes derived from human induced pluripotent stem cells (iPSC) (NP00040-8) were transfected using Lipofectamin 3000 (ThermoFisher Scientific) or nucleofection using the 4D Nucleofector (Lonza, Cologne, Germany) in combination with the P3 Primary Cell 4D Nucleofector Kit according to the manufacturer's instructions. The differentiation of hiPSCs has been previously described [21]. Transfected HT1080 cells were fixed using 4% paraformaldehyde, permeabilized using 0.05% Triton X100, and stained with phalloidin conjugated with Alexa-488. Transfected hiPSC-derived cardiomyocytes were stained with primary antibodies against the Z-band protein α-actinin as a cardiomyocytes specific marker (Sigma-Aldrich, Missouri, MO, USA, #A7732) in combination with secondary antibodies conjugated to Alexa-488 (ThermoFisher). Confocal microscopy was performed as previously described [22].

2.4. Statistical Analysis of Aggregate Formation

A total of 3 to 4 independent transfection experiments were analyzed by counting the number of aggregate forming cells. Non-parametric Kruskal–Wallis for multiple comparison was performed using GraphPad Prism version 8.3.0 for Windows (GraphPad Software, San Diego, CA, USA). *p*-values <0.05 were considered as significant.

2.5. Histopathology, Immunohistochemistry, Desmin Western Blot, and Electron Microscopy

In 5 probands (P1–P4, P6), formalin-fixed paraffin-embedded samples of myocardium were available either from endomyocardial biopsy (P2, P3) and/or from hearts explanted during transplantation (P1, P2, P6) or post-mortem (P4). The samples were snap frozen in liquid nitrogen and stored at −70 °C. Resin-embedded myocardial samples for electron microscopy were analyzed in 4 patients (P1, P2, P4, and P6). A biopsy of skeletal muscle was performed in 3 individuals with

clinical signs of myopathy (P4 and P5: Soleus-, P6: Deltoid muscle). In P4, also we obtained samples of intercostal muscles post-mortem. The excisions from the skeletal muscle (approx. $10 \times 5 \times 5$ mm in size) were snap frozen in isopentane (2-methylbutane; Merck, Kenilworth, NJ, USA) and cooled in liquid nitrogen. Cryosections were examined by routine hematoxylin–eosin staining and a conventional spectrum of histochemical reactions, including myofibrillary ATPase, nicotinamide adenine dinucleotide-tetrazolium reductase (NADH-TR), succinate dehydrogenase (SDH), and cytochrome c oxidase (COX), as described elsewhere [23].

Desmin immunohistochemistry and electron microscopy were performed on both skeletal muscle and myocardium samples according to standard protocols (Supplementary Materials).

2.6. Analysis of Mitochondrial Function in Biopsies

Skeletal muscle homogenate (5%, w/v) was prepared from fresh tissue by using a glass-Teflon homogenizer in a medium containing 150 mM KCl, 50 mM Tris-HCl, 2 mM EDTA, pH 7.4, and 0.2 ug/mL Aprotinin at 4 °C. Mitochondria were isolated from the homogenate by differential centrifugation as described elsewhere [24]. Heart tissue homogenates (7%, w/v) were prepared from −80 °C stored frozen samples of left and right heart ventricles in 0.32 M sucrose, 10 mM Tris-HCl, 1 mM EDTA, pH 7.4, and 1μg/mL PIC (protease inhibitor mixture Sigma P8340) using glass-Teflon and glass-glass Dounce homogenizers. The subsequent methods are described in detail in Supplementary Materials. A western blot analysis of mitochondrial proteins, measurement of mitochondrial DNA content, measurement of activities of respiratory chain complexes and citrate synthase [25], high resolution oxygraphy, and measurement of the content of total coenzyme Q10 were described previously in details and in the Supplementary Materials.

3. Results

3.1. Description of DES Variants and Their Segregation in Families

Probably disease-causing *DES* variants in heterozygous constitution were identified in six index cases (1.8%). Two missense variants were identified within the non-helical head (amino-teminal) domain of desmin, i.e., in P1 with biventricular form of ACM (NM_001927.3: c.127A > G; NP_001918.3: p.(K43E)) and in P2 with DCM (NM_001927.3: c.170C > T; NP_001918.3: p.(S57L)) (Figure 1, Tables S2 and S3). Both of them were previously reported in Clinvar database as variants of uncertain significance. In addition, we analyzed the desmin filament formation in transfected HT1080 and in iPSC-derived cardiomyocytes, revealing an abnormal cytoplasmic aggregation in the DES-p.(K43E) variant and known pathogenic DES-p.(R406W) variant (Figure 2). Two novel variants were found in the highly conserved central α-helical rod domain, i.e., in P3 with familial DCM located in the 1B helical domain (NM_001927.3:c.629C > A; NP_001918.3: p.(A210D)) and in P4 with familial LVNC in combination with skeletal myopathy located in the 2B helical domain (NM_001927.3: c.1092G>T; NP_001918.3: p.(Q364H)) (Figure 1, Tables S2 and S3). The findings in the biopsies are described below. The remaining two probands had the following known *DES* pathogenic variants: P5 with ACM and skeletal myopathy in the 2B helical domain (NM_001927.3: c.1216C>T; NP_001918.3: p.(R406W); HGMD database ((http://www.hgmd.cf.ac.uk/ac/index.php) CM000368) [6] and P6 with RCM and skeletal myopathy within the non-helical tail (carboxy-terminal) domain (NM_001927.3: c.1360C > T; NP_001918.3: p.(R454W); HGMD CM071700) [26] (Figure 1, Tables S2 and S3). Table S4 contains lists of rare genetic variants of further cardiomyopathy associated genes in all probands (frequency in Exac database less than 0.00001). Just the variant of *MYH7* (NM_000257.3) c.4679G > C, p.(Arg1560Pro) in proband 4 could be relevant in a patient with LVNC. However, it was not present in other members of the family tested (II 1, 3, 4; III 1, 2) (Figure 1) and did not co-segregate with the phenotype of LVNC. Importantly, any pathogenic variants in mitochondrial proteins coded by nuclear DNA or mitochondrial DNA were not found in these six probands.

Figure 1 illustrates the segregation of *DES* variants in families. Family history or clinical screening revealed a similar cardiac disease in a first-degree relative in P3, P4, and P6 segregating with occurrence of *DES* variants (Figure 1, Table S2). In the father of P2, heterozygous for *DES* p.(S57L) variant, we observed an incomplete penetrance of the disease with atrioventricular block grade I, right bundle branch block, left anterior hemiblock, normal echocardiography, and a mild elevation of creatinine phosphokinase of 6.1 μkat/l (upper limit of normal 2.3 μkat/L) without clinical signs of myopathy. Cases P1 and P5 seemed to be sporadic (segregation assessed in mother and sister of P1, and three siblings of P5).
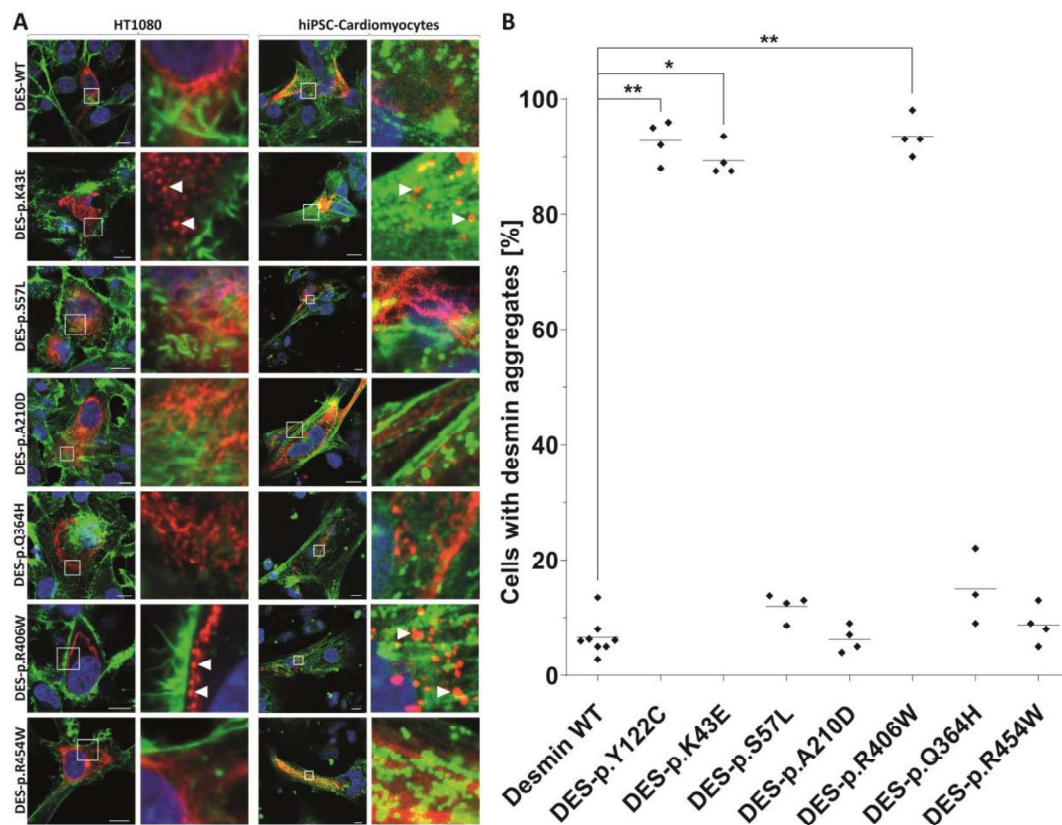
Figure 2. Cell transfection experiments of transfected HT1080 cells and iPSC-derived cardiomyocytes. Mutant and wild-type desmin was expressed with the red fluorescent protein-tag mRuby at the C-terminus (shown in red). Representative confocal images are shown (**A**). In case of HT1080 cells, F-actin was stained using phalloidin-Alexa488 (shown in green) and the nuclei were stained using 4′,6-diamidin-2-phenylindole (shown in blue). In case of iPSC-cardiomyocytes, the cardiomyocyte marker α-actinin was stained using antibodies (shown in green) and the nuclei were stained with DAPI (shown in blue). Scale bars represent 10 μm. (**B**) Quantification of aggregate formation was performed in three to four independent transfection experiments of HT1080 cells. * $p < 0.05$ and ** $p < 0.01$. The variant DES-p.(Y122C) was used as a positive control forming abnormal cytoplasmic aggregates [20].

3.2. Phenotypes of Desminopathy

The initial clinical presentation included cardiac arrest due to ventricular tachycardia in the 2nd decennium (P1), complete atrioventricular blockade in the 3rd decennium (P5, P6), and heart failure in the 3rd to 5th decennium (P2, P3, and P4). Skeletal myopathy and dysfunction of bulbar muscles became apparent during the 4th to 6th decennium in cases 4–6 (Table S2 and S3). An unusual clinical presentation had proband 2. A young female presented with acute heart failure, a severe

Příloha 1a

systolic dysfunction of mildly dilated left ventricle, persistent elevation of troponin T (> 10 times the upper limit of normal) (Table S3), and an extensive mid-wall late gadolinium enhancement of the septum and anterior wall of the left ventricle (Figure 3). These findings mimicked inflammatory cardiomyopathy however, there was no sign of inflammation as assessed by endomyocardial biopsy. Inflammation was absent also in her heart explanted during transplantation three years later. The arrhythmogenic left ventricular cardiomyopathy was considered as an alternative diagnosis in P2. However, her electrocardiogram was unremarkable and ventricular extrasystoles were infrequent. Proband 4 presented with a unique phenotype of LVNC. Magnetic resonance imaging (Figure 3) confirmed the diagnosis of LVNC with a percentage of non-compaction within the total left ventricular mass of 43%. Proband 6 was incorrectly diagnosed with mitochondrial disease based on skeletal muscle biopsy performed several years ago. This diagnosis was reclassified to desminopathy after the identification of known pathogenic desmin mutation (p.(R454W)) and morphological analysis of myocardial samples from the explanted heart. Table S3 illustrates additional clinical and laboratory data of the study group including echocardiography. During a median follow-up of 56 months (31–182), five probands (83%) developed end-stage heart failure.
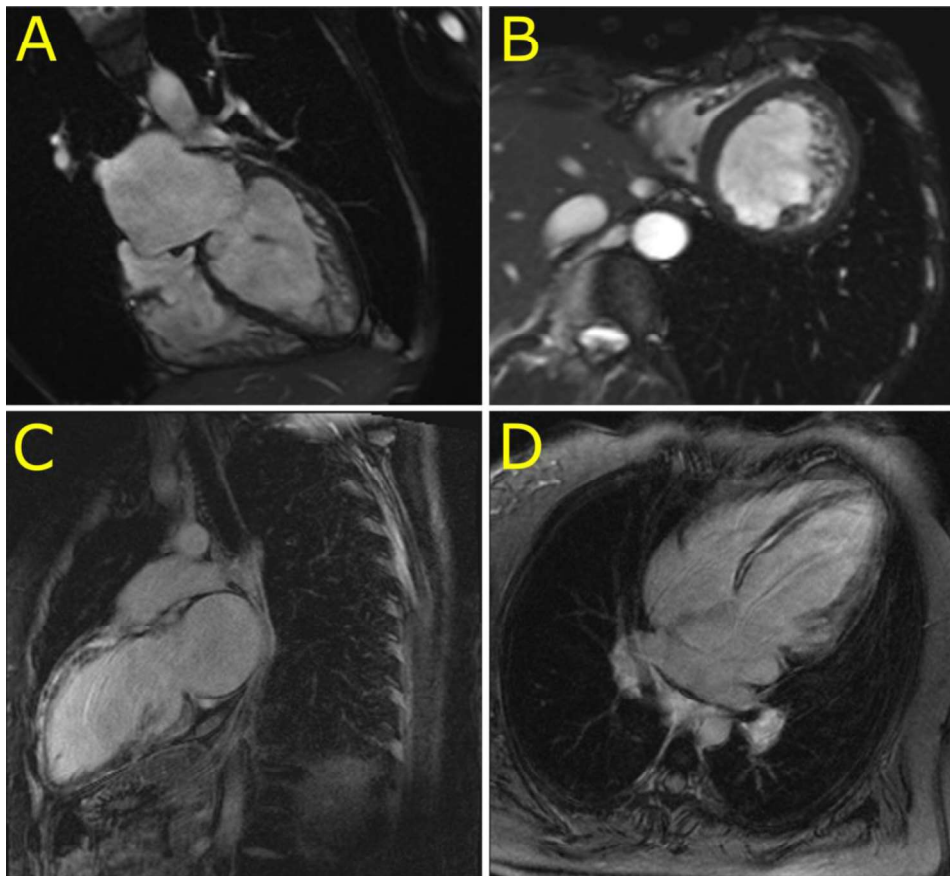
Figure 3. Cardiovascular magnetic resonance imaging in patients with left ventricular non-compaction cardiomyopathy (P4) and dilated cardiomyopathy with an extensive late gadolinium enhancement (P2). (**A,B**): Four chamber and short axis views of left ventricular non-compaction cardiomyopathy in P4. (**C,D**): Two chamber long axis and four chamber views of an extensive late gadolinium enhancement in the ventricular septum and left ventricular anterior wall mimicking inflammatory cardiomyopathy in P2.

3.3. Morphology of Desminopathy in Myocardial and Skeletal Muscle Samples

An immunohistochemical examination of myocardial samples in P1–P3 and P6 showed a diffuse alteration of desmin distribution in cardiomyocytes with a formation of desmin aggregates revealing strong immunoreactivity in the cytoplasm (shown in P1, P3; Figure 4A,E). Electron microscopy of cardiomyocytes in P1, P2, and P6 revealed myofibrillar disruption, streaming Z bands, and deposits of dense, amorphous granulofilamentous material of variable size and shape (shown in P1, P2; Figure 4B,C). In addition, we constructed a set of expression plasmids for the six *DES* missense variants and transfected HT1080 as a cell model without endogenous desmin expression and iPSC-derived cardiomyocytes. These experiments revealed a severe intermediate filament formation defect for *DES*-p.(K43E) and *DES*-p.(R406W) underlining their pathogenicity. Furthermore, electron microscopy of cardiac tissue demonstrated in P2, P4, and P6 focally increased the number of mitochondria, often in clusters, with loss of mitochondrial spatial organization (P2; Figure 4D). Importantly, desmin aggregates were absent in myocardial samples of P4 both at immunohistochemical and ultrastructural analysis. An expression of desmin in myocardium (P2, P4, and P6) was also assessed by Western blot analysis. There was an obvious reduction of the signal in P4 (Figure 1B).

Samples of the skeletal muscle (P4–P5 m. soleus, P4 intercostal muscle, P6 m. deltoideus) showed different findings in P4 and P6 as compared with P5. The morphological analysis in P4 and P6 detected only mild myopathic changes. The light microscopy with hematoxylin-eosin staining showed a marked variability in fiber size and increased number of internal nuclei (P4; Figure 4F). No inclusions were observed by light microscopy. Similarly, desmin immunohistochemistry did not reveal any protein aggregates in the sarcoplasma of P4 and P6 (P4; Figure 4G). In the NADH and SDH reactions, many fibers did not possess the characteristic checkerboard pattern, and in a proportion of fibers there was increased oxidative activity at the periphery of the muscle fibers, indicating the pathological accumulation of mitochondria (P4; Figure 4H). However, no typical ragged red fibers were observed. The distribution of COX reactivity was altered similarly to a NADH/SDH pattern with very few COX-negative fibers present (P4; Figure 4I). On the other hand, the muscle biopsy in P5 showed severe myopathic changes with a large amount of fibro-fatty tissue in the interstitium of the muscle. Desmin immunohistochemistry confirmed in P5 a diffuse alteration of desmin distribution with a formation of desmin aggregates in the cytoplasm of muscle fibers (data not shown).

An ultrastructural analysis of skeletal muscle biopsies revealed a focally increased number of mitochondria, often in clusters, with an altered distribution in P4 and P6 (P4; Figure 4J) however, no ultrastructural abnormality in mitochondria morphology was observed. Typical deposits of dense granulofilamentous material were absent in P4 and were not observed in P6 at the first reading. Thus the first description of the skeletal muscle biopsy in P6 led to the diagnosis of mitochondrial myopathy. Nevertheless, the second reading of the skeletal muscle biopsy performed with the knowledge of the results of genetic tests and abnormal immunostaining of desmin in myocardium discovered a focus of dense amorphous material in a single fiber at electron microscopy (not shown).
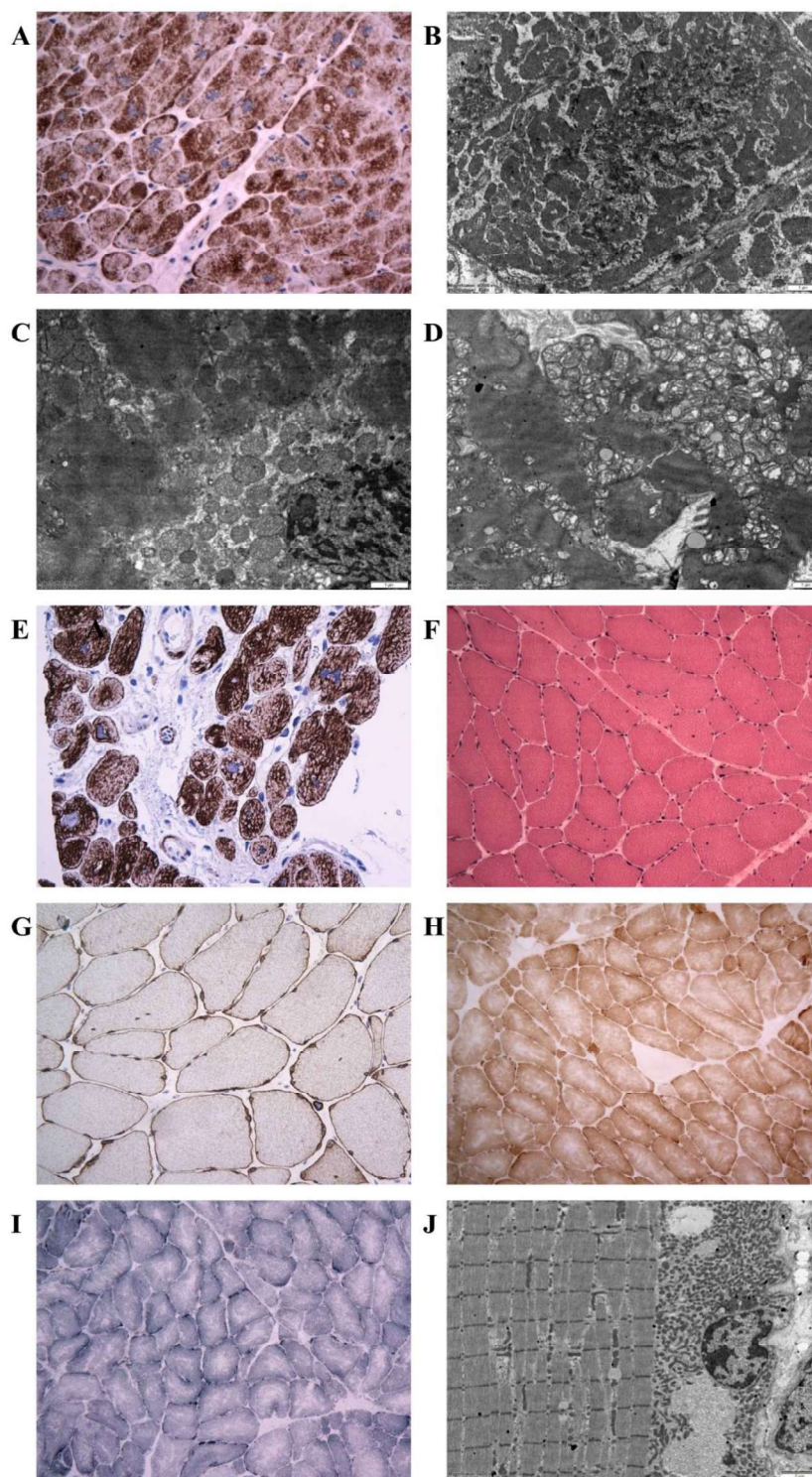
Figure 4. Illustration of histopathology, immunohistochemistry, and electron microscopy in individuals with the novel desmin variants. (**A**): Desmin immunohistochemistry (left ventricular myocardium, explanted heart, P1) documenting a diffuse alteration of desmin distribution with a formation of desmin aggregates revealing strong immunoreactivity in the cytoplasm. Original magnification ×400. (**B**): Electron

Příloha 1a

microscopy (left ventricular myocardium, explanted heart, P1) detects amorphous granulofilamentous material in the cytoplasm of cardiomyocytes compatible with desmin aggregates. Original magnification ×10,000. (**C,D**): Electron microscopy (left ventricular myocardium, explanted heart, P2). (**C**): Pathological dense granulofilamentous inclusions in the cytoplasm of cardiomyocyte. Original magnification ×12,000. (**D**): Increased number of mitochondria in cardiomyocyte, often in clusters, with altered distribution. Original magnification ×8000. (**E**): Desmin immunohistochemistry (right ventricular myocardium, endomyocardial biopsy, P3) revealed an abnormal staining of cardiomyocytes with a formation of desmin positive aggregates. Original magnification ×400. (**F–J**) Diagnostic skeletal muscle biopsy specimens, Soleus muscle, P4, original magnification ×400. (**F**): By light microscopy with hematoxyllin-eosin, there was a marked variability in fiber size, absent inclusions, and increased number of internal nuclei. (**G**): Desmin immunohistochemistry did not reveal any protein aggregates in the sarcoplasma. (**H**): Nicotinamide adenine dinucleotide (NADH) and succinate dehydrogenase (SDH) immunohistochemistry identified few muscle fibers with increased oxidative activity at their periphery, indicating the pathological accumulation of mitochondria. However, no typical ragged red fibers were observed. (**I**): Very few COX-negative fibers were also present. (**J**): Electron-microscopic analysis revealed increased number of mitochondria, often in clusters, with altered distribution. No accumulation of intermediate filaments was observed. Original magnification ×6000.

3.4. Indications for the Pathogenicity of the Novel Desmin Variants

A typical myocardial histopathology and ultrastructure with pathological desmin-immunoreactive aggregates strongly supported the pathogenicity of desmin variants p.(K43E), p.(S57L), and p.(A210D). In addition, the desmin filament formation experiments in transfected HT1080 and in iPSC-derived cardiomyocytes revealed an abnormal cytoplasmic aggregation of DES-p.(K43E). On the other hand, the pathogenicity of the novel desmin variant p.(Q364H) is supported mainly by decreased myocardial desmin expression and co-segregation of the above desmin variant in the family in the absence of other segregating cardiomyopathy-related genes as assessed by WES in the proband.

3.5. Mitochondrial Function and Content in Skeletal Muscle and Heart

An analysis of mitochondrial respiratory enzymes in skeletal muscle homogenates (Table 1) revealed a decreased activity of citrate synthase in P5, the activity of respiratory chain complex IV, and the quantity of mitochondrial respiratory chain proteins were decreased (Figure 5A). An oxygraphy analysis of P6 skeletal muscle fibers further showed a decrease in coupled (state 3-ADP) oxidation of NADH-dependent substrates (pyruvate + malate) to 35% of the mean of the controls (Table 1). More consistent data were provided by the analysis of isolated mitochondria from skeletal muscles of P4–P6. Specific activities of respiratory chain complexes I + III (NADH: Cytochrome c reductase), complex IV (cytochrome c oxidase), and citrate synthase were decreased to 30%–50% of the mean of the controls. Both P5 and P6 had a decreased content of coenzyme Q (Table 1). A low specific content of respiratory chain enzymes, citrate synthase, and porin was further apparent in isolated muscle mitochondria of P4–P6, with the most pronounced decrease observed in P5 (Figure 5A).

Příloha 1a

Table 1. Activities of respiratory chain enzymes in skeletal muscle homogenates (**A**), muscle fibers (**B**), and isolated mitochondria (**C**) of proband P4–P6. For analysis samples of m. tibialis (P4, P5) or m. deltoideus sin. (P6) were used. Enzyme activities and Coenzyme Q10 content are expressed per mg protein.

(A)				
Enzyme Activity of Muscle Homogenates (nmol/min/mg protein)	**P4**	**P5**	**P6**	**Controls** $n = 30$
Complex IV	130.1	38.1	81.8	68–213
Citrate synthase (CS)	109.5	41.4	97.8	48–128
Complex IV/CS	1.19	0.92	0.84	080–160
Coenzyme Q10 content (pmol/mg)	282.9	140.5	112.5	180–460

(B)		
Respiratory Activity of Permeabilized Muscle Fibers (pmol O$_2$/s/mg protein)	**P6**	**Controls** $n = 9$
ADP-stimulated oxidation of NADH-dependent substrates	7.4	16–26
ADP-stimulated oxidation of succinate	10.7	9–18
Cytochrome *c* oxidase respiration	63	43–83

(C)				
Enzyme Activity of Isolated Mitochondria (nmol/min/mg protein)	**P4**	**P5**	**P6**	**Controls** $n = 30$
Complex I	328.5	230.8	131.2	110–290
Complex I+III	94.1	18.7	53.2	126–316
Complex II	69.7	50.5	49.5	21–93
Complex II+III	174.2	92.9	146.7	82–251
Complex III	303.0	342.7	535.0	200–600
Complex IV	578.4	311.6	236.6	658–1552
Citrate synthase	372.5	240.4	384.2	435–1234
Complex I/CS	0.88	0.96	0.34	0.17–0.41
Complex I+III/CS	0.25	0.07	0.13	0.07–0.27
Complex II/CS	0.19	0.21	0.13	0.04–0.12
Complex II+III/CS	0.47	0.39	0.38	0.35–0.36
Complex III/CS	0.81	1.43	1.39	0.56–1.46
Complex IV/CS	1.55	1.30	0.62	0.82–1.88

Abbreviations: ADP–adenosine diphosphate, ATP–adenosine triphosphate, and NADH–reduced form of nicotinamide adenine dinucleotide.

Myocardium of two patients with desminopathy (P2, P6) (Table 2) revealed a general decrease in respiratory chain enzyme activities. An oxidation of NADH and succinate and cytochrome c oxidase respiration decreased to 20%–55% of the controls and activities of respiratory complexes I+III, II+III, and IV decreased to 15%–81%, respectively, indicating more extensive impairment in P2 heart ventricles (Table 2). The impairment of succinate respiration was the most profound with a mean of 277 pmol O$_2$/s/mg. This was much lower than in our historical controls from donor hearts unsuitable for transplantation (653 ± 244 pmol O$_2$/s/mg, $n = 38$) and even myocardium explanted during heart transplantation or ventricular assist device implantation (508 ± 211 pmol O$_2$/s/mg, $n = 91$) [25]. Western blot quantification of mitochondrial proteins showed a decrease in specific content of respiratory chain complexes, also more pronounced in P2, where a very low content of complexes IV and I was associated with the upregulation of complex II (Figure 5B). Other mitochondrial proteins, as porin

(shown in Figure 5A) and adenine nucleotide translocator (not shown) were less affected. Analysis of native forms of respiratory chain complexes by BlueNative electrophoresis (Figure 5C) confirmed a marked reduction of complexes I and IV in P2 heart and further showed that it led to a pronounced decrease of high molecular weight respiratory supercomplexes consisting of complexes I, III, and IV. Similar, yet a smaller decrease of supercomplexes was observed in soleus of R349P desmin knock-in mouse [15] or heart of desmin knockout mouse [27]. The content of mitochondrial DNA (relative to nuclear DNA, D-loop/GAPDH, and 16S RNA/GAPDH) was slightly decreased in P6 heart ventricles (60%–90% of the average value of the controls) but was unchanged in P2 heart. These data indicate mild to pronounced attenuation of the energetic function of mitochondria due to a decreased content and activity of respiratory complexes and supercomplexes in failing hearts of patients with desminopathy.
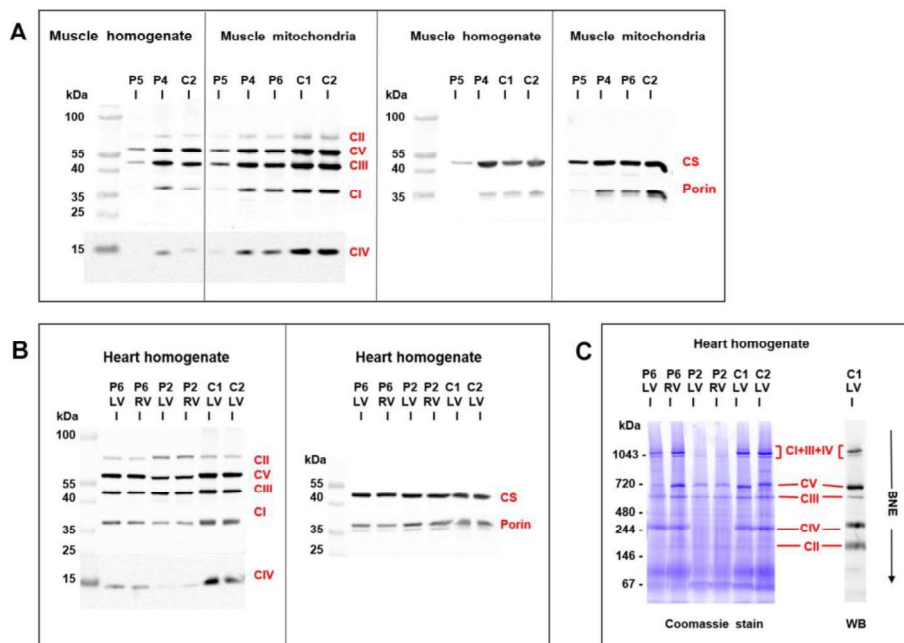
Figure 5. Western blot detection of mitochondrial proteins in skeletal muscle and heart. Analysis of SDS-PAGE resolved proteins from (**A**) muscle homogenates (6 μg protein aliquots) and isolated muscle mitochondria (2 μg protein aliquots) demonstrated a pronounced decrease of respiratory chain complexes (CI-CV), citrate synthase (CS), and porin in skeletal muscle of P5 compared to controls (**C**), P4 and P6 were less affected. Analysis of (**B**) heart homogenates (4 μg protein aliquots) from left and right heart ventricles (LV, RV) demonstrated a marked decrease of respiratory chain enzymes in P2 and a mild decrease in P6 compared to controls (**C**). CS and porin were less affected. BlueNative electrophoresis (**C**) further showed a marked decrease of native respiratory supercomplexes consisting of CI + CIII + CIV in P2 heart ventricles (12 μg protein aliquots).

Table 2. Activities of respiratory chain enzymes and mtDNA content in hearts of proband 2 and 6.

Respiratory/Enzyme Activity	P2 Left Ventricle	P2 Right Ventricle	P6 Left Ventricle	P6 Right Ventricle	Controls $n = 38$
(pmol O_2/s/mg) NADH respiration	245	203	448	229	235–2356
Succinate respiration	295	242	254	319	365–1529
Cytochrome *c* oxidase respiration	766	991	1003	1047	561–4120
(nmol/min/mg) Complex I+III	26.1	30.3	145.1	83.9	44–386
Complex II+III	88.0	71.3	59.5	56.7	27–195
Complex IV	262.6	432.4	430.5	276.8	389–1989
Citrate synthase (CS)	915.9	975.2	562.2	483.6	446–1207
(activity ratio) Complex I+III/CS	0.03	0.03	0.26	0.17	0.09–0.63
Complex II+III/CS	0.10	0.07	0.11	0.12	0.04–0.37
Complex IV/CS	0.29	0.44	0.77	0.57	0.54–2.60
mtDNA content ($2^{-\Delta Ct}$)					
D-loop/GAPDH	4980	5499	2863	3592	2052–10519
16S RNA/GAPDH	11629	10914	8017	7299	3715–15843

Enzyme activities are expressed per mg protein, mtDNA content is expressed as $2^{-\Delta Ct}$ value indicating the number of mtDNA copies per a haploid genome. Abbreviation: GADPH–glyceraldehyde 3-phosphate dehydrogenase.

As changes in mitochondria energetic function can affect a generation of reactive oxygen species, the content of antioxidative enzymes was analyzed by Western blot analysis in skeletal muscle and heart samples from patients with desminopathy (Figure 6). Both P4 and P5 muscle homogenates revealed highly increased glutathione reductase (GR) and superoxide dismutase 1 (SOD1) as well as a variable increase of catalase (CAT) and superoxide dismutase 2 (SOD2). Higher CAT was found in P5 isolated mitochondria, while the most increased SOD1 was of extra-mitochondrial origin (also apparent from the SOD1/SOD2 ratio). An increased content of GR and SOD1 was also found in heart ventricles of P6.
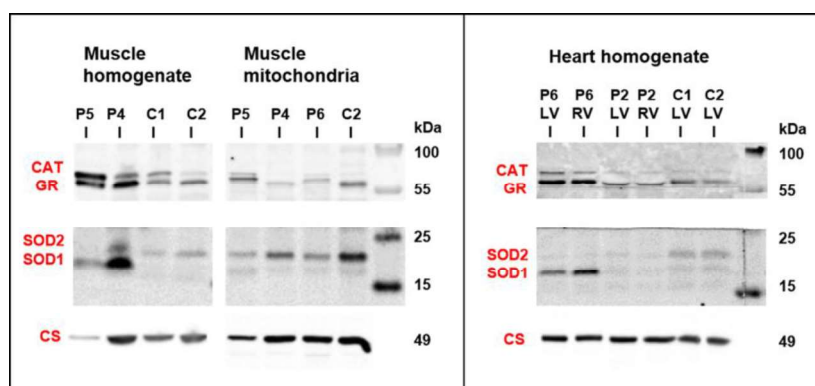

Figure 6. Western blot detection of antioxidative enzymes in skeletal muscle and heart. Both P4 and P5 muscle homogenates revealed variable increase in antioxidative enzymes glutathione reductase (GR), catalase (CAT), and superoxide dismutases 1 and 2 (SOD1, SOD2). Increased content of CAT, GR, and SOD1 was also found in heart ventricles of P6. Protein aliquots–muscle homogenate 30 μg, muscle mitochondria 15 μg, and heart homogenate 20 μg. For comparison, citrate synthase signal (CS) from Figure 5 is shown.

Příloha 1a

4. Discussion

Firstly, the prevalence of desminopathy in a large cohort of patients with an unexplained etiology of cardiomyopathy assessed with WES was 1.8%. Secondly, the presence of pathological desmin aggregates in myocardial/skeletal muscle samples of P1–P3 and decreased myocardial desmin expression in P4 suggested a pathogenicity of two novel *DES* variants and two *DES* variants previously classified as of uncertain significance. Thirdly, a pathogenicity of one variant of uncertain significance (DES-p.(K43E)) was supported also by abnormal desmin filament formation and its cytoplasmic aggregation in transfected HT1080 cells and in iPSC-derived cardiomyocytes. Fourthly, we provided further evidence for LVNC as a novel phenotype of desminopathy. Fifthly, we described secondary mitochondrial dysfunction in skeletal muscle and in myocardium, which was in case of myocardial succinate respiration more profound than in end-stage heart failure of other etiology. To the best of our knowledge, this seems to be the first comprehensive description of mitochondrial dysfunction in human myocardium affected by desminopathy. Finally, secondary mitochondrial dysfunction and/or an extensive left ventricular late gadolinium enhancement in desminopathy may imitate a primary mitochondrial disease or an inflammatory cardiomyopathy.

4.1. Clinical and Histopathological Correlates of Desminopathy

The majority of 68 pathogenic desmin variants that were reported so far are missense or small in-frame deletion variants localized in the helical rod domain [26,28]. A phenotype-genotype correlation meta-analyses revealed that pathogenic variants in the rod 2B domain of *DES* are common among patients with both skeletal and cardiac muscle phenotype, whereas head and tail domain pathogenic variants result mainly in clinically isolated cardiac phenotype [1,29,30]. In agreement with these findings, we found that two *DES* variants in head region (p.(K43E), p.(S57L)) and one novel *DES* variant (p.(A210D)) in the 1B helical domain had in probands isolated cardiac involvement. On the other hand, the novel *DES* mutation located in the 2B helical domain (p.(Q364H)) and two known *DES* variants (p.(R406W), p.(R454W)) affected both the cardiac and skeletal muscle.

Immunohistochemistry revealed pathological desmin aggregates in skeletal or cardiac myocytes in five probands from our study group. Importantly, desmin aggregates were absent in the deltoid muscle of proband 6 (*DES*-p.(R454W)), but present in her myocardial samples. Desmin aggregates were completely absent in proband 4 (*DES*-p.(Q364H)). Immunohistochemistry and electron microscopy of diagnostic muscle soleus biopsy and post-mortem myocardial and intercostal muscle samples failed to detect any pathological protein aggregates. Interestingly, Western blot analysis of the myocardial sample showed a decreased expression of desmin suggesting decreased protein synthesis. This is in agreement with the experience of pathologists that myopathological findings in genetically proven desminopathies may range from no overt pathology over subtle myopathic changes with sporadic protein aggregates to the picture of a vacuolar myopathy [31]. An absence of desmin aggregates has been recently documented both in autosomal dominant [32] and autosomal recessive [33] desminopathy.

4.2. Novel Cardiac Phenotypes of Desminopathy

In addition to known cardiac phenotypes of desminopathy like DCM, RCM HCM, and ACM [1,28,29], we observed LVNC as a relatively novel phenotype. So far, *DES* variants have been associated with LVNC just in a few individuals [34–37]. The first report from Arbustini et al. [34] described a family with a segregation of *DES* variant p.(G84S) with non-obstructive hypertrophic cardiomyopathy and one case of LVNC. Another group [35] reported one sporadic case of LVNC in a child with a *DES* variant p.(L398P). An occurrence of two cases of LVNC in one family has been recently associated with an in-frame mutation of desmin p.(Q113_L115del) affecting the α–helical rod domain [36] with a formation of typical desmin-immunoreactive aggregates. We expanded the available evidence by a description of another familial occurrence of two cases of LVNC associated

with the desmin variant p.(Q364H) with a decreased myocardial expression of desmin and absent desmin aggregates in myocardial/skeletal biopsy.

Recently, a novel phenotype of desminopathy describing left ventricular arrhythmogenic cardiomyopathy was reported to have a significant amount of subepicardial fibrosis [32]. A similar phenotype had our P2, which mimicked inflammatory cardiomyopathy by an extensive late gadolinium enhancement in the left ventricle and persistent elevation of cardiac troponins. However, ventricular ectopy and an inversion of T waves in inferior and precordial leads were absent. Taken together, the presence of desminopathy should be considered also in unexplained cases of LVNC and non-ischemic left ventricular systolic dysfunction with an extensive subepicardial or intramural fibrosis.

4.3. Mitochondrial Dysfunction in Desminopathy

Desminopathy may also imitate a mitochondrial disease, as was shown by Mc Cormic et al. [16]. The presence of SDH positive/COX negative muscle fibers, decreased activities of mitochondrial respiratory chain enzymes, and reduced mitochondrial DNA content in skeletal muscle biopsy lead to the suspicion of mitochondrial disease. We observed similar findings in our patient (P6) with an absence of desmin aggregates and signs of mitochondrial dysfunction in deltoid muscle biopsy. The correct diagnosis in our case provided genetic testing and immunostaining of myocardial samples.

Studies in desmin null mice and patients with recessive desmin-null muscular dystrophy revealed abnormalities in nuclear and mitochondrial localization and morphology, as well as impaired mitochondrial respiratory capacity [13,14]. Secondary mitochondrial dysfunction was also confirmed by Schröder et al. [38] and Vincent et al. [39] in skeletal muscle biopsies of heterozygous patients with desminopathy. Furthermore, Vincent et al. [39] reported a deficiency of respiratory chain complex I and IV compared to age matched controls and a low mitochondrial mass compared to controls. Our morphological and functional data from skeletal muscle samples are in agreement with the above mentioned studies and further evidence [40,41]. We observed a variable mitochondrial dysfunction characterized by a decreased expression of mitochondrial respiratory chain components and other mitochondrial proteins, as well as decreased enzyme activities, suggesting secondary changes in mitochondrial energetic function. The upregulation of several anti-oxidative enzymes, in particular that of superoxide dismutase 1 in homogenates, but not in isolated mitochondria, indicated increased antioxidative defense outside mitochondria.

Novel findings provided our analysis of myocardial energetic function in the explanted failing hearts of two probands with desminopathy. In one case harboring p.(R454W) desmin tail mutation we found a mild decrease in the content and activities of respiratory chain complexes while in the other case with p.(S57L) mutation in the desmin head region was present a very pronounced decrease in mitochondria proteins and an alteration of the bioenergetics function. Interestingly, changes in respiratory chain enzymes thus also caused a downregulation of respiratory supercomplexes that are expected to modulate the catalytic function as well as reactive oxygen species production by the respiratory chain [42]. This was associated with a decrease in several marker proteins of different mitochondrial compartments suggesting a complex mitochondrial dysfunction. The most pronounced was the impairment of myocardial succinate respiration, which was in our patients with desminopathy more profound than in end-stage heart failure of other etiologies.

4.4. Study Limitations

There are several limitations to our study. First, the small study group size reflects the rare occurrence of desminopathy and may limit the general applicability of the study results. Secondly, the small size of affected families limited the segregation studies. However, WES enabled us to exclude the presence of other pathogenic variants in cardiomyopathy- and skeletal myopathy-related genes, including genes coding mitochondrial proteins. Thirdly, an assessment of the mitochondrial function in tissues was possible only in a subgroup of patients with a clinical indication to biopsy or undergoing cardiac surgery. Finally, decreased desmin expression in P4 with a missense variant of *DES* might be

Příloha 1a

related to replacement fibrosis of the myocardium or epigenetic factors. Unfortunately, we cannot provide data supporting any of these hypotheses.

5. Conclusions

Desminopathy is a rare cause of cardiomyopathy and/or skeletal muscle myopathy with a pleomorphic clinical presentation and poor prognosis. This diagnosis should also be considered in individuals with LVNC. Differential diagnosis also includes mitochondrial and inflammatory myocardial diseases.

Abbreviations and Acronyms

ACM	arrhythmogenic cardiomyopathy
CAT	catalase
COX	cytochrome c oxidase
DCM	dilated cardiomyopathy
DES	desmin gene
GADPH	glyceraldehyde 3-phosphate dehydrogenase
GR	glutathione reductase
HCM	hypertrophic cardiomyopathy
LVNC	left ventricular non-compaction cardiomyopathy
NADH	reduced form of nicotinamide adenine dinucleotide
MPS	massively parallel sequencing
RCM	restrictive cardiomyopathy
SDH	succinate dehydrogenase
SOD	superoxide dismutase
WES	whole exome sequencing

References

1. van Spaendonck-Zwarts, K.Y.; van Hessem, L.; Jongbloed, J.D.; de Walle, H.E.; Capetanaki, Y.; van der Kooi, A.J.; van Langen, I.M.; van den Berg, M.P.; van Tintelen, J.P. Desmin-related myopathy. *Clin. Genet.* **2011**, *80*, 354–366. [CrossRef]

Příloha 1a

2. Li, D.; Tapscoft, T.; Gonzalez, O.; Burch, P.E.; Quiñones, M.A.; Zoghbi, W.A.; Hill, R.; Bachinski, L.L.; Mann, D.L.; Roberts, R. Desmin mutation responsible for idiopathic dilated cardiomyopathy. *Circulation* **1999**, *100*, 461–464. [CrossRef]

3. Taylor, M.R.; Slavov, D.; Ku, L.; Di Lenarda, A.; Sinagra, G.; Carniel, E.; Haubold, K.; Boucek, M.M.; Ferguson, D.; Graw, S.L.; et al. Prevalence of desmin mutations in dilated cardiomyopathy. *Circulation* **2007**, *115*, 1244–1251. [CrossRef]

4. Goldfarb, L.G.; Park, K.Y.; Cervenakova, L.; Gorokhova, S.; Lee, H.S.; Vasconcelos, O.; Nagle, J.W.; Semino-Mora, C.; Sivakumar, K.; Dalakas, M.C. Missence mutations in desmin associated with familial cardiac and skeletal myopathy. *Nat. Genet.* **1998**, *19*, 402–403. [CrossRef]

5. Arbustini, E.; Morbini, P.; Grasso, M.; Fasani, R.; Verga, L.; Bellini, O.; Dal Bello, B.; Campana, C.; Piccolo, G.; Febo, O.; et al. Restrictive cardiomyopathy, atrioventricular block and mild to subclinical myopathy in patients with desmin-immunoreactive material deposits. *J. Am. Coll. Cardiol.* **1998**, *31*, 645–653. [CrossRef]

6. Park, K.Y.; Dalakas, M.C.; Semino-Mora, C.; Lee, H.S.; Litvak, S.; Takeda, K.; Ferrans, V.J.; Goldfarb, L.G. Desmin myopathy, a skeletal myopathy with cardiomyopathy caused by mutations in the desmin gene. *N. Engl. J. Med.* **2000**, *342*, 770–780. [CrossRef]

7. Pruszczyk, P.; Kostera-Pruszczyk, A.; Shatunov, A.; Goudeau, B.; Dramiñska, A.; Takeda, K.; Sambuughin, N.; Vicart, P.; Strelkov, S.V.; Goldfarb, L.G.; et al. Restrictive cardiomyopathy with atrioventricular conduction block resulting from a desmin mutation. *Int. J. Cardiol.* **2007**, *117*, 244–253. [CrossRef] [PubMed]

8. Olive, M.; Armstrong, J.; Miralles, F.; Pou, A.; Fardeau, M.; Gonzalez, L.; Martínez, F.; Fischer, D.; Martínez Matos, J.A.; Shatunov, A.; et al. Phenotypic patterns of desminopathy associated with three novel mutations in the desmin gene. *Neuromuscul. Disord.* **2007**, *17*, 443–450. [CrossRef] [PubMed]

9. Otten, E.; Asimaki, A.; Maass, A.; van Langen, I.M.; van der Wal, A.; de Jonge, N.; van den Berg, M.P.; Saffitz, J.E.; Wilde, A.A.; Jongbloed, J.D.; et al. Desmin mutations as a cause of right ventricular heart failure affect the intercalated disks. *Heart Rhythm* **2010**, *7*, 1058–1064. [CrossRef] [PubMed]

10. Klauke, B.; Kossmann, S.; Gaertner, A.; Brand, K.; Stork, I.; Brodehl, A.; Dieding, M.; Walhorn, V.; Anselmetti, D.; Gerdes, D.; et al. De novo desmin mutation N116S is associated with arrhythmogenic right ventricular cardiomyopathy. *Hum. Mol. Genet.* **2010**, *19*, 4595–4607. [CrossRef]

11. Lorenzon, A.; Beffagna, G.; Bauce, B.; De Bortoli, M.; Li Mura, I.E.A.; Calore, M.; Dazzo, E.; Basso, C.; Nava, A.; Thiene, G.; et al. Desmin mutations and arrhythmogenic right ventricular cardiomyopathy. *Am. J. Cardiol.* **2013**, *111*, 400–405. [CrossRef] [PubMed]

12. Capetanaki, Y.; Bloch, R.J.; Kouloumenta, A.; Mavroidis, M.; Psarras, S. Muscle intermediate filaments and their links to membranes and membranous organelles. *Exp. Cell. Res.* **2007**, *313*, 2063–2076. [CrossRef] [PubMed]

13. Milner, D.J.; Mavroidis, M.; Weisleder, N.; Capetanaki, Y. Desmin cytoskeleton linked to muscle mitochondrial distribution and respiratory function. *J. Cell. Biol.* **2000**, *150*, 1283–1298. [CrossRef] [PubMed]

14. Henderson, M.; Waele, L.D.; Hudson, J.; Eagle, M.; Sewry, C.; Marsh, J.; Charlton, R.; He, L.; Blakely, E.L.; Horrocks, I.; et al. Recessive desmin-null muscular dystrophy with central nuclei and mitochondrial abnormalities. *Acta Neuropathol. (Berl.)* **2013**, *125*, 917–919. [CrossRef] [PubMed]

15. Winter, L.; Wittig, I.; Peeva, V.; Eggers, B.; Heidler, J.; Chevessier, F.; Kley, R.A.; Barkovits, K.; Strecker, V.; Berwanger, C.; et al. Mutant desmin substantially perturbs mitochondrial morphology, function and maintenance in skeletal muscle tissue. *Acta Neuropathol.* **2016**, *132*, 453–473. [CrossRef]

16. McCormick, E.M.; Kenyon, L.; Falk, M.J. Desmin common mutation is associated with multi-systemic disease manifestations and depletion of mitochondria and mitochondrial DNA. *Front. Genet.* **2015**, *6*, 199. [CrossRef]

17. Hartmannova, H.; Kubanek, M.; Sramko, M.; Piherova, L.; Noskova, L.; Hodanova, K.; Stranecky, V.; Pristoupilova, A.; Sovova, J.; Marek, T.; et al. Isolated X-linked hypertrophic cardiomyopathy caused by a novel mutation of the Four-and-a-half LIM domain 1 gene. *Circ. Cardiovasc. Genet.* **2013**, *6*, 543–551. [CrossRef]

18. Kalia, S.S.; Adelman, K.; Bale, S.J.; Chung, W.K.; Eng, C.; Evans, J.P.; Herman, G.E.; Hufnagel, S.B.; Klein, T.E.; Korf, B.R.; et al. Recommendations for reporting of secondary findings in clinical exome and genome sequencing, 2016 update (ACMG SF v2.0): A policy statement of the American College of Medical Genetics and Genomics. *Genet. Med.* **2017**, *19*, 249–255. [CrossRef]

Příloha 1a

19. Brodehl, A.; Dieding, M.; Biere, N.; Unger, A.; Klauke, B.; Walhorn, V.; Gummert, J.; Schulz, U.; Linke, W.A.; Gerull, B.; et al. Functional characterization of the novel DES mutation p.L136P associated with dilated cardiomyopathy reveals a dominant filament assembly defect. *J. Mol. Cell. Cardiol.* **2016**, *91*, 207–214. [CrossRef]

20. Brodehl, A.; Pour Hakimi, S.A.; Stanasiuk, C.; Ratnavadivel, S.; Hendig, D.; Gaertner, A.; Gerull, B.; Gummert, J.; Paluszkiewicz, L.; Milting, H. Restrictive Cardiomyopathy is Caused by a Novel Homozygous Desmin (DES) Mutation p.Y122H Leading to a Severe Filament Assembly Defect. *Genes (Basel)* **2019**, *11*, 918. [CrossRef]

21. Debus, J.D.; Milting, H.; Brodehl, A.; Kassner, A.; Anselmetti, D.; Gummert, J.; Gaertner-Rommel, A. In vitro analysis of arrhythmogenic cardiomyopathy associated desmoglein-2 (DSG2) mutations reveals diverse glycosylation patterns. *J. Mol. Cell. Cardiol.* **2019**, *129*, 303–313. [CrossRef] [PubMed]

22. Brodehl, A.; Gaertner-Rommel, A.; Klauke, B.; Grewe, S.A.; Schirmer, I.; Peterschröder, A.; Faber, L.; Vorgerd, M.; Gummert, J.; Anselmetti, D.; et al. The novel αB-crystallin (CRYAB) mutation p.D109G causes restrictive cardiomyopathy. *Hum. Mutat.* **2017**, *38*, 947–952. [CrossRef] [PubMed]

23. Sheehan, D.C.; Hrapchak, B.B. *Theory and Practice of Histotechnology*, 2nd ed.; Mosby: Columbus, OH, USA, 1987.

24. Makinen, M.W.; Lee, C.P. Biochemical studies of skeletal muscle mitochondria. I. Microanalysis of cytochrome content, oxidative and phosphorylative activities of mammalian skeletal muscle mitochondria. *Arch. Biochem. Biophys.* **1968**, *126*, 75–82. [CrossRef]

25. Melenovsky, M.; Petrak, J.; Mracek, T.; Benes, J.; Borlaug, B.A.; Nuskova, H.; Pluhacek, T.; Spatenka, J.; Kovalcikova, J.; Drahota, Z.; et al. Myocardial Iron Content and Mitochondrial Function in Heart Failure: Direct Tissue Analysis. *Eur. J. Heart Fail.* **2017**, *19*, 522–530. [CrossRef]

26. Brodehl, A.; Gaertner-Rommel, A.; Milting, H. Molecular insights into cardiomyopathies associated with desmin (DES) mutations. *Biophys. Rev.* **2018**, *10*, 983–1006. [CrossRef]

27. Diokmetzidou, A.; Soumaka, E.; Kloukina, I.; Tsikitis, M.; Makridakis, M.; Varela, A.; Davos, C.H.; Georgopoulos, S.; Anesti, A.; Vlachou, A.; et al. Desmin and αB-Crystallin Interplay in.Maintenance of Mitochondrial Homeostasis and Cardiomyocyte Survival. *J. Cell Sci.* **2016**, *129*, 3705–3720. [CrossRef]

28. Bär, H.; Goudeau, B.; Wälde, S.; Casteras-Simon, M.; Mücke, N.; Shatunov, A.; Goldberg, Y.P.; Clarke, C.; Holton, J.L.; Eymard, B.; et al. Conspicuous involvement of desmin tail mutations in diverse cardiac and skeletal myopathies. *Hum. Mutat.* **2007**, *28*, 374–386. [CrossRef]

29. Capetanaki, Y.; Papathanasiou, S.; Diokmetzidou, A.; Vatsellas, G.; Tsikitis, M. Desmin related disease: A matter of cell survival failure. *Curr. Opin. Cell Biol.* **2015**, *32*, 113–120. [CrossRef]

30. Kostera-Pruszczyk, A.; Pruszczyk, P.; Kamińska, A.; Lee, H.S.; Goldfarb, L.G. Diversity of cardiomyopathy phenotypes caused by mutations in desmin. *Int. J. Cardiol.* **2008**, *131*, 146–147. [CrossRef]

31. Clemen, C.S.; Herrmann, H.; Strelkov, S.V.; Schröder, R. Desminopathies: Pathology and mechanisms. *Acta Neuropathol.* **2013**, *125*, 47–75. [CrossRef]

32. Bermúdez-Jiménez, F.J.; Carriel, V.; Brodehl, A.; Alaminos, M.; Campos, A.; Schirmer, I.; Milting, H.; Abril, B.Á.; Álvarez, M.; López-Fernández, S.; et al. The Novel Desmin Mutation p.Glu401Asp Impairs Filament Formation, Disrupts Cell Membrane Integrity and Causes Severe Arrhythmogenic Left Ventricular Cardiomyopathy/Dysplasia. *Circulation* **2018**, *137*, 1595–1610. [CrossRef] [PubMed]

33. Cetin, N.; Balci-Hayta, B.; Gundesli, H.; Korkusuz, P.; Purali, N.; Talim, B.; Tan, E.; Selcen, D.; Erdem-Ozdamar, S.; Dincer, P. A novel desmin mutation leading to autosomal recessive limb-girdle muscular dystrophy: Distinct histopathological outcomes compared with desminopathies. *J. Med. Genet.* **2013**, *50*, 437–443. [CrossRef] [PubMed]

34. Arbustini, E.; Favalli, V.; Narula, N.; Serio, A.; Grasso, M. Left Ventricular Noncompaction: A Distinct Genetic Cardiomyopathy? *J. Am. Coll. Cardiol.* **2016**, *68*, 949–966. [CrossRef] [PubMed]

35. van Waning, J.I.; Caliskan, K.; Hoedemaekers, Y.M.; van Spaendonck-Zwarts, K.Y.; Baas, A.F.; Boekholdt, S.M.; van Melle, J.P.; Teske, A.J.; Asselbergs, F.W.; Backx, A.P.C.M.; et al. Genetics, Clinical Features, and Long-Term Outcome of Noncompaction Cardiomyopathy. *J. Am. Coll. Cardiol.* **2018**, *71*, 711–722. [CrossRef]

36. Marakhonov, A.V.; Brodehl, A.; Myasnikov, R.P.; Sparber, P.A.; Kiseleva, A.V.; Kulikova, O.V.; Meshkov, A.N.; Zharikova, A.A.; Koretsky, S.N.; Kharlap, M.S.; et al. Noncompaction cardiomyopathy is caused by a novel in-frame desmin (DES) deletion mutation within the 1A coiled-coil rod segment leading to a severe filament assembly defect. *Hum. Mutat.* **2019**, *40*, 734–741. [CrossRef]

Příloha 1a

37. Miszalski-Jamka, K.; Jefferies, J.L.; Mazur, W.; Głowacki, J.; Hu, J.; Lazar, M.; Gibbs, R.A.; Liczko, J.; Kłyś, J.; Venner, E.; et al. Novel Genetic Triggers and Genotype-Phenotype Correlations in Patients with Left Ventricular. *Noncompact. Circ. Cardiovasc. Genet.* **2017**, *10*, e001763. [CrossRef]

38. Schröder, R.; Goudeau, B.; Simon, M.C.; Fischer, D.; Eggermann, T.; Clemen, C.S.; Li, Z.; Reimann, J.; Xue, Z.; Rudnik-Schöneborn, S.; et al. On noxious desmin: Functional effects of a novel heterozygous desmin insertion mutation on the extrasarcomeric desmin cytoskeleton and mitochondria. *Hum. Mol. Genet.* **2003**, *12*, 657–669. [CrossRef]

39. Vincent, A.E.; Grady, J.P.; Rocha, M.C.; Alston, C.L.; Rygiel, K.A.; Barresi, R.; Taylor, R.W.; Turnbull, D.M. Mitochondrial dysfunction in myofibrillar myopathy. *Neuromuscul. Disord.* **2016**, *26*, 691–701. [CrossRef]

40. Galata, Z.; Kloukina, I.; Kostavasili, I.; Varela, A.; Davos, C.H.; Makridakis, M.; Bonne, G.; Capetanaki, Y. Amelioration of desmin network defects by αB-crystallin overexpression confers cardioprotection in a mouse model of dilated cardiomyopathy caused by LMNA gene mutation. *J. Mol. Cell. Cardiol.* **2018**, *125*, 73–86. [CrossRef]

41. Tsikitis, M.; Galata, Z.; Mavroidis, M.; Psarras, S.; Capetanaki, Y. Intermediate filaments in cardiomyopathy. *Bioph. Rev.* **2018**, *10*, 1007–1031. [CrossRef]

42. Milenkovic, D.; Blaza, J.N.; Larsson, N.G.; Hirst, J. The Enigma of the Respiratory Chain Supercomplex. *Cell Metab.* **2017**, *25*, 765–776. [CrossRef] [PubMed]

ORIGINAL RESEARCH ARTICLE

Danon disease is an underdiagnosed cause of advanced heart failure in young female patients: a LAMP2 flow cytometric study

Jiri Gurka[1], Lenka Piherova[2], Filip Majer[2], Anna Chaloupka[3], Daniela Zakova[4], Ondrej Pelak[5], Alice Krebsova[1], Petr Peichl[1], Jan Krejci[3], Tomas Freiberger[4], Vojtech Melenovsky[1], Josef Kautzner[1], Tomas Kalina[5], Jakub Sikora[2,6] and Milos Kubanek[1]*

[1]*Department of Cardiology, Institute for Clinical and Experimental Medicine, Prague, Czech Republic;* [2]*Research Unit for Rare Diseases, Department of Pediatrics and Adolescent Medicine, First Faculty of Medicine, Charles University and General University Hospital, Prague, Czech Republic;* [3]*1st Internal Cardioangiologic Clinic, Faculty of Medicine, Masaryk University and St. Annes University Hospital, Brno, Czech Republic;* [4]*Centre of Cardiovascular and Transplant Surgery, St. Annes University Hospital, Brno, Czech Republic;* [5]*Department of Paediatric Haematology and Oncology, Childhood Leukaemia Investigation Prague, Second Faculty of Medicine, Charles University and University Hospital Motol, Prague, Czech Republic;* [6]*Institute of Pathology, First Faculty of Medicine, Charles University and General University Hospital, Prague, Czech Republic*

Abstract

Aims   Danon disease (DD) is a rare X-linked disorder caused by mutations in the lysosomal-associated membrane protein type 2 gene (*LAMP2*). DD is difficult to distinguish from other causes of dilated or hypertrophic cardiomyopathy (HCM) in female patients. As DD female patients regularly progress into advanced heart failure (AHF) aged 20–40 years, their early identification is critical to improve patient survival and facilitate genetic counselling. In this study, we evaluated the prevalence of DD among female patients with non-ischemic cardiomyopathy, who reached AHF and were younger than 40 years.
Methods and results   The study cohort comprised 60 female patients: 47 (78%) heart transplant recipients, 2 (3%) patients treated with ventricular assist device, and 11 (18%) patients undergoing pre-transplant assessment. Aetiology of the cardiomyopathy was known in 15 patients (including two DD patients). LAMP2 expression in peripheral white blood cells (WBC) was tested by flow cytometry (FC) in the remaining 45 female patients. Whole exome sequencing was used as an alternative independent testing method to FC. Five additional female DD patients (two with different novel *LAMP2* mutations) were identified by FC. The total prevalence of DD in this cohort was 12%. HCM phenotype (57% vs. 9%, *P = 0.022) and delta waves identified by electrocardiography (43% vs. 0%, **P = 0.002) were significantly more frequent in DD female patients.
Conclusions   Danon disease is an underdiagnosed cause of AHF in young female patients. LAMP2 expression testing in peripheral WBCs by FC can be used as an effective screening/diagnostic tool to identify DD in this patient population.

Introduction

Danon disease (DD, OMIM 300257) is a rare X-linked disorder caused by mutations in the lysosomal-associated membrane protein type 2 gene (*LAMP2*, *Xq24*).[1] All three LAMP2 isoforms (B, A, and C) contribute to lysosomal processing of autophagic substrates.[2] Almost all *LAMP2* mutations result in the absence of the protein [LAMP2 deficiency (LAMP2def)].

X-hemizygous male DD patients present with a complex phenotype that is dominated by cardiomyopathy with massive left ventricular hypertrophy, delta waves by electrocardiography, muscle weakness, and mild cognitive disability. Importantly, male DD patients have extremely poor prognosis due to end-stage congestive heart failure and malignant ventricular arrhytmias. Their mean age at heart transplantation or death is 18–19 years.[3,4]

Unless modified by processes such as formation of syncytia,[5] expression of the mutant *LAMP2* allele is mosaic (mosaic LAMP2def) because of X-chromosome inactivation (XCI) in the tissues of the X-heterozygous female DD patients. As a likely consequence, females present with a milder cardiac DD phenotype with an equal prevalence of (on many occasions isolated) dilated cardiomyopathy (DCM) and hypertrophic cardiomyopathy (HCM). DD female patients also become symptomatic approximately 15 years later than male patients, have an average survival ~35 years, and are less affected by skeletal myopathy and cognitive defects.[3] However, as shown by the latest meta-analysis of published DD studies, similar proportions of DD females and males progress into end-stage heart failure.[6] Some DD females are also at risk of sudden cardiac death.[7] Timely identification of DD female patients is therefore important for their prognostic stratification and family counselling.

Peripheral white blood cells (WBCs) can be used to assess LAMP2 expression/LAMP2 deficiency in suspect male and female DD patients. LAMP2 western blotting in WBCs homogenates was described by Fanin *et al.*[8] who documented the protein deficiency in male DD patients. In their single female DD patient, however, the latter authors showed nearly normal LAMP2 levels and highlighted the inefficiency of this approach due to problematic interpretation of the results in this particular patient group. Flow cytometric (FC) detection of LAMP2 in WBCs was first reported by Regelsberger *et al.*[9] Expanding these seminal studies, we optimized and presented a polychromatic FC protocol that allows quantitation of LAMP2def WBC populations not only in male DD patients but also in female DD patients and somatic mosaic carriers of *LAMP2* mutations.[10–12]

Even though female patients are frequently the first affected individuals in DD families, many are identified retrospectively or even *post-mortem* after the diagnosis is established in their affected male relative(s) (brother or son). To the best of our knowledge, no large-scale study(ies) evaluating prevalence of DD among female patients with cardiologic pathologies has been presented. To fill this unfortunate information gap, we assessed the prevalence and evaluated the clinical characteristics of DD in female patients who reached advanced heart failure (AHF) due to non-ischemic cardiomyopathy and were younger than 40 years of age. LAMP2 FC in WBCs was used as a screening diagnostic method. Whole-exome sequencing (WES) served as an alternative independent testing approach.

Methods

Study design and patient cohort

This was a two-centre cohort study. The study group was recruited from patients of the two Czech heart transplant centres. From November 2016 to October 2018, 60 female patients with AHF due to non-ischemic cardiomyopathy were identified and agreed to inclusion in the study (*Figure 1A*). All patients were younger than 40 years at the time of heart transplantation or at pre-transplant assessment and were either living female heart transplant recipients, female patients on mechanical circulatory support or female patients referred to pre-transplant assessment. The selected cut-off age of 40 years was based on previously presented data of mean age of cardiac transplant (32.3 ± 14.5 years)[3] and median age of end-stage cardiomyopathy [28 years (18.0–50.0)][6] in female DD patients.

The study was approved by the Ethics Committee of the authors' home institution and was conducted in accordance with the principles of the Declaration of Helsinki. All patients provided a written informed consent prior to participating in the study.

Study protocol

Medical records of the 60 female patients were reviewed, and their clinical data, electrocardiographic, and echocardiographic findings were collected. Abnormal electrocardiograms suggesting pre-excitation were reviewed by an electrophysiologist blinded to the aetiology of the cardiomyopathy, to confirm/exclude the presence of delta waves. Among the 60 patients (*Figure 1A*, *Table 1*), 15 female patients (25%) had a known aetiology of the cardiomyopathy (for details, see supporting information). Two patients (#1 and #2, *Table 2*) who were diagnosed with DD prior the start of this study were among these 15 patients. The remaining 45 patients (75%) underwent LAMP2 FC in WBCs and WES analyses. For these analyses, 5 ml of peripheral venous blood were collected into an EDTA-containing tube(s). Samples for FC were maintained at room temperature and tested within 24 h of collection.

LAMP2 flow cytometry in white blood cells

Intracellular LAMP1 and LAMP2 protein content in peripheral WBCs was assessed by polychromatic FC based on previously reported protocols.[11] In short, leukocytes were isolated by sedimentation over 2% dextran, fixed and permeabilized (BD FACS Lyse and Perm solution (BD Bioscience, San Jose, CA, USA)), and then incubated with fluorochrome-conjugated antibodies anti-LAMP2 (CD107b, clone H4B4) phycoerythrin, anti-LAMP1 (lysosomal-associated membrane protein type 1, CD107a, clone H4A3) Alexa Fluor 488, anti-CD45 PerCP, anti-CD19 APC, anti-CD3 Alexa Fluor 700 and anti-CD14 Pacific Blue (all from Exbio Praha, Vestec, Czech Republic), anti-CD15 Brilliant Violet 510 (BioLegend, Inc, San Diego, CA, USA), for 30 min, washed twice, and measured using BD LSRII flow

Příloha 1a

Figure 1 LAMP2 flow cytometric screening in the patient cohort. (A) Schematic summary of the findings in the patient cohort. Symbols correspond to panel B. Summary of the whole-exome sequencing findings is provided in the supporting information. (B) % fractions of LAMP2 deficiency (LAMP2def) granulocytes identified by the LAMP2 flow cytometry screening in 45 female patients. The numbers correspond to individual female DD patients as listed in Table 2. Values shown for Patients #1[10] and #2[13] were measured prior the start of this screening study. The threshold of 5% of LAMP2def granulocytes is highlighted by the dashed line. The minute fraction of LAMP2def granulocytes (2.6%) in Patient #4 is a result of her unique Xq24 molecular pathology resulting in extremely skewed X-chromosome inactivation ratios in white blood cells (Table 2 and also Majer et al.[14] for further details including the LAMP1/LAMP2 scatterplots in monocytes and granulocytes of patient #4). (C) LAMP1/LAMP2 flow cytometry scatterplots demonstrating the typical profiles seen healthy control, female DD patient (Patient #7 is shown), and male DD patient (patient III.3 from Majer et al. [10] is shown). LAMP2def and LAMP2+ granulocytes are gated. The deficit is mosaic (LAMP2def and LAMP2+ cells are found) and corresponds to white blood cell X-chromosome inactivation ratios in the X-heterozygous female DD patient, whereas it is uniform (only LAMP2def cells are found) in X-hemizygous male DD patient. DD, Danon disease.
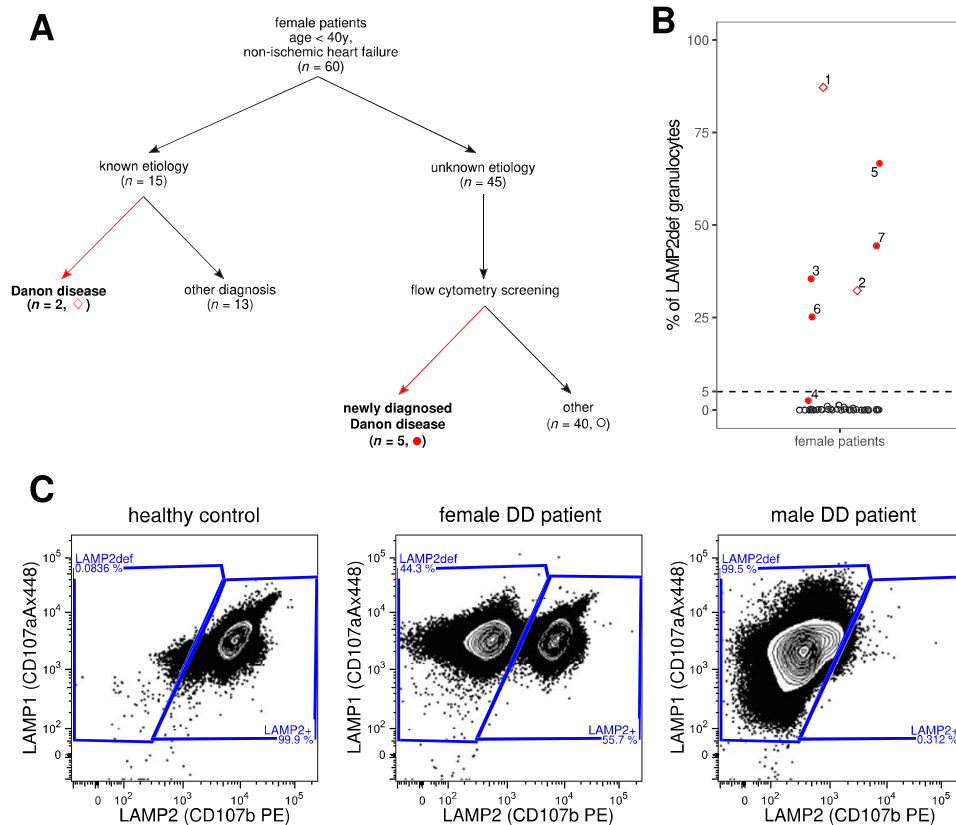
cytometer (BD Biosciences) equipped with 405, 488, and 633 nm lasers. Technical details (sample processing/staining protocol and gating strategy), interpretation, and representative examples of positive results in female and male DD patients are summarized in a Standard Operating Protocol, which is included in the supporting information (pages 7–9).

Populations of LAMP2def granulocytes and LAMP2def monocytes were analysed by FC specialists (T.K. and O.P.) blinded to the aetiology of cardiomyopathy and results of the WES analyses. Anti-LAMP1 staining served as a permeabilization control. A threshold of 5% of LAMP2def granulocytes (or monocytes) was set to calculate the sensitivity and specificity of the FC assay. This value was selected because ~98.3% of healthy adult females have WBC XCI ratios within the >5:95/<95:5 range.[15]

Molecular genetic analyses

To detect causal genetic variants, WES was performed according to internationally accepted guidelines.[16] Full technical details are provided in the supporting information. Analyses of

the *LAMP2* genomic DNA, full-length isoform *LAMP2* messenger RNAs/complementary DNAs and HUMARA XCI assays in DD patients #5, #6, and #7 were performed as reported previously.[10,11]

Myocardial LAMP2 immunohistochemistry

In DD patients #5, #6 and #7, myocardial LAMP2 immunohistochemistry (IHC) was performed in endomyocardial biopsies, explanted hearts or excisions from the left ventricle obtained at implantation of ventricular assist devices. The staining protocol followed previous studies.[10,14]

Statistical analyses of the clinical, electrocardiographic, and echocardiographic data

Categorical data were expressed as percentages and compared using a χ^2-test or Fisher's exact test. Normally distributed continuous variables were expressed as a mean and standard deviation. Abnormally distributed continuous variables were given as a median and interquartile range. Continuous variables were compared using the Student's *t*-tests or by the non-parametric Mann–Whitney *U* test, where appropriate. For all tests, a probability value of $P < 0.05$ was considered significant. All analyses were performed using the statistical software SPSS, version 17.0 (Chicago, Illinois, USA).

Results

Clinical findings in the patient cohort

The study group of 60 female patients included 47 (78%) heart transplant recipients, 2 individuals (3%) treated by a ventricular assist device, and 11 patients (18%) in the pre-transplant phase. *Table 1* summarizes the clinical findings. Median ages at disease onset, surgery or pre-transplant assessment, and the LAMP2 FC screening were

Table 1 Study group characteristics and comparison of clinical and instrumental findings between individuals with Danon disease and other aetiologies of non-ischemic heart failure

Characteristic	Danon disease (*n* = 7)	Non-Danon disease (*n* = 53)	Overall (*n* = 60)	*P* value
Age at first symptoms (year)	16 (15–24)	24 (12–32)	22 (12–31)	0.398
Age at progression (year)	25 (21–28)	30 (19–36)	28 (20–35)	0.228
Cardiomypathy type				0.022[*]
Hypertrophic	4 (57%)	5 (9%)	9 (15%)	
Dilated	3 (43%)	43 (81%)	46 (77%)	
Restrictive	0 (0%)	4 (8%)	4 (6%)	
Left-ventricular non-compaction	0 (0%)	1 (2%)	1 (2%)	
NYHA functional class	(*n* = 7)	(*n* = 45)	(*n* = 52)	0.754
I	1 (14%)	3 (7%)	4 (8%)	
II	1 (14%)	10 (22%)	11 (21%)	
III	4 (58%)	21 (47%)	25 (48%)	
IV	1 (14%)	11 (24%)	12 (23%)	
Arrhythmia				0.052
Atrial fibrillation	3 (43%)	4 (8%)	7 (12%)	
Ventricular tachyarrhythmia	0 (0%)	5 (10%)	5 (8%)	
Electrocardiogram	(*n* = 7)	(*n* = 42)	(*n* = 49)	
PR duration (ms)	154 (152–160)	166 (159–184)	162 (154–184)	0.268
QRS duration (ms)	144 (137–187)	96 (80–110)	102 (83–121)	0.001[**]
Delta-waves	3 (43%)	0 (0%)	3 (6%)	0.002[**]
LBBB	3 (43%)	5 (12%)	8 (16%)	0.068
Echocardiography	(*n* = 7)	(*n* = 46)	(*n* = 53)	
LVEDD (mm)	62 (49–67)	61 (56–69)	62 (56–68)	0.537
LVEF (mm)	20 (20–39)	25 (20–30)	24 (20–30)	0.749
Interventricular septum (mm)	14 (9–14)	8 (7–9)	8 (7–9)	0.001[**]
Posterior wall (mm)	12 (10–14)	8 (7–9)	8 (7–9)	0.002[**]
Mitral regurgitation	(*n* = 7)	(*n* = 50)	(*n* = 57)	0.899
None or trace	4 (58%)	20 (40%)	24 (42%)	
Mild	1 (14%)	10 (20%)	11 (19%)	
Moderate	1 (14%)	12 (24%)	13 (23%)	
Severe	1 (14%)	8 (16%)	9 (16%)	

LBBB, left bundle branch block; LVEDD, left ventricular end-diastolic diameter; LVEF, left ventricular ejection fraction; NYHA, New York Heart Association.
[*]*P* ‹ 0.05.
[**]*P* ‹ 0.01.

22, 28, and 37 years, respectively. DCM was found in 46 patients (77%), HCM in nine patients (15%), restrictive cardiomyopathy in three patients (5%), and left ventricular non-compaction cardiomyopathy in one patient (2%).

LAMP2 flow cytometry in white blood cells

Patients #1[10] and #2,[13] who were diagnosed with DD prior the start date of this study, had fractions of LAMP2def granulocytes larger than 5% (Figure 1A,B, Table 2).

Of the 45 female patients tested by FC in this study, populations of LAMP2def granulocytes larger than 5% were identified in four female patients (Patients #3, #5, #6, and #7) (Figure 1A,B, Table 2). Additional five female patients had distinct populations of LAMP2def granulocytes that were smaller than 5% (0.17–2.6%). The most suspect of DD was the values of 2.6% LAMP2def granulocytes and 3.9% LAMP2def monocytes in a single patient. This result was later explained by identifying a very complex LAMP2 molecular pathology[14] that skewed WBC XCI ratios in DD patient #4 (Figure 1B and Table 2). No LAMP2 mutation was detected in the remaining four patients harbouring the very small LAMP2def cellular subsets. The remaining 36 samples did not contain any distinct populations of LAMP2def granulocytes.

Including patients #1 and #2, the total prevalence of DD in this cohort of female patients with non-ischemic heart failure was 12% (7/60). At a threshold of 5% LAMP2def granulocytes or monocytes, DD female patients were identified with a sensitivity of 86% and specificity of 100%. Positive predictive value (PPV) and negative predictive value (NPV) of the test were 100% and 98%, respectively. The presence of any distinct subpopulation of LAMP2def granulocytes identified DD female patients with a sensitivity of 100%, specificity of 92%, PPV 63%, and NPV 100%.

Whole-exome sequencing analyses, LAMP2 mutations, HUMARA X-chromosome inactivation ratios, and immunohistochemistry assessment of the myocardial samples

Whole-exome sequencing results are summarized in the supporting information. ACMG class 3–5 variants in disease-related genes were found in 24 patients (53%) including the five newly identified DD patients (Figure 1A,B). Importantly, characterization of the LAMP2 mutations in DD patients #3 and #4 mandated an individualized methodological approach that was far beyond the standard WES analytics in both patients.[13,14] WES testing was negative or inconclusive in 21 patients (47%).

Table 2 summarizes the molecular genetic analyses, WBC XCI, and myocardial LAMP2 IHC findings in the female DD

Table 2 LAMP2 flow cytometry, LAMP2 molecular genetic analyses, and LAMP2 myocardial expression in Danon disease female patients

Patient	LAMP2def granulocytes (%)	LAMP2def monocytes (%)	XCI in WBCs (HUMARA)	LAMP2 mutation/ LAMP2 cardiac IHC	Note
#1[b]	87.2	84.9	Not informative	p.[Ala314Glnfs*32];[=] / mosaic expression	III.2 in Majer et al.[10]
#2[b]	32.3	38.0	30:70	g.19925_45401[del25477];[=], deletion of LAMP2 exons 4–9C/no tissue available	II.1 (family 2) in reference Majer et al.[13]
#3[c]	35.5	49.1	40:60	g.17916_29069[del111154];[=], deletion of LAMP2 exons 4–8/no tissue available	II.1 (family 1) in Majer et al.[13]
#4[c]	2.6	3.9	96:4[a]	Heterozygous deletion of CUL4B, LAMP2, ATP1B4, TMEM255A, and ZBTB33 genes/mosaic expression	II.1 in Majer et al.[14]
#5[c]	66.7	70.8	57:44	p.[Asp149Phefs*2];[=] /mosaic expression	Novel LAMP2 mutation (Supporting Information, Figure S1A)
#6[c]	25.2	28.9	20:80	p.[Gln240*];[=] / mosaic expression	Known LAMP2 mutation (Figure S1B)[17]
#7[c]	44.3	52.7	46:54	p.[Leu139Phefs*8];[=] / mosaic expression	Novel LAMP2 mutation (Figure S1C)

DD, Danon disease; HUMARA, human androgen receptor assay; IHC, immunohistochemistry
[a]Skewed WBC XCI ratios are an effect of the parallel mutation in the CUL4B gene.
[b]DD diagnosis established prior the LAMP2 FC screening study.
[c]DD diagnosis established by the LAMP2 FC screening study.

Table 3 Clinical findings in Danon disease female patients

Patient	Age at disease onset (years)	Age at HTx (years)	Age at DD diagnosis (years)	Cardiac phenotype	QRS width (ms)	Delta waves	LVEDD (mm)	LVEF (%)	IVS (mm)	PW (mm)
#1	15	29	33	DCM	140	I, aVL, V4–6	67	15	10	10
#2	11	—	17	HCM	134	I, II, III, aVF, V5–6	33	60	22	21
#3	12	21	42	HCM	208	Absent	68	20	15	15
#4	25	26	36	DCM	112	Absent	62	20	8	7
#5	25	28	48	HCM	200	Absent	68	20	14	14
#6	16	27	25	HCM	174	I, II, III, aVF, V4–6	40	55	14	12
#7	23	24	23	DCM	144	Absent	59	23	9	10

DCM, dilated cardiomyopathy; DD, Danon disease; HCM, hypertrophic cardiomyopathy; HTx, heart transplantation; IVS, interventricular septum end-diastolic thickness; LVEDD, left-ventricular end-diastolic diameter; LVEF, left-ventricular ejection fraction; PW, left-ventricular posterior wall end-diastolic thickness.

patients. Patient #1 was heterozygous for a frame-shift c.del940G *LAMP2* mutation.[10] Patients #2 and #3 carried heterozygous deletion exon copy number variants encompassing *LAMP2* exons 4-9C and 4-8, respectively.[13] Patient #4 had an *Xq24* re-arrangement that caused a heterozygous deletion of several C-terminal exons of *CUL4B* and the complete deletion of *LAMP2, ATP1B4, TMEM255A*, and *ZBTB33* genes.[14] Patient #5 was heterozygous for a novel frameshift *c.445_449delGACCT* mutation in the *LAMP2* exon 4 (Supporting Information, *Figure S1A*). A previously reported[17] heterozygous *c.718C>T* non-sense mutation (*Figure S1B*) in the *LAMP2* exon 5 was found in patient #6. Patient #7 was heterozygous for a novel frameshift *c.418delC* mutation in the *LAMP2* exon 4 (*Figure S1C*).

White blood cell XCI ratios were within the >5:95/<95:5 range and corresponded to percentages of LAMP2def granulocytes and monocytes in patients #2, #3, #5, #6, and #7. The extremely skewed WBC XCI ratios in patient #4 (96:4) were an effect of the parallel mutation in the *CUL4B* gene.[14] *LAMP2* expression in cardiomyocytes was mosaic in all DD patients from whom tissue samples were available (*Table 2*).

Family screening in newly identified Danon disease patients

Patients #3,[13] #4,[14] and #7 (*Figure S1C*) were the only affected individuals in their families. Patient #5 transmitted the *LAMP2* mutation to her daughter (III.3, *Figure S1A*). At 30 years of age, the daughter had a sinus rhythm with a short PQ interval (98 ms) and discrete delta waves in leads I, II, aVF, and V4–V6. Her echocardiography showed a borderline systolic function of the non-dilated left ventricle (end-diastolic diameter 49 mm, ejection fraction 50–55%, and interventricular septum thickness 10 mm). The populations of her LAMP2def granulocytes and monocytes were 22.1% and 27.2%, respectively. XCI ratios by HUMARA were 33:67. Patient #6 had the most complex family history (*Figure S1B*). Her mother (an obligatory heterozygote for the *LAMP2* mutation) had a DCM and died at 27 years of age. Hypertrophic cardiomyopathy was diagnosed in the patient's brother who carried the same *LAMP2* mutation as Patient #6 and died aged 18 years. For additional clinical details see supporting information.

Clinical characteristics of Danon disease female patients

Hypertrophic cardiomyopathy phenotype (57% vs. 9%, [*]*P* = 0.022) and delta waves by electrocardiograms (43% vs. 0%, [**]*P* = 0.002) were significantly more frequent in DD female patients in comparison with the rest of the patients in

the cohort. The presence of HCM identified DD female patients with a sensitivity of 57%, specificity of 91%, PPV of 44%, and NPV of 94%. Delta waves identified DD female patients with a sensitivity of 43%, a specificity of 100%, PPV of 100%, and NPV of 93%. The sensitivity of these clinical variables was thus much lower than sensitivity of the LAMP2 FC test. The increased thickness of the left ventricular walls and broader QRS complexes in DD female patients corresponded to higher prevalence of HCM and delta waves in these individuals (*Table 1*). Electrocardiograms of DD female patients are shown in Supporting Information, *Figure S2*.

Discussion

To the best of our knowledge, we present the first study specifically assessing the prevalence of DD among female patients with AHF. This is also the first large-scale study that uses LAMP2 flow cytometry as a primary screening tool in this particular patient group.

Our key findings are (i) the prevalence of DD among young female patients (≤40 years of age) with AHF due to non-ischemic cardiomyopathy is relatively high (12%), (ii) LAMP2 FC in WBCs is an effective screening/diagnostic tool to detect female (and also male) DD patients, and (iii) despite more frequent than in non-DD patients, DD female patients cannot be reliably identified based on the presence of hypertrophic cardiomyopathy and/or delta waves in their electrocardiograms.

Danon disease screening studies

The overall population frequency as well as population ratio of male and female DD patients is, to the best of our knowledge, not known. The recent extensive review of the available DD literature documented 90 male and only 56 female patients.[6] It is very likely that female patients heterozygous for pathogenic *LAMP2* variants remain an underdiagnosed DD patient group despite they are often the first affected family members. Furthermore, DD affects female patients in their reproductive age. Timely and correct diagnosis is therefore also critical for genetic counselling in their families.

There are several studies that used molecular genetic testing and evaluated the frequency of DD in specifically selected patient cohorts. Again, male DD patients predominated among probands identified by most of these studies.

Prevalence of DD was suggested to be ~1–3% among patients with HCM.[18,19] The values are higher among similarly affected paediatric patients (4–6%)[20] or patients with end-stage HCM (7.7%).[21] DD is, nonetheless, most frequent (~33%) among patients presenting with both HCM and preexcitation.[22] When tested among patients, who underwent endomyocardial biopsy because of suspected

cardiac storage disease, the prevalence of DD reached 8% after exclusion of patients with amyloidosis.[23] Interestingly, a large scale study that combined oligonucleotide hybridization-based and dideoxy-based DNA sequencing techniques of selected genes including *LAMP2* did not identify any DD individual among 558 HCM patients.[24]

Almost all reported *LAMP2* mutations (106–108 in December 2019 by the authors' review of literature) putatively result in the absence of the protein. *LAMP2* missense mutations are very rare in DD patients.[6] Residual LAMP2 was unambiguously documented for very few variants (e.g. a leaky splice-site mutation[25] or a mutation in the isoform specific exon 9B[26]). Given this mutation spectrum, LAMP2 protein testing identifies uniform LAMP2 deficiency in cells and tissues of male DD patients (*Figure 1C*).

XCI triggers mosaic expression of the wild-type and mutant *LAMP2* alleles in tissues of female DD patients (*Figure 1B, C*).[10,12-14] Setting thresholds for skewing or extreme skewing of XCI is arbitrary. Importantly, ~98% of females have WBC XCI ratios within the >5:95/<95:5 range.[15] A large-scale survey evaluating XCI ratios in DD female patients has never been reported; however, a systematic extreme skewing beyond the aforementioned range is unlikely in these patients based on the dataset presented in this manuscript. The only patient in our cohort (#4), who had extremely skewed WBC XCI ratios resulting in fractions of LAMP2def granulocytes (and monocytes) <5%, had a complex *Xq24* re-arrangement that deleted not only the entire *LAMP2* but also several C-terminal exons of the neighbouring *CUL4B* gene.[14] Although clinically asymptomatic, female patients heterozygous for mutations in the latter gene have extremely skewed WBC XCI ratios as a result of selective pressure, most likely tissue-specific, against the CUL4B deficient cellular clones.[14]

Critical for interpretation of the sensitivity and specificity values of the LAMP2 FC assay in WBCs, all six female DD patients (#1–3 and #5–7) with mutations impacting solely the *LAMP2* gene had unambiguously detectable LAM2def populations larger than 5%. Identifying patient #4 among the individuals with LAMP2def fractions <5% supports the robustness of the method. Rather than expression-related, we attribute the LAMP2def populations <5% in the other four patients with no *LAMP2* molecular abnormality to sample collection/processing-induced errors.

Clinical implications

Prognostic stratification of patients with non-ischemic heart failure is difficult. It is particularly problematic in patients with recent-onset DCM, because clinical outcomes in these patients may range from full recovery to sudden death or progressive heart failure.[27] Clarification of a monogenic aetiology (DD in this case) may considerably improve the risk assessment and facilitate family counselling. Although no

Příloha 1a

specific therapy is currently available, further development of efficient diagnostic algorithms for DD is substantiated by the currently ongoing *LAMP2B* gene-therapy trial in male patients.[28]

It is not easy to establish the diagnosis of DD in male patients. However, identification of female patients is even more complicated.[6] As we show in this study, hypertrophic cardiomyopathy and/or the presence of delta waves may suggest DD. Documenting these clinical clues, however, does not have the sufficient sensitivity and specificity to effectively support the diagnosis in female patients. A study by Boucek *et al*.[3] evaluated 18 DD female patients and reported pre-excitation in 27% of them. Brambatti *et al*.[6] identified pre-excitation in 32% of 56 DD female patients included into their review of previously published DD reports. The slightly higher fraction of patients with delta waves (43%), that we observed in our study, potentially reflects a combined effect of the relatively limited number of evaluated DD female patients and stringent electrocardiogram assessment criteria.

Laboratory diagnostic implications

Massively parallel sequencing technologies increased the efficiency of molecular genetic DD diagnostics.[17] However, pathogenicity validation/prediction of many of the variants identified by these methods is often inconclusive and certain *LAMP2* mutation types (e.g. copy number variants) can be easily missed.[13] Contrary to these high-throughput genomic analytical techniques, the outlined FC method is a selective protein-level expression test. Unlike to analyses of WBCs homogenates by western blotting,[8] the fraction of LAMP2def cells is directly quantified by the FC method. The FC test identifies uniform LAMP2 deficiency in X-hemizygous male patients as well as mosaic LAMP2 deficiency in X-heterozygous female DD patients (*Figure 1C*). In specific pedigree situations, the test may also be modified to allow identification of individuals with extremely small LAMP2def populations (<1%) resulting from somatic mosaicism.[11,12]

Sample collection is minimally invasive, the FC test uses commercially available reagents and the turnover time is short (<24 h). Flow cytometers are a standard laboratory equipment and the overall cost of the test is low. Most importantly, the test is easy to set-up—Standard Operating Protocol is part of the supporting information (pages 7–9) for those interested in using the methodology in their local diagnostic practice.

Given the high prevalence of DD among young female patients with non-ischemic cardiomyopathy, that we identified in this study, we suggest screening of similarly affected patients by flow cytometry since this technique allows direct assessment of the (XCI-driven) mosaic expression of the mutant *LAMP2* allele. Additionally, the information about the presence or absence of LAMP2def cells may facilitate molecular genetic testing and expedite the correct diagnostic classification.

Study limitations

Patients with AHF constitute ~5% of the patients with heart failure.[29] AHF is also rare among female patients aged 20–40 years (e.g. 6–23 cases per one million people in a study by authors from Northeast France[30]). Genetic cardiomyopathies, myocarditis, and peripartum cardiomyopathy are the most common causes of heart failure in young female patients. Contrary to infectious and pregnancy-related insults, genetic defects almost exclusively result in irreversible cardiac damage. The high prevalence (12%) of DD seen in our cohort likely reflects a combination of the listed reasons—that is, small number of young female AHF patients in the general population and possible proportional increase of patients with genetic causes of cardiomyopathy in the tested population.

Patients included in our study were gathered from two centres that participate in the nation-wide heart transplantation program and jointly serve the entire population of the Czech Republic (~10 million). The studied population of female patients with non-ischemic heart failure younger than 40 years is not composed of patients who were followed long-term to reach the inclusion criteria but rather is a snapshot group of young female patients recruited within 24 months, who lived with a heart transplant, ventricular assist device or were undergoing a pre-transplant assessment.

Lastly, almost all of currently known *LAMP2* pathogenic variants result in the absence of the protein. The set-up of the LAMP2 FC assay allows identification of LAMP2 deficient cells. Given the spectrum of *LAMP2* variants identified in the Czech DD patient cohort, samples of patients with residual LAMP2 were not tested.

Conclusions

Danon disease is an underdiagnosed cause of AHF in young female patients. LAMP2 flow cytometry in peripheral WBCs can be used as an effective screening method to facilitate the timely diagnosis, treatment, and family counselling in these patients.

Acknowledgements

Příloha 1a

Conflict of interest

None declared.

Supporting information

Additional supporting information may be found online in the Supporting Information section at the end of the article.

Figure S1. Family pedigrees and *LAMP2* mutations.
Figure S2. ECG curves in female DD patients.

References

1. Nishino I, Fu J, Tanji K, Yamada T, Shimojo S, Koori T, Mora M, Riggs JE, Oh SJ, Koga Y, Sue CM, Yamamoto A, Murakami N, Shanske S, Byrne E, Bonilla E, Nonaka I, DiMauro S, Hirano M. Primary LAMP-2 deficiency causes X-linked vacuolar cardiomyopathy and myopathy (Danon disease). *Nature* 2000; **406**: 906–910.
2. Rowland TJ, Sweet ME, Mestroni L, Taylor MRG. Danon disease—dysregulation of autophagy in a multisystem disorder with cardiomyopathy. *J Cell Sci* 2016; **129**: 2135–2143.
3. Boucek D, Jirikowic J, Taylor M. Natural history of Danon disease. *Genet Med* 2011; **13**: 563–568.
4. D'Souza RS, Levandowski C, Slavov D, Graw SL, Allen LA, Adler E, Mestroni L, Taylor MR. Danon disease: clinical features, evaluation, and management. *Circ Heart Fail* 2014; **7**: 843–849.
5. Wu H, Luo J, Yu H, Rattner A, Mo A, Wang Y, Smallwood PM, Erlanger B, Wheelan SJ, Nathans J. Cellular resolution maps of X chromosome inactivation: implications for neural development, function, and disease. *Neuron* 2014; **81**: 103–119.
6. Brambatti M, Caspi O, Maolo A, Koshi E, Greenberg B, Taylor MRG, Adler ED. Danon disease: gender differences in presentation and outcomes. *Int J Cardiol* 2019; **286**: 92–98.
7. Miani D, Taylor M, Mestroni L, D'Aurizio F, Finato N, Fanin M, Brigido S, Proclemer A. Sudden death associated with Danon disease in women. *Am J Cardiol* 2012; **109**: 406–411.
8. Fanin M, Nascimbeni AC, Fulizio L, Spinazzi M, Melacini P, Angelini C. Generalized lysosome-associated membrane protein-2 defect explains multisystem clinical involvement and allows leukocyte diagnostic screening in Danon disease. *Am J Pathol* 2006; **168**: 1309–1320.
9. Regelsberger G, Höftberger R, Pickl WF, Zlabinger GJ, Körmöczi U, Salzer-Muhar U, Luckner D, Bodamer OA, Mayr JA, Muss WH, Budka H, Bernheimer H. Danon disease: case report and detection of new mutation. *J Inherit Metab Dis* 2009; **32**: S115–S122.
10. Majer F, Vlaskova H, Krol L, Kalina T, Kubanek M, Stolnaya L, Dvorakova L, Elleder M, Sikora J. Danon disease: a focus on processing of the novel LAMP2 mutation and comments on the beneficial use of peripheral white blood cells in the diagnosis of LAMP2 deficiency. *Gene* 2012; **498**: 183–195.
11. Majer F, Pelak O, Kalina T, Vlaskova H, Dvorakova L, Honzik T, Palecek T, Kuchynka P, Masek M, Zeman J, Elleder M, Sikora J. Mosaic tissue distribution of the tandem duplication of LAMP2 exons 4 and 5 demonstrates the limits of Danon disease cellular and molecular diagnostics. *J Inherit Metab Dis* 2014; **37**: 117–124.
12. Sikora J, Majer F, Kalina T. LAMP2 flow cytometry in peripheral white blood cells is an established method that facilitates identification of heterozygous Danon disease female patients and mosaic mutation carriers. *J Cardiol* 2015; **66**: 88–89.
13. Majer F, Piherova L, Reboun M, Stara V, Pelak O, Norambuena P, Stranecky V, Krebsova A, Vlaskova H, Dvorakova L, Kmoch S, Kalina T, Kubanek M, Sikora J. LAMP2 exon-copy number variations in Danon disease heterozygote female probands: infrequent or underdetected? *Am J Med Genet A* 2018; **176**: 2430–2434.
14. Majer F, Kousal B, Dusek P, Piherova L, Reboun M, Mihalova R, Gurka J, Krebsova A, Vlaskova H, Dvorakova L, Krihova J, Liskova P, Kmoch S, Kalina T, Kubanek M, Sikora J. Alu-mediated contiguous Xq24 deletion encompassing CUL4B, LAMP2, ATP1B4, TMEM255A, and ZBTB33 genes causes Danon disease in a female patient. *Am J Med Genet A* 2020; **182**: 219–223.
15. Amos-Landgraf JM, Cottle A, Plenge RM, Friez M, Schwartz CE, Longshore J, Willard HF. X chromosome-inactivation patterns of 1,005 phenotypically unaffected females. *Am J Hum Genet* 2006; **79**: 493–499.
16. Kalia S, Adelman K, Bale S, Chung WK, Eng C, Evans JP, Herman GE, Hufnagel SB, Klein TE, Korf BR, McKelvey KD. Recommendations for reporting of secondary findings in clinical exome and genome sequencing, 2016 update (ACMG SF v2.0): a policy statement of the American College of Medical Genetics and Genomics. *Genet Med* 2017; **19**: 249–255.
17. Fu L, Luo S, Cai S, Hong W, Guo Y, Wu J, Liu T, Zhao C, Li F, Huang H, Huang M, Wang J. Identification of LAMP2 mutations in early-onset Danon disease with hypertrophic cardiomyopathy by targeted next-generation sequencing. *Am J Cardiol* 2016; **118**: 888–894.
18. Charron P, Villard E, Sébillon P, Laforêt P, Maisonobe T, Duboscq-Bidot L, Romero N, Drouin-Garraud V, Frébourg T, Richard P, Eymard B, Komajda M. Danon's disease as a cause of hypertrophic cardiomyopathy: a systematic survey. *Heart* 2004; **90**: 842–846.
19. Arad M, Maron BJ, Gorham JM, Johnson WH Jr, Saul JP, Perez-Atayde AR, Spirito P, Wright GB, Kanter RJ, Seidman CE, Seidman JG. Glycogen storage diseases presenting as hypertrophic cardiomyopathy. *N Engl J Med* 2005; **352**: 362–372.
20. Yang Z, McMahon CJ, Smith LR, Bersola J, Adesina AM, Breinholt JP, Kearney DL, Dreyer WJ, Denfield SW, Price JF, Grenier M, Kertesz NJ, Clunie SK, Fernbach SD, Southern JF, Berger S, Towbin JA, Bowles KR, Bowles NE. Danon disease as an underrecognized cause of hypertrophic cardiomyopathy in children. *Circulation* 2005; **112**: 1612–1617.
21. Garcia-Pavia P, Vázquez ME, Segovia J, Salas C, Avellana P, Gómez-Bueno M, Vilches C, Gallardo ME, Garesse R, Molano J, Bornstein B, Alonso-Pulpon L. Genetic basis of end-stage hypertrophic cardiomyopathy. *Eur J Heart Fail* 2011; **13**: 1193–1201.
22. Liu Y, Chen X, Wang F, Liang Y, Deng H, Liao H, Zhang Q, Zhang B, Zhan X, Fang X, Shehata M, Wang X, Xue Y, Wu S. Prevalence and clinical characteristics

of Danon disease among patients with left ventricular hypertrophy and concomitant electrocardiographic preexcitation. *Mol Genet Genomic Med* 2019; **7**: e638.

23. Cheng Z, Cui Q, Tian Z, Xie H, Chen L, Fang L, Zhu K, Fang Q. Danon disease as a cause of concentric left ventricular hypertrophy in patients who underwent endomyocardial biopsy. *Eur Heart J* 2012; **33**: 649–656.

24. Li Q, Gruner C, Chan RH, Care M, Siminovitch K, Williams L, Woo A, Rakowski H. Genotype-positive status in patients with hypertrophic cardiomyopathy is associated with higher rates of heart failure events. *Circ Cardiovasc Genet* 2014; **7**: 416–422.

25. Cetin H, Wöhrer A, Rittelmeyer I, Gencik M, Zulehner G, Zimprich F, Ströbel T,

Zimprich A. The c.65-2A>G splice site mutation is associated with a mild phenotype in Danon disease due to the transcription of normal LAMP2 mRNA. *Clin Genet* 2016; **90**: 366–371.

26. van der Kooi AJ, van Langen IM, Aronica E, van Doorn PA, Wokke JHJ, Brusse E, Langerhorst CT, Bergin P, Dekker LRC, dit Deprez RH, de Visser M. Extension of the clinical spectrum of Danon disease. *Neurology Apr* 2008; **70**: 1358–1359.

27. Givertz MM, Mann DL. Epidemiology and natural history of recovery of left ventricular function in recent onset dilated cardiomyopathies. *Curr Heart Fail Rep* 2013; **10**: 321–330.

28. ClinicalTrials.gov [Internet]. Bethesda (MD): National Library of Medicine (US). 2000 Feb 29. Identifier

NCT03882437, Gene therapy for male patients with Danon disease using RP-A501; AAV9.LAMP2B; 2019 20. https://clinicaltrials.gov/ct2/show/study/NCT03882437 (12 January 2020).

29. Costanzo MR, Mills RM, Wynne J. Characteristics of "Stage D" heart failure: insights from the Acute Decompensated Heart Failure National Registry Longitudinal Module (ADHERE LM). *Am Heart J* 2008; **155**: 339–347.

30. Zannad F, Briancon S, Juilliere Y, Mertes PM, Villemot JP, Alla F, Virion JM. Incidence, clinical and etiologic features, and outcomes of advanced chronic heart failure: the EPICAL Study. Epidemiologie de l'Insuffisance Cardiaque Avancee en Lorraine. *J Am Coll Cardiol* 1999; **33**: 734–742.

WILEY medical genetics

CLINICAL REPORT

LAMP2 exon-copy number variations in Danon disease heterozygote female probands: Infrequent or underdetected?

Filip Majer[1†] | Lenka Piherova[1†] | Martin Reboun[1] | Veronika Stara[2] | Ondrej Pelak[3] |

Patricia Norambuena[4] | Viktor Stranecky[1] | Alice Krebsova[5] | Hana Vlaskova[1] |

Lenka Dvorakova[1] | Stanislav Kmoch[1] | Tomas Kalina[3] | Milos Kubanek[5] | Jakub Sikora[1] [iD]

[1]Research Unit for Rare Diseases, Department of Pediatrics and Adolescent Medicine, 1st Faculty of Medicine, Charles University and General University Hospital, Prague, Czech Republic

[2]Department of Pediatrics, 2nd Faculty of Medicine, Charles University and University Hospital Motol, Prague, Czech Republic

[3]Department of Paediatric Haematology and Oncology, Childhood Leukaemia Investigation Prague, 2nd Faculty of Medicine, Charles University and University Hospital Motol, Prague, Czech Republic

[4]Department of Biology and Medical Genetics, 2nd Faculty of Medicine, Charles University and University Hospital Motol, Prague, Czech Republic

[5]Department of Cardiology, Institute for Clinical and Experimental Medicine, Prague, Czech Republic

Correspondence
Jakub Sikora, Research Unit for Rare Diseases, Department of Pediatrics and Adolescent Medicine, 1st Faculty of Medicine, Charles University and General University Hospital, Ke Karlovu 2, 128 00, Prague 2, Czech Republic.
Email: jakub.sikora@lf1.cuni.cz

Funding information
Grantová Agentura, Univerzita Karlova, Grant/Award Number: GAUK 580716; Ministerstvo Školství, Mládeže a Tělovýchovy, Grant/Award Number: NCMG LM2015091, NPU I no. LO1604; Ministerstvo Zdravotnictví České Republiky, Grant/Award Number: AZV-MZ ČR 15-27682A, AZV-MZ ČR 15-33297A, RVO-VFN 64165/2012, VZ IKEM (00023001); Univerzita Karlova v Praze, Grant/Award Number: PROGRESS Q26, PRVOUK P24

Danon disease (DD) is an X-linked disorder caused by mutations in the lysosomal-associated membrane protein 2 (*LAMP2*) gene (*Xq24*). DD is characterized by cognitive deficit, myopathy, and cardiomyopathy in male patients. The phenotype is variable and mitigated in females. The timely identification of *de-novo LAMP2* mutated family members, many of whom are heterozygous females, remains critical for their treatment and family counseling. DD laboratory testing builds on minimally invasive quantification of the LAMP2 protein in white blood cells and characterization of the specific mutation. This integrative approach is particularly helpful when assessing suspect female heterozygotes. *LAMP2* exon-copy number variations (eCNVs) were so far reported only in X-hemizygous male DD probands. In heterozygous female DD probands, the wild-type allele may hamper the identification of an eCNV even if it results in the complete abolition of *LAMP2* transcription and/or translation. To document the likely underappreciated rate of occurrence and point out numerous potential pitfalls of detection of the *LAMP2* eCNVs, we present the first two DD heterozygote female probands who harbor novel multi-exon *LAMP2* deletions. Critical for counseling and recurrence prediction, we also highlight the need to search for somatic-germinal mosaicism in DD families.

KEYWORDS

Danon disease, X-chromosome, lysosomal-associated membrane protein 2, female heterozygotes, flow cytometry, exon-copy number variations

1 | INTRODUCTION

Danon disease (DD, MIM #300257) is a rare X-linked disorder characterized by cognitive deficit, cardiomyopathy and skeletal myopathy in males. DD is caused by mutations in the lysosomal-associated

membrane protein 2 (*LAMP2, Xq24*) (Nishino et al., 2000). The alternative *LAMP2* exons 9 (B, A, and C) code three protein variants differing in C-termini. The majority of the mutations affect the isoform shared regions (exons 1–8) of the gene and result in the complete and uniformly distributed absence of the LAMP2 protein in tissues of male DD patients (Boucek, Jirikowic, & Taylor, 2011; D'Souza et al., 2014). *LAMP2* exon-copy number variations (eCNVs) have, thus far, all been

[†]These authors contributed equally to the work

reported in X-hemizygous male probands (Lines et al., 2014; Majer et al., 2014; Yang et al., 2010).

Heterozygous females for *LAMP2* mutations also develop DD. However, the tissue expression of their two *LAMP2* alleles is mosaic due to X-chromosome inactivation (XCI). In fact, the healthy allele may actually hamper characterization of the complementary *LAMP2* mutation in tissue homogenates from DD females, making eCNVs particularly difficult to identify during molecular genetic and/or genomic diagnostics.

To document the probable higher frequency of occurrence and demonstrate the numerous potential pitfalls posed by X-heterozygosity, we present the first two heterozygote female DD probands who harbor novel multi-exon deletions in the *LAMP2* gene.

2 | CLINICAL REPORTS

2.1 | Family 1—Proband II.1[F1]

II.1[F1] (Figure 1a) was diagnosed with hypertrophic cardiomyopathy at 12 years old. By 16 years of age, the patient's left ventricular (LV) hypertrophy had reached 22–25 mm, however the systolic function remained preserved. At 21 years, II.1[F1] developed end-stage heart failure with severe LV systolic dysfunction and underwent

cardiac transplantation. A recent re-evaluation of her pretransplant electrocardiogram identified sinus rhythm and delta waves in most limb leads. Unfortunately, myocardial samples from her explanted heart were not available for histological, immunohistochemical, or ultrastructural testing. The plasma/serum activity levels of aminotransferases and creatine kinase were/are normal. II.1[F1] has a mild cognitive deficit and normal muscle strength and is currently 42 years old.

2.2 | Family 2—Proband II.1[F2]

II.1[F2] (Figure 2a) was diagnosed with hypertrophic cardiomyopathy and pre-excitation at 11 years of age. The patient's electrocardiogram showed sinus rhythm with delta waves in inferior and precordial leads. At 14 years, the patient underwent radiofrequency ablation of two right-sided atrio-ventricular accessory pathways with a high capacity of antegrade conduction. At 15 years, the concentric LV hypertrophy (without obstruction of the outflow tract) reached 15–16 mm. Plasma/serum aspartate aminotransferase activity (0.95–1.45 μkat/l; normal range 0.16–0.78 μkat/l) and myoglobin levels (62–66 μg/l; normal range 19–51 μg/l) were slightly elevated throughout the patient's late childhood/adolescence. The patient experienced two episodes of palpitations at 17 and 18 years of age. Electrocardiography showed no arrhythmia at that time. At 19 years, the concentric LV hypertrophy
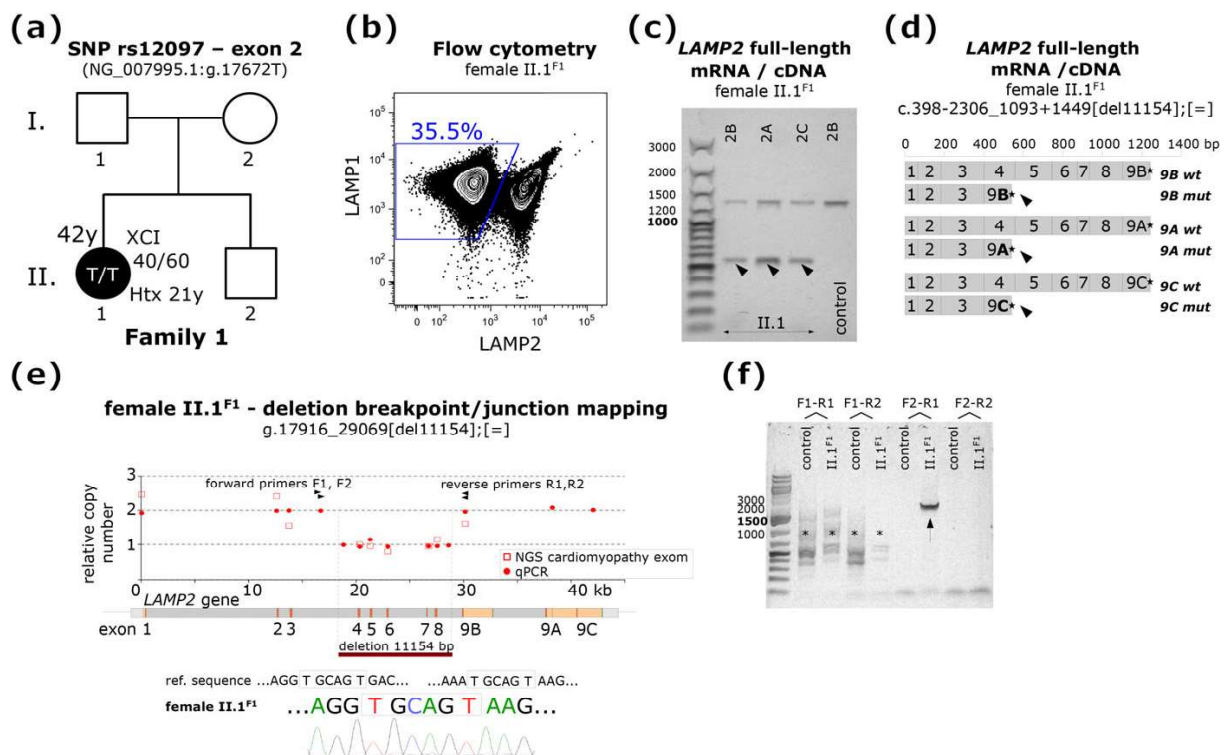

FIGURE 1 DD family 1—proband II.1[F1]. (a) Current age, setup of the *LAMP2* exon 2 rs12097 SNP, and WBC XCI ratio are given for II.1[F1]. I.1, I.2, and II.2 were not available for analyses. (b) LAMP1/LAMP2 coexpression FC profile shows LAMP2def granulocytes (blue gate) in II.1[F1]. (c, d) Short aberrant *LAMP2* mRNA/cDNA isoforms (black arrowheads) lack exons 4–8. (e) qPCR (red dots) and NGS (red squares) values of *LAMP2* exon-copy number in II.1[F1]. Black arrowheads mark positions and orientation of primers used to map the deletion breakpoint/junction. The deletion is flanked by short identical sequences. (f) Specific detection of the deletion junction (arrow), the wild-type allele, and/or the length of the product(s) may compromise PCR efficiency and specificity (*) [Color figure can be viewed at wileyonlinelibrary.com]
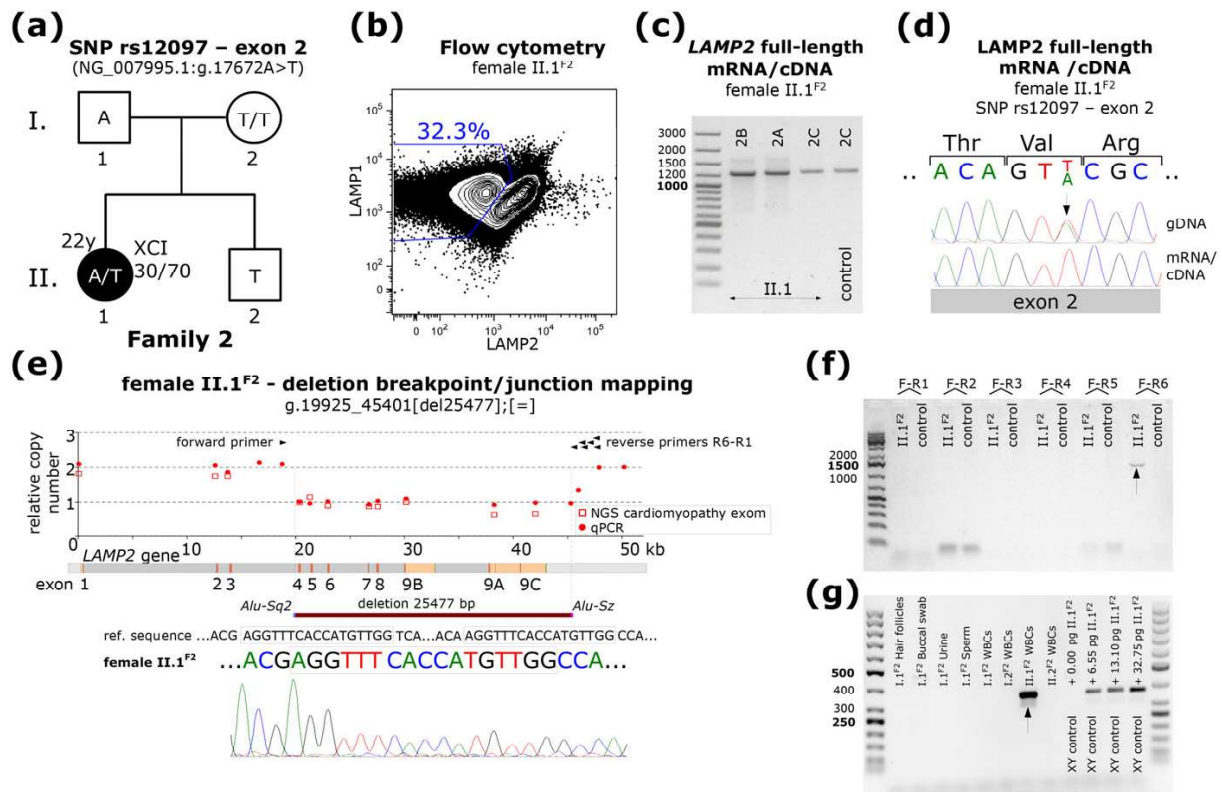
FIGURE 2 DD family 2—proband II.1[F2]. (a) Current age and WBC XCI ratio are given for II.1[F2]. Setup of the *LAMP2* exon 2 rs12097 SNP is shown for all family members. (b) LAMP1/LAMP2 coexpression FC profile shows LAMP2def granulocytes (blue gate) in II.1[F2]. (c) Profile of the full-length *LAMP2* mRNA/cDNA isoforms (B, A, and C) in II.1[F2] is normal. (d) gDNA and mRNA/cDNA sequence analyses of the exon 2 rs12097 SNP show exclusive expression of the maternal *LAMP2* allele in WBCs of II.1[F2] (see also Supporting information Table S2 for NGS data). (e) qPCR (red dots) and NGS (red squares) values of *LAMP2* exon-copy number in II.1[F2]. Black arrowheads mark positions and orientation of primers used to map the deletion breakpoint/junction site. The deletion is flanked by *Alu-Sq2* and *Alu-Sz* sequences. (f) Specific detection of the deletion junction (arrow) in II.1[F2]. (g) PCR screening in the family identified the mutation only in WBCs of II.1[F2]. 0.00, 6.55, 13.10, or 32.75 pg of II.1[F2] WBC gDNA were mixed with 50 ng of XY control gDNA to demonstrate the efficiency of the nested PCR (Supporting information Table S1). These ratios correspond (Dolezel, Bartos, Voglmayr, & Greilhuber, 2003) to 0, 1, 2, or 5 mutant X-chromosome templates in the reaction mix and suggest that 1 cell carrying the mutation can be identified in ~7800 diploid or ~15600 haploid cells [Color figure can be viewed at wileyonlinelibrary.com]

progressed to 21–22 mm, nonetheless the LV systolic function remained normal. Recurrent syncopes and nonsustained ventricular tachycardia were treated by implantation of a dual-chamber cardio-verted defibrillator. II.1[F2] is currently 22 years old and has normal intellect and skeletal muscle strength.

Parents and brothers of both probands are without symptoms of DD.

3 | MATERIALS AND METHODS

To diagnose DD in both probands, LAMP2 expression was tested by flow cytometry (FC) in peripheral white blood cells (WBCs), and *LAMP2* molecular genetic analyses were performed. Informed consent (approved by the Ethics Committee of the authors' home institution) for participation and presentation of results was obtained from all tested individuals.

LAMP1/LAMP2 FC, polymerase chain reaction (PCR), and sequence analyses of the coding gDNA and full-length *LAMP2* mRNA/cDNAs, quantitative PCR (qPCR) *LAMP2* exon-copy number testing,

and XCI HUMARA assay were performed in WBCs as previously described (Majer et al., 2012, 2014).

Primers used for *LAMP2* exon dosage qPCR assessment, mapping of the breakpoint/junctions, and mutation-specific screening in Family 2 are listed in Table S1 (Supporting information).

LAMP2 exon dosage was also tested by next generation sequencing (NGS) using targeted enrichment panels and sequenced using the MiSeq platform (Illumina, San Diego, CA). The maternal/paternal *LAMP2* gDNA and mRNA/cDNA ratios, as well as the presence of the paternal wild-type *LAMP2* allele in II.1[F2], were tested by NGS. For additional details see Supporting Materials and Methods (Supporting information).

4 | RESULTS

4.1 | Flow cytometry

FC identified ~35% (Figure 1b) and ~33% (Figure 2b) of LAMP2 deficient (LAMP2def) granulocytes in II.1[F1] and II.1[F2], respectively.

LAMP2 profiles were retested after one year in II.1[F2] with the same result. FC findings corresponded with the XCI ratios by HUMARA assay in both probands (Figures 1a and 2a).

4.2 | Full-length *LAMP2* isoform mRNA/cDNA analyses and comparison to gDNA

In II.1[F1], a shorter (~550 bp) variant was detected in all three isoform mRNA/cDNAs in addition to the normal *LAMP2* splicing products (Figure 1c). Direct sequencing showed that these abnormal *LAMP2* mRNAs/cDNAs lack exons 4–8 (Figure 1d).

In II.1[F2], the profile of the *LAMP2* full-length mRNA/cDNAs was usual (Figure 2c), and the sequencing of all three isoforms did not identify any abnormality. However, analyses of her *LAMP2* gDNA coding regions revealed heterozygosity (A/T) for a known single nucleotide polymorphism (SNP) (rs12097) in exon 2. Comparison to the mRNA/cDNA sequences (using both direct sequencing and NGS) showed exclusive expression of the maternal *LAMP2* allele in II.1[F2] (Figure 2a,d and Supporting information Table S2).

4.3 | *LAMP2* gDNA exon-copy number testing, deletion breakpoint/junction mapping, and mutation specific screening

gDNA qPCR eCNV analyses revealed abnormal (1 instead of 2) relative copy number of *LAMP2* exons 4–8 and 4–9C in II.1[F1] and II.1[F2], respectively. Identical results were observed by NGS when evaluating normalized read depth coverage (Figures 1e and 2e and Supporting Materials and Methods in Supporting information).

To characterize the breakpoint/junctions in both probands, primer pairs were designed to span the presumed deleted gDNA regions. Alignment of the resultant PCR products (Figure 1f and 2f) to the reference *LAMP2* gene sequence (NG_007995.1) identified the TGCAGT motif to flank the breakpoint/junction in II.1[F1] (Figure 1e) and *Alu-Sq2* and *Alu-Sz* repeats in II.1[F2] (Figure 2e).

Mutation-specific screening was performed in gDNA from WBCs of I.1[F2], I.2[F2], and II.2[F2]. To test for somatic-germinal mosaicism, hair folliculi, buccal swabs, urine epithelia, and sperm were tested in I.1[F2]. The deletion found in II.1[F2] was not detected in any of these samples (Figure 2g). Similarly, the wild-type paternal *LAMP2* allele was not detected (using three SNPs in *LAMP2* intron 5) in WBCs of II.1[F2] by NGS (Table S3, Supporting information).

These analyses were not performed in Family 1 because of advanced age of I.1[F1] and I.2[F1].

5 | DISCUSSION

Heterozygous females for *LAMP2* mutations still likely remain an underdiagnosed DD patient group despite the growing body of information about their phenotype. Clinical presentation in heterozygous females is more variable (Toib et al., 2010) and mitigated in comparison to male DD patients (Boucek et al., 2011). Yet, early onset and/or malignant DD was documented in a number of females (Bottillo et al., 2016; Samad et al., 2017; Sugie et al., 2016). DD females were also

reported at risk of sudden death and timely ICD implantation was suggested as an appropriate therapeutic intervention (Miani et al., 2012).

To minimize late or retrospective (postmortem included) diagnosis, the clinical and laboratory DD workup should therefore account for pitfalls posed by X-chromosome heterozygosity. Minimally invasive and quantitative analyses of the cellular LAMP2 protein content in WBCs combined with comparative gDNA and full-length isoform *LAMP2* mRNAs/cDNAs testing meet such requirements (Fanin et al., 2006; Majer et al., 2012, 2014; Regelsberger et al., 2009; Sikora, Majer, & Kalina, 2015). To further document the robustness of this protocol and highlight additional potential detection problems, we present the first two female DD probands affected by *LAMP2* eCNVs.

Clinical presentation was indicative of DD in the patients. However, it was the discrete populations of LAMP2def WBCs found by *LAMP2* FC that provided unambiguous evidence and advocated further *LAMP2* molecular genetic analyses in both females. Whereas the deletion of exons 4–8 in II.1[F1] was anticipated based on the presence of the abnormally short PCR products while testing full-length *LAMP2* isoform mRNAs/cDNAs, II.1[F2] unexpectedly showed a normal profile. The absence of the aberrant mRNA/cDNA species (lacking exons 4–9C) in II.1[F2] is likely the result of decay of the truncated *LAMP2* mRNAs. Rationale for continued exploration of an eCNV was based on results from the *LAMP2* exon 2 SNP genotyping of the parents that suggested exclusive expression of the maternal *LAMP2* allele in II.1[F2].

Although unable to categorize the flanking elements (TGCAGT) of the breakpoint/junction in II.1[F1], the results suggest that the underlying mutagenic mechanism in both patients is a recombination mediated by repetitive sequences. Both deletions start/end in *LAMP2* intron 3. This localization is identical to four out of five *LAMP2* eCNVs reported in male DD patients (Lines et al., 2014; Majer et al., 2014; Yang et al., 2010). Moreover, the rearrangement in II.1[F2] encompasses the same *AluSq2* repeat as that involved in an earlier reported duplication of *LAMP2* exons 4 and 5 (Lines et al., 2014). Collectively, these data imply that the *LAMP2* intron 3 could be a recombination hotspot and therefore warrants specific analysis of eCNVs in suspected patients.

DD is an important differential diagnostic option among patients with (hereditary) cardiomyopathies. The current diagnostic schemes for such patient cohorts frequently employ nonselective NGS-based approaches (Fu et al., 2016). Our findings document that *LAMP2* eCNVs not only occur in female DD probands but also constitute at least 10% of all reported (78–80 in March 2018 by the authors' review of the literature) *LAMP2* mutations. To avoid false-negative diagnostic conclusions and similar to others (Mates et al., 2018), we strongly suggest systematic (re)evaluation of NGS datasets for this type of molecular *LAMP2* pathology in suspected individuals.

Although frequent and critical for determining risk of recurrence in the siblings and progenies of the affected probands, mosaicism remains generally under-recognized in counseling practice (Campbell et al., 2014). For example, instances of maternal somatic-germinal mosaicism were previously shown (Chen et al., 2012; Majer et al., 2014; Takahashi et al., 2002) but also missed in DD (Sikora et al., 2015). To the best of our knowledge, a paternal variant of this phenomenon has never been presented in DD. As II.1[F2] carries the

mutation on the paternal *LAMP2* allele, we examined an array of the father's somatic tissues and sperm but did not identify the deletion-specific sequence. Moreover, high-resolution analyses of WBCs from II.1[F2] did not detect the paternal wild-type *LAMP2* allele, suggesting homogenous distribution of the abnormal variant.

To conclude, *LAMP2* eCNVs are an important type of mutation causing DD and can be found in female probands. To avoid missing such variants, the outlined integrative approach to clinical, protein, and molecular genetic/genomic DD diagnostics is fully advocated, particularly in suspect females.

ACKNOWLEDGMENTS

CONFLICT OF INTEREST

The authors declared that they have no conflict of interest.

ORCID

Jakub Sikora http://orcid.org/0000-0003-4104-2023

REFERENCES

Bottillo, I., Giordano, C., Cerbelli, B., D'Angelantonio, D., Lipari, M., Polidori, T., ... Grammatico, P. (2016). A novel LAMP2 mutation associated with severe cardiac hypertrophy and microvascular remodeling in a female with Danon disease: A case report and literature review. *Cardiovascular Pathology*, 25(5), 423–431.

Boucek, D., Jirikowic, J., & Taylor, M. (2011). Natural history of Danon disease. *Genetics in Medicine*, 13(6), 563–568.

Campbell, I. M., Yuan, B., Robberecht, C., Pfundt, R., Szafranski, P., McEntagart, M. E., ... Stankiewicz, P. (2014). Parental somatic mosaicism is underrecognized and influences recurrence risk of genomic disorders. *American Journal of Human Genetics*, 95(2), 173–182.

Chen, X. L., Zhao, Y., Ke, H. P., Liu, W. T., Du, Z. F., & Zhang, X. N. (2012). Detection of somatic and germline mosaicism for the *LAMP2* gene mutation c.808dupG in a Chinese family with Danon disease. *Gene*, 507(2), 174–176.

D'Souza, R. S., Levandowski, C., Slavov, D., Graw, S. L., Allen, L. A., Adler, E., ... Taylor, M. R. (2014). Danon disease: Clinical features, evaluation, and management. *Circulation. Heart Failure*, 7(5), 843–849.

Dolezel, J., Bartos, J., Voglmayr, H., & Greilhuber, J. (2003). Nuclear DNA content and genome size of trout and human. *Cytometry. Part A*, 51(2), 127–128.

Fanin, M., Nascimbeni, A. C., Fulizio, L., Spinazzi, M., Melacini, P., & Angelini, C. (2006). Generalized lysosome-associated membrane protein-2 defect explains multisystem clinical involvement and allows leukocyte diagnostic screening in Danon disease. *The American Journal of Pathology*, 168(4), 1309–1320.

Fu, L., Luo, S., Cai, S., Hong, W., Guo, Y., Wu, J., ... Wang, J. (2016). Identification of LAMP2 mutations in early-onset Danon disease with hypertrophic

cardiomyopathy by targeted next-generation sequencing. *The American Journal of Cardiology*, 118(6), 888–894.

Lines, M. A., Hewson, S., Halliday, W., Sabatini, P. J., Stockley, T., Dipchand, A. I., ... Siriwardena, K. (2014). Danon disease due to a novel LAMP2 microduplication. *JIMD Report*, 14, 11–16.

Majer, F., Pelak, O., Kalina, T., Vlaskova, H., Dvorakova, L., Honzik, T., ... Sikora, J. (2014). Mosaic tissue distribution of the tandem duplication of LAMP2 exons 4 and 5 demonstrates the limits of Danon disease cellular and molecular diagnostics. *Journal of Inherited Metabolic Disease*, 37(1), 117–124.

Majer, F., Vlaskova, H., Krol, L., Kalina, T., Kubanek, M., Stolnaya, L., ... Sikora, J. (2012). Danon disease: A focus on processing of the novel LAMP2 mutation and comments on the beneficial use of peripheral white blood cells in the diagnosis of LAMP2 deficiency. *Gene*, 498(2), 183–195.

Mates, J., Mademont-Soler, I., Del Olmo, B., Ferrer-Costa, C., Coll, M., Perez-Serra, A., ... Brugada, R. (2018). Role of copy number variants in sudden cardiac death and related diseases: Genetic analysis and translation into clinical practice. *European Journal of Human Genetics*, 26(7), 1014–1025.

Miani, D., Taylor, M., Mestroni, L., D'Aurizio, F., Finato, N., Fanin, M., ... Proclemer, A. (2012). Sudden death associated with Danon disease in women. *The American Journal of Cardiology*, 109(3), 406–411.

Nishino, I., Fu, J., Tanji, K., Yamada, T., Shimojo, S., Koori, T., ... Hirano, M. (2000). Primary LAMP-2 deficiency causes X-linked vacuolar cardiomyopathy and myopathy (Danon disease). *Nature*, 406(6798), 906–910.

Regelsberger, G., Hoftberger, R., Pickl, W. F., Zlabinger, G. J., Kormoczi, U., Salzer-Muhar, U., ... Bernheimer, H. (2009). Danon disease: Case report and detection of new mutation. *Journal of Inherited Metabolic Disease*, 32 Suppl 1, S115–22.

Samad, F., Jain, R., Jan, M. F., Sulemanjee, N. Z., Menaria, P., Kalvin, L., ... Tajik, A. J. (2017). Malignant cardiac phenotypic expression of Danon disease (LAMP2 cardiomyopathy). *International Journal of Cardiology*, 245, 201–206.

Sikora, J., Majer, F., & Kalina, T. (2015). LAMP2 flow cytometry in peripheral white blood cells is an established method that facilitates identification of heterozygous Danon disease female patients and mosaic mutation carriers. *Journal of Cardiology*, 66(1), 88–89.

Sugie, K., Yoshizawa, H., Onoue, K., Nakanishi, Y., Eura, N., Ogawa, M., ... Ueno, S. (2016). Early onset of cardiomyopathy and intellectual disability in a girl with Danon disease associated with a de novo novel mutation of the *LAMP2* gene. *Neuropathology*, 36(6), 561–565.

Takahashi, M., Yamamoto, A., Takano, K., Sudo, A., Wada, T., Goto, Y., ... Saitoh, S. (2002). Germline mosaicism of a novel mutation in lysosome-associated membrane protein-2 deficiency (Danon disease). *Annals of Neurology*, 52(1), 122–125.

Toib, A., Grange, D. K., Kozel, B. A., Ewald, G. A., White, F. V., & Canter, C. E. (2010). Distinct clinical and histopathological presentations of Danon cardiomyopathy in young women. *Journal of the American College of Cardiology*, 55(4), 408–410.

Yang, Z., Funke, B. H., Cripe, L. H., Vick, G. W., 3rd, Mancini-Dinardo, D., Pena, L. S., ... Vatta, M. (2010). LAMP2 microdeletions in patients with Danon disease. *Circulation. Cardiovascular Genetics*, 3(2), 129–137.

SUPPORTING INFORMATION

Additional supporting information may be found online in the Supporting Information section at the end of the article.

How to cite this article: Majer F, Piherova L, Reboun M, et al. *LAMP2* exon-copy number variations in Danon disease heterozygote female probands: Infrequent or underdetected? *Am J Med Genet Part A*. 2018;1–5. https://doi.org/10.1002/ajmg.a.40430

CLINICAL REPORT

AMERICAN JOURNAL OF
medical genetics A PART WILEY

Alu-mediated Xq24 deletion encompassing CUL4B, LAMP2, ATP1B4, TMEM255A, and ZBTB33 genes causes Danon disease in a female patient

Filip Majer[1] | Bohdan Kousal[1,2] | Petr Dusek[3,4] | Lenka Piherova[1] |
Martin Reboun[1] | Romana Mihalova[5] | Jiri Gurka[6] | Alice Krebsova[6] |
Hana Vlaskova[1] | Lenka Dvorakova[1] | Jana Krihova[7] | Petra Liskova[1,2] |
Stanislav Kmoch[1] | Tomas Kalina[8] | Milos Kubanek[6] | Jakub Sikora[1,9] [ID]

[1]Research Unit for Rare Diseases, Department of Pediatrics and Adolescent Medicine, 1st Faculty of Medicine, Charles University and General University Hospital, Prague, Czech Republic

[2]Department of Ophthalmology, 1st Faculty of Medicine, Charles University and General University Hospital, Prague, Czech Republic

[3]Department of Neurology and Center of Clinical Neuroscience, 1st Faculty of Medicine, Charles University and General University Hospital, Prague, Czech Republic

[4]Department of Radiology, 1st Faculty of Medicine, Charles University and General University Hospital, Prague, Czech Republic

[5]Institute of Biology and Medical Genetics, 1st Faculty of Medicine, Charles University and General University Hospital, Prague, Czech Republic

[6]Department of Cardiology, Institute for Clinical and Experimental Medicine, Prague, Czech Republic

[7]Department of Psychology, Thomayer Hospital, Prague, Czech Republic

[8]Department of Paediatric Haematology and Oncology, Childhood Leukaemia Investigation Prague, 2nd Faculty of Medicine, Charles University and University Hospital Motol, Prague, Czech Republic

[9]Institute of Pathology, 1st Faculty of Medicine, Charles University and General University Hospital, Prague, Czech Republic

Correspondence
Jakub Sikora, Research Unit for Rare Diseases, Department of Pediatrics and Adolescent Medicine, 1st Faculty of Medicine, Charles University and General University Hospital, Ke Karlovu 2, 128 00 Prague 2, Czech Republic.
Email: jakub.sikora@lf1.cuni.cz

Abstract

Cullin 4B (CUL4B), lysosomal-associated membrane protein Type 2 (LAMP2), ATP1B4, TMEM255A, and ZBTB33 are neighboring genes on Xq24. Mutations in CUL4B result in Cabezas syndrome (CS). Male CS patients present with dysmorphic, neuropsychiatric, genitourinary, and endocrine abnormalities. Heterozygous CS females are clinically asymptomatic. LAMP2 mutations cause Danon disease (DD). Cardiomyopathy is a dominant feature of DD present in both males and heterozygous females. No monogenic phenotypes have been associated with mutations in ATP1B4, TMEM255A, and ZBTB33 genes. To facilitate diagnostics and counseling in CS and DD families, we present a female DD patient with a de novo Alu-mediated Xq24 rearrangement causing a deletion encompassing CUL4B, LAMP2, and also the other three neighboring genes. Typical to females heterozygous for CUL4B mutations, the patient was CS asymptomatic, however, presented with extremely skewed X-chromosome inactivation (XCI) ratios in peripheral white blood cells. As a result of the likely selection against CUL4B deficient clones, only minimal populations (~3%) of LAMP2 deficient leukocytes were identified by flow cytometry. On the contrary, myocardial LAMP2 protein expression suggested random XCI. We demonstrate that contiguous CUL4B and LAMP2 loss-of-function

copy number variations occur and speculate that male patients carrying similar defects could present with features of both CS and DD.

KEYWORDS

Cabezas syndrome, cullin 4B, Danon disease, female heterozygotes, lysosomal-associated membrane protein 2

1 | INTRODUCTION

Cullin 4B (*CUL4B*), lysosomal-associated membrane protein type 2 (*LAMP2*), ATPase Na+/K+ transporting family member beta 4 (*ATP1B4*), transmembrane protein 255A (*TMEM255A*), and KAISO (*ZBTB33*) are neighboring genes that occupy ~300 kb of *Xq24*.

Cabezas syndrome (CS, MIM #300354) is caused by mutations in *CUL4B* (Tarpey et al., 2007; Zou et al., 2007). Male CS patients express developmental, neuropsychiatric, genitourinary, endocrine, and dysmorphic symptoms. Females heterozygous for *CUL4B* mutations are clinically asymptomatic but skewed ratios of X-chromosome inactivation (XCI) in their peripheral blood suggest a selection against CUL4B deficient leukocyte clones (Ravn, Lindquist, Nielsen, Dahm, & Tumer, 2012; Zou et al., 2007).

Danon disease (DD, MIM #300257) results from mutations in *LAMP2*. DD is characterized by cognitive deficit, cardiomyopathy, and myopathy in male patients while delayed progression and cardiomyopathy dominate in heterozygous females (Brambatti et al., 2019).

No monogenic clinical phenotypes have been linked to variants in *ATP1B4*, *TMEM255A*, and *ZBTB33* genes.

Loss-of-function copy number variations (CNVs) in either *CUL4B* or *LAMP2* were reported in CS and DD families, respectively (Brambatti et al., 2019; Isidor, Pichon, Baron, David, & Le Caignec, 2010; Ravn et al., 2012). Despite their proximity, a simultaneous deficiency of the two genes has not yet been documented (Isidor et al., 2010).

To demonstrate the pitfalls of diagnostic assessment and facilitate counseling in CS and DD families, we present clinical, tissue and molecular findings in a female DD patient who carried a unique de novo *Alu*-mediated *Xq24* rearrangement causing a deletion encompassing *CUL4B*, *LAMP2*, *ATP1B4*, *TMEM255A*, and *ZBTB33* genes.

2 | CLINICAL REPORT

Aged 25 years, the proband (II.1) was diagnosed with dilated cardiomyopathy and severe bilateral heart failure. The left ventricle (LV) had normal wall thickness by echocardiography. LV ejection fraction was 20%. Moderate mitral and tricuspid valve regurgitation were also detected. A pulsatile biventricular assist device was implanted after 10 months of pharmacological treatment due to refractory cardiogenic shock with liver and kidney failure. Heart transplantation was performed 3 months later. Reevaluation (at the age of 36 years) of the proband's pretransplantation electrocardiograph identified discrete delta waves in lateral leads (Figure S1a).

The Wechsler Adult Intelligence Scale-III test in the proband (performed at the age of 37 years) suggested mild mental retardation (verbal IQ−66, performance IQ−68, full-scale IQ−64), with verbal scores worse than performance subtest scores (see Supporting Materials and Methods for index and subtest scores). No additional psychiatric abnormalities were identified by the evaluation of anamnestic data.

No abnormalities were found by neurological examination and brain MRI (Figure S1b-e).

The patient has no subjective visual complaints. Best-corrected visual acuity is 1.0 in both eyes. Fundus examination in dilatation revealed salt and pepper retinopathy (Figure S2a-d), altered autofluorescence distribution that spared the foveal and parafoveal zones (Figure S2e,f) and mild visual field defects (Figure S2g,h). High-resolution spectral-domain optical coherence tomography detected deposits in the retinal pigment epithelium/Bruch's membrane layer and hyper-reflective foci in the outer nuclear layer. OCT angiography revealed normal retinal vasculature (Figure S2k,l). The hyperreflective signal was noted in the avascular central zone (Figure S2m,n) by automated segmentation. Retinal nerve fiber layer thickness of the right and left eye was normal (Figure S2o,p). The patient has a normal perception of colors, but her contrast sensitivity is bilaterally decreased to 1.20.

The cardiologic examination was normal in the proband's mother and brother. The father has mild hypertrophy (13 mm) of the interventricular septum as a likely consequence of arterial hypertension.

3 | MATERIALS AND METHODS

3.1 | Editorial policies and ethical considerations

The study was approved by the Ethics Committee of the authors' home institution. Informed consent (also approved by the Ethics Committee of the authors' home institution) for presentation of the results was obtained from all participants.

Standard laboratory protocol based on LAMP2 protein assessment and molecular genetic studies (Majer et al., 2014; Majer et al., 2018; Sikora, Majer, & Kalina, 2015) confirmed DD in the clinically highly suspect proband (II.1, Figure 1a). Multicolor flow cytometry (FC) of the lysosomal-associated membrane protein Type 1 (LAMP1) and LAMP2, PCR and sequence analyses of the coding gDNA and full-length *LAMP2* mRNA/cDNAs, quantitative PCR (qPCR) *LAMP2* exon-copy number testing, and XCI HUMARA assay were performed in
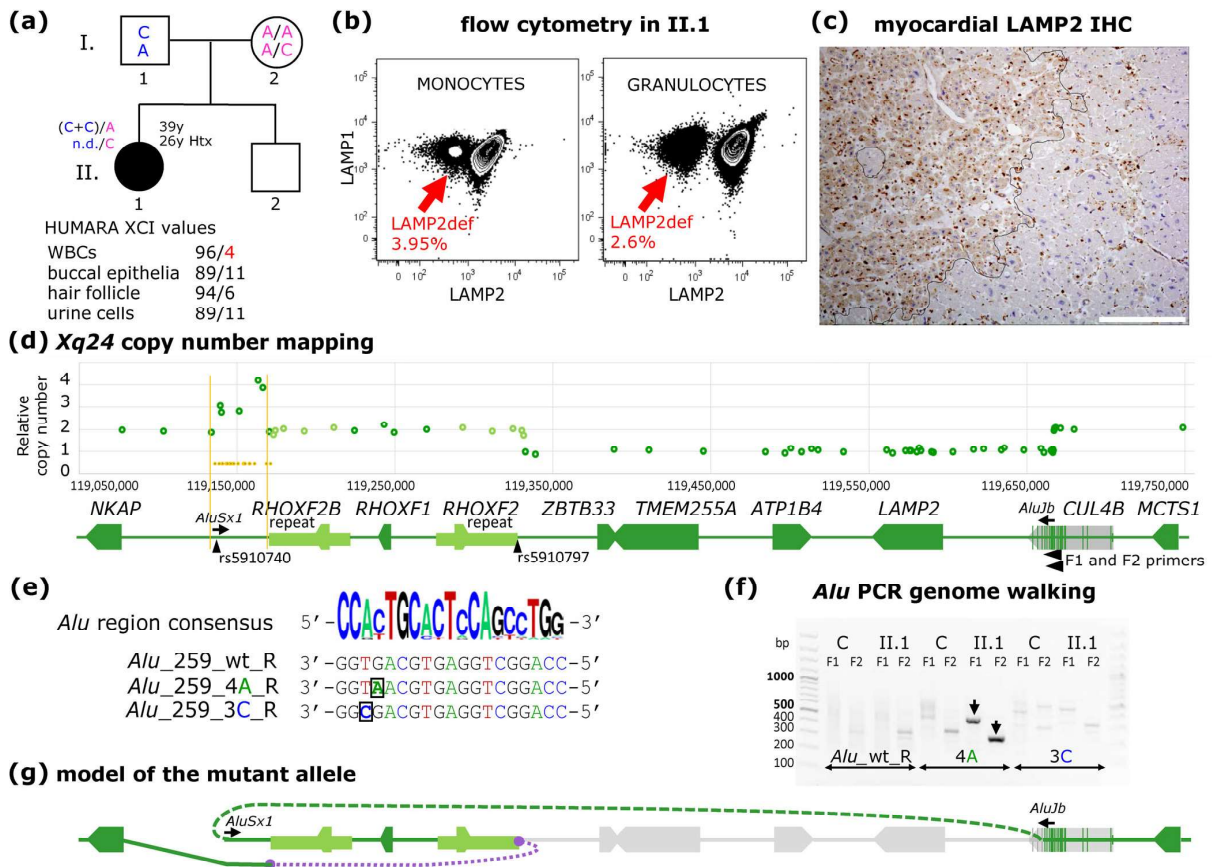
FIGURE 1 (a) Family pedigree. Current age and age at heart transplantation (Htx) are shown for II.1. Two SNPs (rs5910740 and rs5910797—positions are highlighted in Figure 1d and Figure S7) helped to identify, which of the parental alleles was affected by the rearrangement in the proband. The genetic setup of rs5910740 (upper) and rs5910797 (lower) is color-coded in both parents and the proband. rs5910740 localizes to a region with relative copy number 3 (Figure 1d). Paternal variant of rs5910797 was not detected (n.d.) in the proband (see also Figure S7). XCI ratios were assessed by the HUMARA assay. (b) FC dot plots show LAMP2def monocytes and granulocytes (red arrows) with normal presence of LAMP1 in II.1. (c) representative image of the mosaic LAMP2 expression (brown signal) in the patient's myocardium of the interventricular septum (borderline of LAMP2def and LAMP+ patches is highlighted, for further details see Figure S3), scale bar = 200 μm. (d) qPCR relative copy number values (green circles) in the critical *Xq24* region. *Alu* elements in the region with abnormally increased copy number values 3 and 4 are highlighted in orange. Black arrowheads indicate the position and orientation of the forward (F1 and F2) *Alu* PCR genome walking primers used to map the *CUL4B* breakpoint/junction site. Positions and orientation of *AluJb* and *AluSx1* elements are shown by arrows. (e) Sequences of *Alu* elements in the *Xq24* region with the copy number 3 or 4 were aligned (Figure S5) and three reverse primers for *Alu* PCR genome walking were designed. *Alu_259_wt_R* aligned to the most abundant and conserved part of the *Alu* sequence. *Alu_259_4A_R* and *Alu_259_3C_R* aligned to the most frequent 3′ *Alu* variants. (f) Agarose gel of *Alu* PCR genome walking reactions. Specific products (black arrows) were gained only with the *Alu_259_4A_R* primer (4A). The size difference (~177 bp), corresponds to the difference in position of primers F1 and F2 (Figure S6 shows the breakpoint junction sequence in detail). C—control sample. (g) A model of the complex rearrangement at the mutant allele. The orientation of the *AluSx1* element that participates in the *CUL4B* breakpoint junction highlights the presumed inversion of the *RHOXF* gene cluster. Violet dotted line marks the breakpoint junction that was not characterized [Color figure can be viewed at wileyonlinelibrary.com]

peripheral white blood cells (WBCs) as previously described (Majer et al., 2012, 2014). Primers used for all the PCR-based analyses are listed in Table S1. Cytogenetic analyses of peripheral blood samples followed standard protocols (Verma & Babu, 1995).

Quantification of the ratio of LAMP2+ and LAMP2 deficient (LAMP2def) cardiomyocytes was performed on immunohistochemically (IHC) stained sections from the formalin-fixed and paraffin-embedded explanted heart. For additional details see Supporting Materials and Methods.

4 | RESULTS

4.1 | FC, XCI analyses, and myocardial (immuno) histopathology

FC detected small but distinct populations of LAMP2def monocytes (~4%) and granulocytes (~3%) in the proband (Figure 1b). This corresponded with XCI ratios assessed by HUMARA (Figure 1a). HUMARA also showed that the inactive androgen receptor allele was of paternal origin.

Myocardial histopathology showed patchy hypertrophy and vacuolization of cardiomyocytes and fibrosis (Figure S3a,b). LAMP2 expression in cardiomyocytes was mosaic (Figure 1c) by IHC. The cell counts of the LAMP2def and LAMP2+ cardiomyocytes were comparable (Figure 1c, Supplementary Materials and Methods and Figure S3c–f).

4.2 | LAMP2 molecular studies

Profile and sequence of the three full-length *LAMP2* isoform mRNAs/cDNAs were normal in the proband (Figure S4). gDNA qPCR analyses identified ~300 kb long *Xq24* region with abnormally reduced relative copy number (1 instead of 2). The deletion started in *CUL4B* intron 19 (see Figure S6 for details) and encompassed the distal part of *CUL4B* (including exons 20–22 that code the last 140 amino acids of the protein and also the 3′ untranslated sequences with poly(A) sites), and the entire *LAMP2*, *ATP1B4*, *TMEM255A*, and *ZBTB33* genes. Five qPCR probes downstream of the *RHOXF2/RHOXF1/RHOXF2* homeobox gene cluster showed abnormally increased copy number values of 3 or 4 (Figure 1d). *Alu* PCR genome walking method was used to characterize the *CUL4B* breakpoint/junction site (Figure 1e,f). We identified residual sequences of *AluJb* (strand-) from intron 19 of *CUL4B* and *AluSx1* (strand+) (Figure S6) from the *Xq24* region with relative copy numbers of 3 and 4 (Figure 1d). G-banded chromosome analysis identified a normal female (46, XX) karyotype. Genotyping of two *Xq24* single nucleotide polymorphisms (SNPs; rs5910740 and rs5910797) in the proband and her parents (Figure 1a, Figure S7, and Table S1) suggested that the *Xq24* rearrangement affected the proband's paternal allele. The mutation-specific sequences were not identified in WBCs of either parent or the father's sperm (Figure S8).

5 | DISCUSSION

We present clinical findings and results of laboratory analyses in a female proband with a unique complex de novo *Xq24* rearrangement (Figure 1g) that caused a deletion impacting the distal part of *CUL4B* and the complete sequences of *LAMP2*, *ATP1B4*, *TMEM255A*, and *ZBTB33* genes.

The ophthalmic symptoms, myocardial histopathology, and mosaic LAMP2 expression corresponded to findings in DD female patients (Brambatti et al., 2019). In contrast to the latter study, however, the patient reached the end-stage heart failure more than 10 years earlier than DD females presenting with dilated cardiomyopathy.

Instability (and most probably also decay) of the putative *CUL4B* transcript is expected in the proband. Any truncated CUL4B protein (773 instead of 914 amino acids in length) would also likely not be stable, not complex with its partners, and fail the ubiquitination function (see Figure S9). Similar to other *CUL4B* female heterozygotes, our patient was asymptomatic in nonpsychiatric clinical domains that are usually impacted in male CS patients (Tarpey et al., 2007; Zou et al., 2007). Her mild mental retardation could be caused by the pathogenic effects of both *LAMP2* and *CUL4B* mutations. However, the

contribution of the pathogenic variants in either of the two genes to this particular phenotype is impossible to establish.

An additional finding typical for female CS heterozygotes, XCI ratios were extremely skewed (presumably due to selection against CUL4B deficient cellular clones) in several of the proband's tissues including peripheral blood (Zou et al., 2007). This phenomenon was reflected by minimal but distinct LAMP2def populations of peripheral WBCs. On the contrary, the fraction of *LAMP2*def cardiomyocytes was comparable to the number of cardiomyocytes that expressed LAMP2 normally. This tissue-specific discrepancy suggests that the selection may not be universal to all cell types/tissues. Interestingly, a similar phenomenon was suggested in heterozygous female *Cul4b* knock-out mice (Jiang et al., 2012).

Little is known about the function of the three other deleted genes (*ATP1B4*, *TMEM255A*, and *ZBTB33*). ATP1B4 is a muscle-specific protein of the inner nuclear envelope (Zhao, Pestov, Korneenko, Shakhparonov, & Modyanov, 2004), TMEM255A is a predicted transmembrane protein (UniProtKB), and ZBTB33 (KAISO) is a zinc-finger containing transcriptional factor involved in cell cycle regulation and cancer progression (Schackmann, Tenhagen, van de Ven, & Derksen, 2013). Variants in these three genes have not been associated with any defined human genetic phenotype. Contribution of their reduced copy number to the proband's phenotype is thus speculative.

As repetitive elements often contribute to *LAMP2* CNVs (Majer et al., 2018), we used the *Alu* PCR genome walking technique and identified residual *AluJb* and *AluSx1* sequences in the breakpoint junction (Figure 1e and Figures S5 and S6). Detailed analysis of this junctional sequence suggested an inversion of the *RHOXF2/RHOXF1/RHOXF2* homeobox cluster as part of the complex *Xq24* rearrangement. The full characterization of the other breakpoint(s) (violet dots in Figure 1g) was not completed because of the high content of repetitions in the region.

Overall, our data demonstrate that deletion CNVs contiguously affecting *CUL4B* and *LAMP2* occur. In reference to findings in the presented proband, the clinical phenotype in heterozygous females with similar genetic setup is expected to be dominated by cardiac DD symptoms. The values of XCI ratios in WBCs and quantitation of the LAMP2def leukocyte populations in these patients should, however, be interpreted cautiously, because the results of these tests may be impacted by the (likely tissue-specific) effects of the *CUL4B* mutation. In male patients, on the contrary, a contiguous *CUL4B* and *LAMP2* loss-of-function CNV could result in a phenotype combining symptoms of CS and DD.

CONFLICT OF INTEREST

The authors have no conflict of interest.

DATA AVAILABILITY STATEMENT

The data that support the findings of this study are available on request from the corresponding author. The data are not publicly available due to privacy or ethical restrictions.

ORCID

Jakub Sikora https://orcid.org/0000-0003-4104-2023

REFERENCES

Brambatti, M., Caspi, O., Maolo, A., Koshi, E., Greenberg, B., Taylor, M. R. G., & Adler, E. D. (2019). Danon disease: Gender differences in presentation and outcomes. *International Journal of Cardiology*, *286*, 92–98.

Isidor, B., Pichon, O., Baron, S., David, A., & Le Caignec, C. (2010). Deletion of the CUL4B gene in a boy with mental retardation, minor facial anomalies, short stature, hypogonadism, and ataxia. *American Journal of Medical Genetics, Part A*, *152A*(1), 175–180.

Jiang, B., Zhao, W., Yuan, J., Qian, Y., Sun, W., Zou, Y., … Gong, Y. (2012). Lack of Cul4b, an E3 ubiquitin ligase component, leads to embryonic lethality and abnormal placental development. *PLoS One*, *7*(5), e37070.

Majer, F., Pelak, O., Kalina, T., Vlaskova, H., Dvorakova, L., Honzik, T., … Sikora, J. (2014). Mosaic tissue distribution of the tandem duplication of LAMP2 exons 4 and 5 demonstrates the limits of Danon disease cellular and molecular diagnostics. *Journal of Inherited Metabolic Disease*, *37*(1), 117–124.

Majer, F., Piherova, L., Reboun, M., Stara, V., Pelak, O., Norambuena, P., … Sikora, J. (2018). LAMP2 exon-copy number variations in Danon disease heterozygote female probands: Infrequent or underdetected? *American Journal of Medical Genetics, Part A*, *176*(11), 2430–2434.

Majer, F., Vlaskova, H., Krol, L., Kalina, T., Kubanek, M., Stolnaya, L., … Sikora, J. (2012). Danon disease: A focus on processing of the novel LAMP2 mutation and comments on the beneficial use of peripheral white blood cells in the diagnosis of LAMP2 deficiency. *Gene*, *498*(2), 183–195.

Ravn, K., Lindquist, S. G., Nielsen, K., Dahm, T. L., & Tumer, Z. (2012). Deletion of CUL4B leads to concordant phenotype in a monozygotic twin pair. *Clinical Genetics*, *82*(3), 292–294.

Schackmann, R. C., Tenhagen, M., van de Ven, R. A., & Derksen, P. W. (2013). p120-catenin in cancer - Mechanisms, models and opportunities for intervention. *Journal of Cell Science*, *126*(Pt 16), 3515–3525.

Sikora, J., Majer, F., & Kalina, T. (2015). LAMP2 flow cytometry in peripheral white blood cells is an established method that facilitates identification of heterozygous Danon disease female patients and mosaic mutation carriers. *Journal of Cardiology*, *66*(1), 88–89.

Tarpey, P. S., Raymond, F. L., O'Meara, S., Edkins, S., Teague, J., Butler, A., … Partington, M. (2007). Mutations in CUL4B, which encodes a ubiquitin E3 ligase subunit, cause an X-linked mental retardation syndrome associated with aggressive outbursts, seizures, relative macrocephaly, central obesity, hypogonadism, pes cavus, and tremor. *American Journal of Human Genetics*, *80*(2), 345–352.

UniProtKB. https://www.uniprot.org/uniprot/Q5JRV8.

Verma, R., & Babu, A. (1995). *Human chromosomes: Principles & techniques* (2nd ed.). New York: McGraw-Hill, Inc.

Zhao, H., Pestov, N. B., Korneenko, T. V., Shakhparonov, M. I., & Modyanov, N. N. (2004). Accumulation of beta (m), a structural member of X,K-ATPase beta-subunit family, in nuclear envelopes of perinatal myocytes. *American Journal of Physiology Cell Physiology*, *286*(4), C757–C767.

Zou, Y., Liu, Q., Chen, B., Zhang, X., Guo, C., Zhou, H., … Gong, Y. (2007). Mutation in CUL4B, which encodes a member of cullin-RING ubiquitin ligase complex, causes X-linked mental retardation. *American Journal of Human Genetics*, *80*(3), 561–566.

SUPPORTING INFORMATION

Additional supporting information may be found online in the Supporting Information section at the end of this article.

How to cite this article: Majer F, Kousal B, Dusek P, et al. *Alu*-mediated *Xq24* deletion encompassing *CUL4B*, *LAMP2*, *ATP1B4*, *TMEM255A*, and *ZBTB33* genes causes Danon disease in a female patient. *Am J Med Genet Part A*. 2019;1–5. https://doi.org/10.1002/ajmg.a.61416